Reliability of Modular Multilevel Converters

Impact of Redundancy, Modularity, and Reconfigurability

Ahmadi, M.

DOI
10.4233/uuid:0ad53f7a-fbdb-448d-9aac-676fb1dd5c65

Publication date
2025

Document Version
Final published version

Citation (APA)
Ahmadi, M. (2025). *Reliability of Modular Multilevel Converters: Impact of Redundancy, Modularity, and Reconfigurability*. [Dissertation (TU Delft), Delft University of Technology].
https://doi.org/10.4233/uuid:0ad53f7a-fbdb-448d-9aac-676fb1dd5c65

Important note
To cite this publication, please use the final published version (if applicable).
Please check the document version above.

Reliability of Modular Multilevel Converters

Impact of Redundancy, Modularity, and Reconfigurability

RELIABILITY OF MODULAR MULTILEVEL CONVERTERS

IMPACT OF REDUNDANCY, MODULARITY, AND RECONFIGURABILITY

Dissertation,

for the purpose of obtaining the degree of doctor
at Delft University of Technology
by the authority of rector Magnificus prof.dr.ir T. H. J. J. van der Hagen
chair of the Board for Doctorates
to be defended publicly on
Friday 16th of May 2025 at 10 o'clock

by

Miad AHMADI

Master of Science in Electrical Engineering, Politecnico di Milano, Italy
born in Kermanshah, Iran

This dissertation has been approved by the promotor.

Composition of the doctoral committee:

Rector Magnificus,	Chairman
Prof. dr. ir. P. Bauer,	Delft University of Technology, promotor
Dr. ir. A. Shekhar,	Delft University of Technology, copromotor

Independent members:

Prof. dr. ir. W.D. Van Driel,	Delft University of Technology
Prof. dr. D. Vinnikov,	Tallinn University of Technology, Estonia
Prof. dr. G. Papafotiou,	Eindhoven University of Technology
Prof. ir. P.T.M. Vaessen,	Delft University of Technology
Dr. ir. J.L. Rueda Torres,	Delft University of Technology

Printed by Gildeprint

Cover designed by Fatemeh Kazemi

ISBN/EAN: 978-94-6518-041-0

An electronic version of this dissertation is available at
http://respsitory.tudelft.nl/.

With love to my family and wife

CONTENTS

SUMMARY

This thesis focuses on advancing modular multilevel converters' (MMCs') reliability and fault tolerance. MMC is a popular converter in high-power applications due to its scalability, efficiency, and modular design. Despite their advantages, MMCs are susceptible to reliability issues, which can compromise continuous operation. To address these challenges, the research introduces a series of strategies and methodologies to enhance the resilience of MMCs through improved reliability assessments, optimized redundancy strategies, and fault-tolerant reconfigurability techniques.

The work begins with a comparative analysis of reliability assessment methods, including the Military Handbook, FIDES, and Mission Profile approaches. By examining the strengths and limitations of each, the thesis provides a foundation for selecting the most suitable method for evaluating MMC reliability in diverse operational contexts. This step is crucial as it addresses the challenge of accurately predicting MMC lifespan under variable conditions, paving the way for more reliable converter designs.

The Monte Carlo simulation framework is developed to evaluate the effectiveness of different redundancy strategies. This framework allows for modeling complex, real-world operational stresses and testing redundancy schemes. Through this approach, the thesis explores various configurations, such as Fixed-Level Active Redundancy and Standby Redundancy, demonstrating how each impacts overall reliability. The insights from these simulations provide a data-driven foundation for optimizing redundancy strategies tailored to specific application requirements.

The thesis proposes a cost-effective design methodology to address the trade-off between modularity, redundancy, and cost. By optimizing switch voltage ratings, this methodology balances capital and operational expenditures with reliability goals, allowing for scalable, modular designs without compromising durability. This approach reduces the initial costs associated with MMCs and ensures that performance standards are maintained under typical operating conditions.

To optimize the reliability of MMCs, a Mixed Redundancy Strategy (MRS) is introduced, combining active and spare redundant submodules (SMs) within the converter structure. This strategy offers an optimal balance between reliability improvement and cost containment. Through sensitivity analyses and simulations, the MRS is validated as a practical approach to enhancing MMC resilience, ensuring continuous operation despite faults without high redundancy costs.

Finally, the thesis develops a reconfigurability method enabling MMCs to operate continuously under fault conditions by dynamically bypassing faulty SMs or reconfiguring. This fault-tolerant reconfiguration technique is experimentally validated, demonstrating its effectiveness in detecting, localizing, and isolating faults in real-time. The proposed method provides a practical solution to enhance fault tolerance, enabling the MMC to maintain functionality with minimal impact on performance.

Overall, this thesis presents a comprehensive framework for advancing the reliability and cost-efficiency of MMCs through targeted improvements in reliability assessment, redundancy management, and fault-tolerant design. These contributions represent a significant advancement for power electronic systems where robustness and continuous operation are paramount, providing valuable insights and methodologies for developing resilient power converters.

SAMENVATTING

Deze scriptie richt zich op het verbeteren van de betrouwbaarheid en fouttolerantie van modulaire multilevel-omvormers (MMC's). MMC is een populaire omvormer in hoogvermogentoepassingen vanwege zijn schaalbaarheid, efficiëntie en modulaire ontwerp. Ondanks hun voordelen zijn MMC's vatbaar voor betrouwbaarheidsproblemen, wat de continuïteit van de werking kan compromitteren. Om deze uitdagingen aan te pakken, introduceert het onderzoek een reeks strategieën en methodologieën om de veerkracht van MMC's te vergroten door verbeterde betrouwbaarheidsbeoordelingen, geoptimaliseerde redundantie-strategieën en fouttolerante herconfigureerbaarheidstechnieken.

Het werk begint met een vergelijkende analyse van betrouwbaarheidsbeoordelingsmethoden, waaronder de Military Handbook-, FIDES- en Mission Profile-benaderingen. Door de sterke en zwakke punten van elk te onderzoeken, biedt de scriptie een basis voor het selecteren van de meest geschikte methode voor het evalueren van de betrouwbaarheid van MMC's in diverse operationele contexten. Deze stap is cruciaal omdat het de uitdaging aanpakt om de levensduur van MMC's nauwkeurig te voorspellen onder variabele omstandigheden, wat de weg vrijmaakt voor betrouwbaardere omvormerontwerpen.

Het Monte Carlo-simulatiekader is ontwikkeld om de effectiviteit van verschillende redundantie-strategieën te evalueren. Dit kader maakt het mogelijk om complexe, realistische operationele spanningen te modelleren en redundantie-schema's te testen. Via deze benadering verkent de scriptie verschillende configuraties, zoals Fixed-Level Active Redundancy en Standby Redundancy, waarbij wordt gedemonstreerd hoe elk de algehele betrouwbaarheid beïnvloedt. De inzichten uit deze simulaties bieden een datagedreven basis voor het optimaliseren van redundantie-strategieën die zijn afgestemd op specifieke toepassingsvereisten.

De scriptie stelt een kosteneffectieve ontwerpmethodologie voor om de afweging tussen modulariteit, redundantie en kosten aan te pakken. Door het optimaliseren van de spanningswaarden van schakelaars balanceert deze methodologie kapitaal- en operationele uitgaven met betrouwbaarheidsdoelen, waardoor schaalbare, modulaire ontwerpen mogelijk zijn zonder in te leveren op duurzaamheid. Deze aanpak vermindert de initiële kosten die geassocieerd zijn met MMC's en zorgt ervoor dat prestatiestandaarden worden gehandhaafd onder typische bedrijfsomstandigheden.

Om de betrouwbaarheid van MMC's te optimaliseren, wordt een Mixed Redundancy Strategy (MRS) geïntroduceerd, die actieve en reserve redundante submodules (SM's) combineert binnen de omvormerstructuur. Deze strategie biedt een optimale balans tussen betrouwbaarheidverbetering en kostbeheersing. Door middel van gevoeligheidsanalyses en simulaties wordt de MRS gevalideerd als een praktische benadering om de veerkracht van MMC's te vergroten, waardoor continue werking ondanks fouten wordt verzekerd zonder hoge redundantie-kosten.

Ten slotte ontwikkelt de scriptie een herconfigureerbaarheidsmethode die MMC's in staat stelt continu te werken onder foutcondities door dynamisch defecte SM's te omzeilen of te herconfigureren. Deze fouttolerante herconfiguratietechniek wordt experimenteel gevalideerd en toont zijn effectiviteit aan bij het detecteren, lokaliseren en isoleren van fouten in real-time. De voorgestelde methode biedt een praktische oplossing om de fouttolerantie te verbeteren, waardoor de MMC functionaliteit behoudt met minimale impact op de prestaties.

Over het geheel genomen presenteert deze scriptie een uitgebreid kader voor het verbeteren van de betrouwbaarheid en kostenefficiëntie van MMC's door gerichte verbeteringen in betrouwbaarheidsbeoordeling, redundantiebeheer en fouttolerant ontwerp. Deze bijdragen vertegenwoordigen een significante vooruitgang voor vermogenselektronische systemen waar robuustheid en continue werking van het grootste belang zijn, en bieden waardevolle inzichten en methodologieën voor het ontwikkelen van veerkrachtige vermogensomvormers.

List of Tables

LIST OF FIGURES

1

INTRODUCTION

This chapter aims to provide a framework for improving the reliability of power electronic converters. In general, achieving higher reliability often incurs additional costs, either in terms of increased capital expenditure (e.g., higher-quality components, redundancy) or higher operational costs (e.g., maintenance, monitoring). Therefore, optimal design requires a careful balance between improving reliability—such as reducing failure rates or extending system lifetime—and managing both capital and operational costs.

A part of this chapter is published in:

- M. Ahmadi, A. Shekhar and P. Bauer, "Reconfigurability, Modularity and Redundancy Trade-offs for Grid Connected Power Electronic Systems," in IEEE 20th International Power Electronics and Motion Control Conference (PEMC), 2022.

1

1.1. BACKGROUND

In recent years, alongside the power electronics devices development [1], voltage source converters (VSC) such as modular multilevel converters (MMCs), two-level converter (2L-VSC), three-level converters (3L-VSCs) among other types, showed a significant increase of applications in power grids [2]. On the other hand, the penetration of distributed systems such as renewable energy sources (RES), charging stations, storage systems, etc., has risen considerably [3]. Additionally, the demand for electricity has increased sharply—not only due to population growth, but also because of the electrification of various sectors such as transportation, industry, and heating—highlighting the growing need for a reliable power supply [4]. Therefore, a growing number of installed electrical energy systems (load and supplier) increase the demand for reliable power systems to decrease the likelihood of blackouts [4].

It is important to modernize the grid-connected power electronics systems to increase the system reliability and decrease greenhouse gas emissions by integrating RES, e-mobility technologies, and storage units into the power systems [5, 6]. For such energy transition goals, the role of power electronics is pivotal in enabling grid integration with power electronic converters as efficient and reliable interfaces [7, 8].

It is worth mentioning that grid-connected power electronic converters play a key role in advanced configurations such as meshed transmission systems with multiple terminals [9]—including medium-voltage and high-voltage VSC-based multi-terminal DC (VSC-MTDC) systems—which are becoming increasingly attractive due to their high controllability, power transfer capability, and operational flexibility [10]. But, utilizing more power electronic-based systems can pose challenges to reliable planning and operation of the system [6]. Furthermore, power electronic converters are composed of many components, including power switches, capacitors, etc., which can be a source of failure and negatively affect the reliable operation of the power systems [11]. For instance, in grid-connected power electronic converters, converters can contribute to unplanned downtime of RES where the cost losses are significant [12].

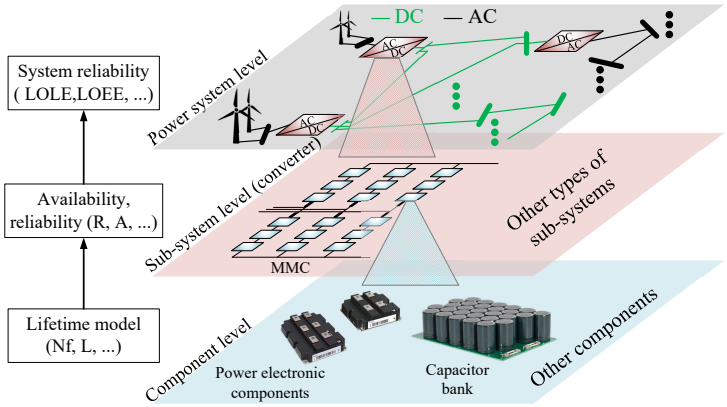

Figure 1.1: Physical layers of reliability from component to power system levels.

As shown in Fig. 1.1, the reliability analysis is gaining attention in grid-connected

power electronic converters in which the reliability evaluation can be done at component-level [5, 6, 13], converter-level [3, 9, 10, 14–18] and system level[4, 7, 19–24]. The most common corresponding reliability indicators are also given at each level, where LOLE is the loss of load expectation, LOEE is the loss of energy expectation, R is reliability, A is availability, Nf is the number of thermal cycles to failure caused by temperature variations induced by fundamental (50 Hz) and low-frequency power cycles, and L is the lifetime of the considered components.

Most studies regarding reliability analysis at the converter and system level only evaluate reliability without proposing how to enhance it. However, applying design strategies such as redundancy, modularity, and reconfigurability (RMR) can significantly improve the reliability of grid-connected power electronic converters. These strategies can be implemented during the design, planning, and operational stages to enhance system reliability in a cost-efficient manner. Therefore, this thesis provides an overview of how RMR can be used to improve system reliability, particularly as the penetration of power electronic converters in the grid continues to increase.

1.2. MOTIVATION

As summarized in Fig. 1.2, the development of MMC has revolutionized the field of power electronics, particularly for medium and high-voltage applications. MMCs offer numerous advantages, including improved power quality, scalability, and higher efficiency, making them an essential component in modern power electronic systems. These converters are extensively used in applications such as renewable energy integration, high-voltage direct current (HVDC) transmission, and flexible alternating current transmission systems (FACTS). However, as the demand for more reliable and efficient power electronic systems grows, addressing the challenges associated with MMC reliability becomes increasingly critical.

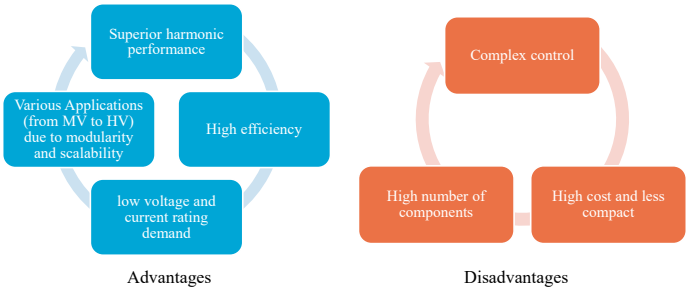

Figure 1.2: Advantages and disadvantages of using MMC in different applications.

Reliability is a fundamental concern in the design and operation of MMCs due to the significant impact of component failures on system performance, safety, and cost. In power electronic systems, failures can lead to costly downtime, extensive maintenance requirements, and potential safety hazards. The modular nature of MMCs, while providing flexibility and scalability, also introduces complexity in reliability assessment and maintenance strategies. As a result, developing robust methodologies to predict and

1

enhance the reliability of MMCs is essential for their successful deployment in critical applications.

One of the primary challenges in ensuring the reliability of MMCs is the diverse range of operating conditions and environmental factors they encounter. MMCs are exposed to varying thermal, electrical, and mechanical stresses, as well as environmental stresses such as moisture, dust, and contamination. These factors can significantly influence the failure rates of their components. Traditional reliability assessment methods, such as the Military Handbook (MIL-HDBK-217), have provided a baseline for reliability prediction.

The economic implications of MMC reliability cannot be overlooked. The cost associated with system failures, maintenance, and downtime can be substantial, particularly in large-scale power electronic installations. This highlights the need for a cost-effective reliability assessment and enhancement approach, considering initial investment and long-term operational expenses.

Hence, the concept of RMR is pivotal in achieving high reliability but cost-efficient, as given in Fig. 1.3. To achieve this, firstly, a very brief insight into the concept of each term in MMC is provided as follows:

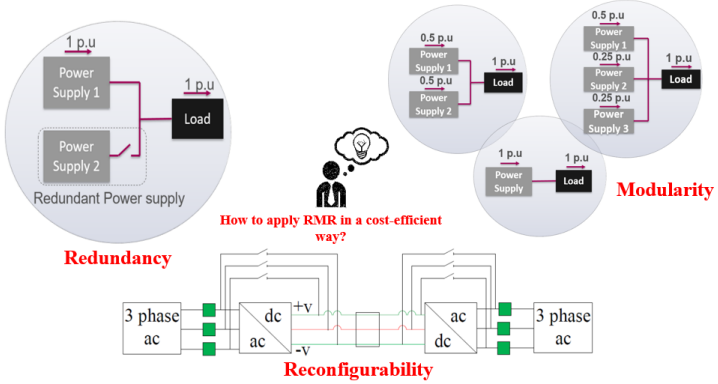

Figure 1.3: General overview of RMR application for reliability improvement.

1.2.1. CONVERTER-LEVEL REDUNDANCY

The simple definition of redundancy means the inclusion of additional components within the system's structure that are not necessary to function, and they are used in case of other components' failure. So, redundancy is one of the approaches to embed the fault-tolerance ability within the system structure. The MMC comprises SMs connected in series to reach the desired DC-link voltage. In this type of converter, to increase the converter reliability in case of SM failure and without degrading the post-fault operation, redundant SMs are used in the MMC, as shown in Fig. 1.4.

Regarding the operation of MMC with redundant SM, various strategies are proposed wherein, in each strategy, the redundant components can be operational or remain idle. For example, in the non-redundant configuration of Fig 1.4 (a), if any one of the SMs within the MMC fails, the converter should shut down (or, in some cases, it can operate

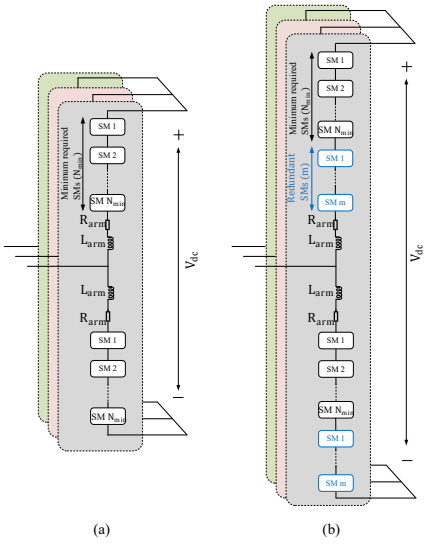

Figure 1.4: The MMC configuration (a) without (b) and with redundancy.

at a derated power) whereas, in a redundant configuration, if an SM fails (open circuit or short-circuit) it can be bypassed. As a result, the converter continues to operate at the rated power [14].

1.2.2. CONVERTER-LEVEL MODULARITY

Modularity is the degree to which system components might be separated in power converter applications, providing the system with flexibility and a higher number of choices for component selection. Modularity can be applied at MMC's arm level by considering the cost and reliability. Therefore, optimal choices could be based on the number of levels or power switch rating, which essentially determines the modularity level. The characteristics of various switches determine the system's reliability, efficiency, and cost. For example, Fig 1.5 represents the MMC with two modularity scenarios, which can be obtained by applying [25]:

$$N_{\text{min}} = ceil[\frac{V_{\text{dc}}}{S_{\text{f}} \times V_{\text{IGBT}}}] \tag{1.1}$$

where the safety factor S_{f} ranges from 0.4 to 0.75 [26] which are the voltage limits for the design of SM for different applications. In this part, the value of 0.6 is assumed that is the voltage limit for the safe switching. N_{min} is the minimum number of levels and V_{IGBT} is the IGBT blocking voltage. Considering an applied voltage of $V_{\text{dc}} = 28$ kV to the DC link, if the voltage rating of the power switch is 1.7 kV, the N_{min} is 28. If the voltage rating of the power switches is 3.3 kV, the N_{min} will be 15.

As shown in Fig 1.5, many choices exist regarding the MMC modularity. Each modularity scenario has advantages and disadvantages, and the optimal configuration can be selected based on assumptions, system requirements, reliability, cost, efficiency, etc.

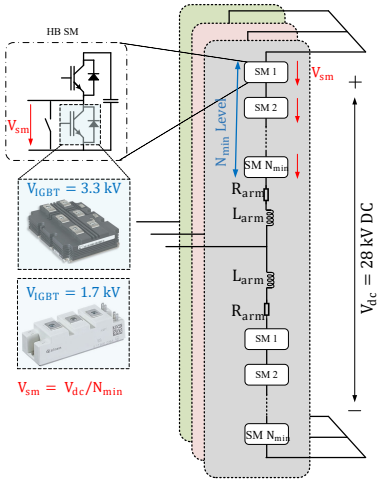

Figure 1.5: The MMC general configuration with two modularity scenarios.

For instance, in Fig. 1.5, if N_{min}= 28, there are more SMs within the MMC compared to N_{min}= 15, and the reliability of such a system might be lower since there is a higher number of components and the chance of SM failure is higher. Also, the efficiency of the MMC with N_{min}= 15 could be higher than N_{min}= 28 since there are fewer power modules, and consequently, the lower conduction losses (higher efficiency) will be [14, 18]. However, the modularity of MMC with N_{min}= 28 gives higher flexibility and smoother modulation, consequently decreasing the harmonic distortion and filter size [25, 27, 28]. All these concepts will be detailed in chapter 4.

1.2.3. CONVERTER-LEVEL RECONFIGURABILITY

In general, the ability of the system to rearrange its various parts in case of failure is called reconfigurability. This is another way of meeting fault tolerance capability. The reliability of the converter can be improved if reconfigurability is embedded within its structure [29] that in some cases is compulsory such as grid-connected converter for offshore wind turbines where maintenance could be challenging and not cost-efficient [30]. Hence, reconfigurability is required to increase the system's reliability and availability. For example, in [31], a three-level neutral-point-clamped (NPC) converter with an extra flying capacitor (FC) is proposed, wherein, in case of fault, the FC leg will take over, and the converter continues its operation. Other examples of the reconfigurable converter are presented in [32, 33], in which reconfigurable DC-DC converters are proposed to embed the fault tolerance within their structures.

It is worth mentioning that fault tolerance ability in various converter topologies has been explored, and the converter is fault-tolerant because of redundancy and/or reconfigurability. There are two ways of reaching fault tolerance: redundancy and reconfigurability. However, there is a distinction between redundancy and reconfigurability. With redundancy, the configuration of the converter after a fault and before a fault is iden-

tical, whereas, with reconfigurability, the post-fault structure of the system is different than before fault occurrence [31–36].

1.3. THESIS OBJECTIVES AND RESEARCH QUESTIONS

The main objective of this thesis is as follows:

"Enhancing the MMC reliability in a cost-efficient manner by applying Redundancy, modularity, and reconfigurability (RMR) through a comprehensive analysis of reliability methods, redundancy strategies, cost-optimized designs, and the integration of reconfigurability, culminating in practical recommendations."

The objective of this thesis is divided into the following four research questions.

Q1: How can the reliability of MMCs be accurately assessed using comprehensive methodologies?

Chapters 2 and 3 address the need for accurate and comprehensive reliability assessment methodologies for MMCs. Chapter 2 introduces and compares three distinct methodologies: the Military Handbook (MIL-HDBK-217), FIDES, and the Mission Profile Methodology. Each method is detailed for calculating failure rates by considering environmental conditions, operational stresses, and specific mission profiles. The Military Handbook method provides standardized failure rates, the FIDES methodology incorporates technical controls over manufacturing and operational processes, and the Mission Profile Methodology focuses on modeling the operational environment and specific conditions of the MMC. Chapter 3 complements this analysis by applying Monte Carlo Simulations (MCS) to these methodologies. MCS is used to evaluate the reliability of MMC under different redundancy strategies. The MCS can quantify reliability outputs where the analytical approach is challenging or unavailable. These chapters provide a holistic approach to reliability assessment, combining traditional methods with MCS to offer a more accurate and practical reliability prediction.

Key challenges:

- Each method will result in different reliability results, which makes it difficult to determine which method gives the most realistic outputs due to the variability of failure rate data.
- Calculating the MMC reliability under the mission profile method with specific redundancy strategies is unavailable due to analytical challenges. So, an alternative solution is required to solve the problem.
- The Monte Carlo Simulation method could be a valuable tool for reliability evaluation, but there is no literature on implementing it. Hence, it is desired to implement the Monte Carlo simulation for reliability analysis as another valuable method in scenarios where analytical methods are very challenging to apply.

Q2: How can the trade-offs between cost, modularity, and reliability be optimized in the design of MMCs?

Chapter 4 examines the cost-oriented design of MMCs, focusing on the trade-offs between modularity, redundancy, and overall system cost. It begins by discussing the importance of modularity and redundancy in achieving high reliability and flexibility in MMCs. The chapter then presents a detailed analysis of different modularity options to optimize the cost, reliability, and efficiency of MMCs. It includes case studies comparing various design options' capital investment and operational costs, considering switch voltage ratings, SM configurations, and loading conditions. The chapter also explores sensitivity analyses to evaluate the impact of different parameters, such as failure rates, component lifetimes, and energy prices, on the overall cost and reliability of the system. By comprehensively evaluating these trade-offs, the chapter offers practical guidelines for selecting the optimal switch raring to have cost-effective and reliable MMCs, emphasizing the need to balance initial investment with long-term operational expenses.

Key challenges:

- Selecting the optimal modularity level is affected by many factors, including capital costs, operational loss, redundancy level, and reliability requirements. Hence, providing an optimized switch rating selection method to consider all these aspects is not straightforward.
- Since there are different methods in reliability analysis, all lead to different reliability outputs, which can significantly change the output. Hence, generalization and sensitivity must be performed, which is difficult as the load and switch characteristics differ for each scenario.
- For each switch rating, different available commercial choices are there. Each has different characteristics and price considerations, which change the whole results. This consideration is of importance for generalization.

Q3: How can a mixed redundancy strategy improve the reliability and cost-effectiveness of MMCs?

Chapter 5 focuses on a mixed redundancy strategy (MRS) for MMCs, which combines active and spare redundant SMs to enhance system reliability and cost-effectiveness. The chapter introduces the MRS and its working principles. It details how MRS can be implemented by integrating a combination of active redundant SMs that are always in operation and spare SMs that only replace faulty SMs during maintenance. The chapter includes comprehensive reliability assessments through analytical methods, and MCS is applied to validate the effectiveness of such methodology. It also presents case studies and sensitivity analyses to evaluate the impact of different configurations and operating conditions on the system's reliability and cost. The findings highlight the advantages of MRS in providing a more balanced and flexible approach to redundancy, offering improved reliability without significantly increasing costs. The chapter concludes by discussing the practical implications of implementing MRS and providing recommendations for optimizing its design and operation.

Key challenges:

- Almost all the literature evaluates the reliability of the MMC only by considering redundancy. Still, after each maintenance, a system composed of newly replaced

subparts and some parts operating for several years will change the reliability outputs. So, no analytical method exists to solve this problem; hence, a new method is required.
- Since the analytical model is not available in the literature, how can we be sure it is correct? Hence, another method should be developed to validate the results.
- The obtained concept should be generalized for different MMC characteristics to make a valuable study for various systems. But, this requires the choice of switch rating, costs, and other aspects, which is challenging.

Q4: How can reconfigurability be utilized to enhance fault tolerance and reliability in MMCs, particularly during open-circuit faults (OCFs), while maintaining operational efficiency and minimizing system downtime?

Chapter 6 addresses ensuring continuous operation in MMCs when component failures occur, specifically in IGBTs. The chapter investigates how reconfigurability, combined with fault detection and localization algorithms, can provide a cost-effective solution to bypass faulty components or reconfigure the system without needing additional hardware. By exploring the integration of fault tolerance into the control logic, this research aims to develop methodologies to detect and recover from faults while minimizing system disruptions and maintaining optimal performance.

Key challenges:

- Detecting which specific IGBT has failed in an open-circuit manner is challenging, particularly due to the identical characteristics of certain switch pairs.
- Ensuring continuous operation of the converter in the presence of an OCF is complex, especially when maintaining original functionality without hardware modifications.
- Setting up a lab-scale prototype to experimentally validate the purpose of this chapter is another real challenge.

1.4. RESEARCH CONTRIBUTIONS

The main contributions of this thesis focus on enhancing the reliability and cost-efficiency of MMCs through innovative approaches in reliability assessment, redundancy strategies, design optimization, and fault tolerance. The contributions of the thesis are as follows:

- A comparative analysis of reliability assessment methods (Military Handbook, FIDES, and Mission Profile) was conducted, highlighting each method's unique strengths (**Chapter 2**).

- Developed and implemented Monte Carlo simulations to evaluate different redundancy strategies where an analytical approach is not feasible, offering a comprehensive reliability assessment under real-world operating conditions (**Chapter 3**).

- Proposed a methodology for cost-efficient MMC design by balancing modularity

and redundancy, optimizing switch voltage ratings based on capital investment, operational costs, and reliability (**Chapter 4**).

- Introduced a Mixed Redundancy Strategy (MRS), combining active and spare redundant SMs to optimize reliability and cost, validated through sensitivity analyses and Monte Carlo simulations (**Chapter 5**).
- Developed a reconfigurability method to enhance fault tolerance, allowing continuous operation by bypassing faulty components, validated experimentally to ensure efficient fault detection, localization, and reconfiguration (**Chapter 6**).

1.5. THESIS OUTLINE

The thesis is structured to address the research questions and contributions outlined above systematically as shown in Fig. 1.6. The following chapters are included:

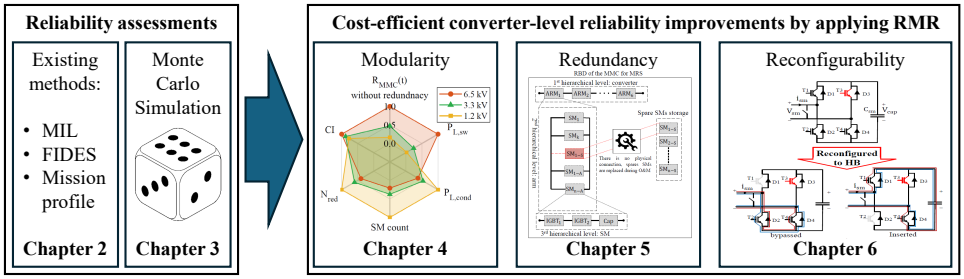

Figure 1.6: Outline of the thesis: definitions of the parts, the chapters, and their connections.

Chapter 2: Reliability Assessment Methods
Introduces and compares Military Handbook (MIL-HDBK-217), FIDES, and Mission Profile Methodology for reliability assessment of MMCs.
Chapter 3: Reliability Assessment for MMCs Using Monte Carlo Simulations
Explores various redundancy strategies and their evaluation through Monte Carlo simulations.
Chapter 4: Cost-Oriented Redundancy and Modularity-Based Design of MMC
Discusses the trade-offs between cost, modularity, and reliability, providing optimal design solutions.
Chapter 5: Mixed Redundancy Strategy for MMCs
Introduces a mixed redundancy strategy, combining active and spare redundant SMs to optimize system reliability and cost.
Chapter 6: Reconfigurability in MMC
Explores methods to integrate reconfigurability into MMCs to enhance their adaptability and reliability.

REFERENCES

[1] W. Liu and Y. Xu, *Reliability modeling of mmc-based flexible interconnection controller considering the uncertainty of current loading,* **25** (2019), 10.1007/s00542-018-4070-4.

[2] G. Konstantinou, J. Pou, S. Ceballos, and V. G. Agelidis, *Active redundant submodule configuration in modular multilevel converters,* IEEE Transactions on Power Delivery **28**, 2333 (2013).

[3] H. Li, X. Xie, A. S. McDonald, Z. Chai, T. Yang, Y. Wu, and W. Yang, *Cost and reliability optimization of modular multilevel converter with hybrid submodule for offshore dc wind turbine,* International Journal of Electrical Power & Energy Systems **120**, 105994 (2020).

[4] J. Contreras-Jiménez, F. Rivas-Dávalos, J. Song, and J. Guardado, *Multi-state system reliability analysis of hvdc transmission systems using matrix-based system reliability method,* International Journal of Electrical Power & Energy Systems **100**, 265 (2018).

[5] S. Peyghami, F. Blaabjerg, and P. Palensky, *Incorporating power electronic converters reliability into modern power system reliability analysis,* IEEE Journal of Emerging and Selected Topics in Power Electronics **9**, 1668 (2021).

[6] S. Peyghami, M. Fotuhi-Firuzabad, and F. Blaabjerg, *Reliability evaluation in microgrids with non-exponential failure rates of power units,* IEEE Systems Journal **14**, 2861 (2020).

[7] Y. Guo, H. Gao, and Q. Wu, *A combined reliability model of vsc-hvdc connected offshore wind farms considering wind speed correlation,* IEEE Transactions on Sustainable Energy **8**, 1637 (2017).

[8] S. Peyghami, P. Palensky, and F. Blaabjerg, *An overview on the reliability of modern power electronic based power systems,* IEEE Open Journal of Power Electronics **1**, 34 (2020).

[9] L. Guo, Y. Ding, M. Bao, C. Shao, P. Wang, and L. Goel, *Nodal reliability evaluation for a vsc-mtdc-based hybrid ac/dc power system,* IEEE Transactions on Power Systems **35**, 2300 (2020).

[10] G. Abeynayake, G. Li, T. Joseph, J. Liang, and W. Ming, *Reliability and cost-oriented analysis, comparison and selection of multi-level mvdc converters,* IEEE Transactions on Power Delivery , 1 (2021).

[11] S. Peyghami, P. Palensky, M. Fotuhi-Firuzabad, and F. Blaabjerg, *System-level design for reliability and maintenance scheduling in modern power electronic-based power systems,* IEEE Open Access Journal of Power and Energy **7**, 414 (2020).

[12] Y. Ye, J. Lutz, G. Zeng, R. Alvarez, and P. Correa, *Thermal calculation methodology for lifetime estimation of semiconductor devices in mmc application,* in *PCIM Europe 2017; International Exhibition and Conference for Power Electronics, Intelligent Motion, Renewable Energy and Energy Management* (2017) pp. 1–6.

[13] H. Wang and F. Blaabjerg, *Reliability of capacitors for dc-link applications in power electronic converters—an overview,* IEEE Transactions on Industry Applications **50**, 3569 (2014).

[14] P. Tu, S. Yang, and P. Wang, *Reliability- and cost-based redundancy design for modular multilevel converter,* IEEE Transactions on Industrial Electronics **66**, 2333 (2019).

[15] J. Guo, J. Liang, X. Zhang, P. D. Judge, X. Wang, and T. C. Green, *Reliability analysis of mmcs considering submodule designs with individual or series-operated igbts,* IEEE Transactions on Power Delivery **32**, 666 (2017).

[16] J. Guo, X. Wang, J. Liang, H. Pang, and J. Gonçalves, *Reliability modeling and evaluation of mmcs under different redundancy schemes,* IEEE Transactions on Power Delivery **33**, 2087 (2018).

[17] J. Xu, H. Jing, and C. Zhao, *Reliability modeling of mmcs considering correlations of the requisite and redundant submodules,* IEEE Transactions on Power Delivery **33**, 1213 (2018).

[18] J. V. M. Farias, A. F. Cupertino, V. d. N. Ferreira, H. A. Pereira, S. I. Seleme, and R. Teodorescu, *Reliability-oriented design of modular multilevel converters for medium-voltage statcom,* IEEE Transactions on Industrial Electronics **67**, 6206 (2020).

[19] M. Ahmadi, A. Bertinato, and I. Boussaad, *Reliability analysis of the bus-bar systems in multiterminal hvdc systems,* in *2021 23rd European Conference on Power Electronics and Applications (EPE'21 ECCE Europe)* (2021) pp. P.1–P.10.

[20] B. Tourgoutian, A. Yanushkevich, and R. Marshall, *Reliability and availability model of offshore and onshore vsc-hvdc transmission systems,* in *11th IET International Conference on AC and DC Power Transmission* (2015) pp. 1–8.

[21] J. Zhou, W. Li, J. Lu, and W. Yan, *Incorporating aging failure mode and multiple capacity state model of hvdc system in power system reliability assessment,* Electric Power Systems Research **77**, 910 (2007).

[22] B. Wang, X. Wang, X. Wang, C. Shao, and S. Liu, *Reliability evaluation of voltage-source converter-based multi-terminal direct current integrated offshore wind plants,* Iet Renewable Power Generation **10**, 761 (2016).

[23] S. Zadkhast, M. Fotuhi-Firuzabad, F. Aminifar, R. Billinton, S. O. Faried, and A.-A. Edris, *Reliability evaluation of an hvdc transmission system tapped by a vsc station,* IEEE Transactions on Power Delivery **25**, 1962 (2010).

[24] Y. Ding, L. Cheng, Y. Zhang, and Y. Xue, *Operational reliability evaluation of restructured power systems with wind power penetration utilizing reliability network equivalent and time-sequential simulation approaches,* Journal of Modern Power Systems and Clean Energy **2**, 329 (2014).

[25] A. Shekhar, T. B. Soeiro, Z. Qin, L. Ramírez-Elizondo, and P. Bauer, *Suitable submodule switch rating for medium voltage modular multilevel converter design,* in *2018 IEEE Energy Conversion Congress and Exposition (ECCE)* (2018) pp. 3980–3987.

[26] R. Alvarez, M. Wahle, H. Gambach, and J. Dorn, *Optimum semiconductor voltage level for mmc submodules in hvdc applications,* in *2016 18th European Conference on Power Electronics and Applications (EPE'16 ECCE Europe)* (2016) pp. 1–9.

[27] N.-T. Quach, S. H. Chae, J. H. Ahn, and E.-H. Kim, *Harmonic analysis of a modular multilevel converter using double fourier series,* Journal of Electrical Engineering and Technology **13**, 298 (2018).

[28] A. Shekhar, L. B. Larumbe, T. B. Soeiro, Y. Wu, and P. Bauer, *Number of levels, arm inductance and modulation trade-offs for high power medium voltage grid-connected modular multilevel converters,* in *2019 10th International Conference on Power Electronics and ECCE Asia (ICPE 2019 - ECCE Asia)* (2019) pp. 1–8.

[29] A. Bennani-Ben Abdelghani, H. Ben Abdelghani, F. Richardeau, J.-M. Blaquière, F. Mosser, and I. Slama-Belkhodja, *Versatile three-level fc-npc converter with high fault-tolerance capabilities: Switch fault detection and isolation and safe postfault operation,* IEEE Transactions on Industrial Electronics **64**, 6453 (2017).

[30] R. Selvaraj, K. Desingu, T. R. Chelliah, D. Khare, and C. Bharatiraja, *Fault tolerant operation of parallel-connected 3l-neutral-point clamped back-to-back converters serving to large hydro-generating units,* IEEE Transactions on Industry Applications **54**, 5429 (2018).

[31] S. Ceballos, J. Pou, I. Gabiola, J. L. Villate, J. Zaragoza, and D. Boroyevich, *Fault-tolerant multilevel converter topology,* in *2006 IEEE International Symposium on Industrial Electronics*, Vol. 2 (2006) pp. 1577–1582.

[32] S. Bhattacharya, C. Willich, P. Hoenicke, and J. Kallo, *A novel re-configurable llc converter for electric aircraft,* in *2021 IEEE 12th Energy Conversion Congress Exposition - Asia (ECCE-Asia)* (2021) pp. 32–37.

[33] J. L. Soon, D. D.-C. Lu, J. C.-H. Peng, and W. Xiao, *Reconfigurable nonisolated dc–dc converter with fault-tolerant capability,* IEEE Transactions on Power Electronics **35**, 8934 (2020).

[34] K. Hu, Z. Liu, Y. Yang, F. Iannuzzo, and F. Blaabjerg, *Ensuring a reliable operation of two-level igbt-based power converters: A review of monitoring and fault-tolerant approaches,* IEEE Access **8**, 89988 (2020).

[35] A. Cordeiro, J. Palma, J. Maia, and M. Resende, *Fault-tolerant design of a classical voltage-source inverter using z-source and standby redundancy,* in *11th International Conference on Electrical Power Quality and Utilisation* (2011) pp. 1–6.

[36] L. Ferreira Costa and M. Liserre, *Failure analysis of the dc-dc converter: A comprehensive survey of faults and solutions for improving reliability,* IEEE Power Electronics Magazine **5**, 42 (2018).

2

RELIABILITY ASSESSMENT METHODS

This chapter delves into the reliability assessment methods of MMCs, an essential component in modern power electronic systems. The primary objective is to compare and contrast three methodologies used for calculating reliability: the Military Handbook (MIL-HDBK-217), FIDES (French acronym for "Reliability in Electronic Systems"), and the Mission Profile Methodology. Each method brings a unique perspective and set of tools to reliability assessment, considering different factors such as environmental conditions, operational stresses, and specific application requirements. This analysis aims to comprehensively understand how these methodologies can be applied to evaluate reliability in various operational contexts.

This chapter is based on:

- M. Ahmadi, F. Kardan, A. Shekhar, P. Bauer, "Reliability Assessment of Modular Multilevel Converters: A Comparative Study of MIL and Mission Profile Methods," in 13th International Conference on Integrated Power Electronics Systems (CIPS), 2024.
- M. Ahmadi, A. Shekhar, P. Bauer, "Comparison of Military Handbook and the FIDES Methodology for Failure Rate Estimation of Modular Multilevel Converters," in IEEE 17th International Conference on Compatibility, Power Electronics and Power Engineering (CPE-POWERENG), 2023.
- M. Ahmadi, A. Shekhar and P. Bauer, "Impact of the Various Components Consideration on Choosing Optimal Redundancy Strategy in MMC," in IEEE 20th International Power Electronics and Motion Control Conference (PEMC), 2022.

2.1. INTRODUCTION

In this chapter, three distinct methodologies for calculating the reliability of MMCs are introduced and analyzed in detail. These methodologies are:

2

Military Handbook (MIL-HDBK-217):
The Military Handbook method provides a standardized approach to reliability prediction, primarily used in military and aerospace applications. It considers the base failure rates of components and adjusts them using various factors that account for environmental conditions, quality levels, and specific stress factors. For instance, the failure rate of film capacitors and Insulated Gate Bipolar Transistors (IGBTs) is adjusted based on temperature, voltage, series resistance, and other operational parameters [1–5].

FIDES Methodology:
The FIDES methodology offers a more comprehensive approach by incorporating mission-specific conditions and technical controls over manufacturing, field operation, and maintenance processes. It calculates the failure rates of electronic components by considering physical failures and specific environmental and operational stresses during different mission phases. This method is recognized for providing a more accurate and current estimation of failure rates, reflecting real-world conditions more closely than traditional methods [6–10].

Mission Profile Methodology:
This methodology uses detailed modeling of the MMC's operational environment and mission-specific conditions. It includes thermal modeling to estimate the power losses and junction temperatures of components like IGBTs and capacitors. By using the rainflow algorithm and fitting the Weibull distribution, this method captures the stochastic nature of the system, providing reliability estimates based on the actual thermal cycles and stresses experienced during operation. The Mission Profile Methodology is particularly practical in applications with detailed operational data [11–19].

2.2. MILITARY HANDBOOK

The probability of IGBTs and capacitors experiencing failure depends on the temperature and voltage they are subjected to. Hence, any formula used to calculate their failure rate must consider these factors [20]. This holds true, especially for capacitors, as their likelihood of failure can be notably impacted by these conditions:

$$\lambda_{\text{MIL-Cap}} = \lambda_{\text{base-Cap}} \pi_{\text{T}} \pi_{\text{V}} \pi_{\text{SR}} \pi_{\text{Q}} \pi_{\text{E}} \pi_{\text{C}} \tag{2.1}$$

In (2.1), film capacitors' base failure rate is 0.000876 occurrences per year. The impact of the capacitor's series resistance is accounted for through the incorporation of the π_{SR} factor, which has a value of 0.1. The quality of the capacitor is represented by the factor π_Q, which assumes a value of 10 for commercially available capacitors. The environmental factor π_{E}, which is equal to 1 in controlled environments, is another factor that influences the capacitor's failure rate. The capacitance factor π_C is determined by equation (2.2), while the voltage stress factor π_V can be obtained by applying equation (2.3).

The temperature factor π_T is calculated using equation (2.4). All these factors with details on how to choose are provided in [20]. It is one of the shortcomings of the MIL method that these coefficients can change the calculated failure rate greatly.

$$\pi_C = (C)^{0.09} \tag{2.2}$$

$$\pi_V = [\frac{V_{\text{operating}}}{0.6 \times V_{\text{rated}}}]^5 + 1 \tag{2.3}$$

$$\pi_T = exp[\frac{-0.15}{8.617 \times 10^{-5}}[\frac{1}{T_{vj}+273} - \frac{1}{298}]] \tag{2.4}$$

In which T_{vj} is the temperature of the capacitor, and C in (2.2) is in μF. The failure rate of the IGBT is given by:

$$\lambda_{\text{MIL-IGBT}} = \lambda_{\text{base-IGBT}}\pi_{\text{T}}\pi_{\text{S}}\pi_{\text{A}}\pi_{\text{R}}\pi_{\text{E}} \tag{2.5}$$

$$\pi_{\text{T}} = exp[-2114 \times [\frac{1}{T_{\text{j}}+273} - \frac{1}{298}]] \tag{2.6}$$

$$\pi_{\text{S}} = 0.045 \times exp[3.1\frac{V_{\text{applied}}}{V_{\text{rated}}}] \tag{2.7}$$

Equation (2.5) provides the base failure rate of IGBTs, which is determined to be 0.000876 occurrences per year. The temperature factor π_T required to calculate the failure rate of IGBTs can be obtained by utilizing equation (2.6) [20]. Similar to capacitors, the voltage stress factor π_S is a variable factor that plays a crucial role in determining the actual failure rate of IGBTs and is expressed by equation (2.7) [20]. IGBTs are utilized for various applications, with the factor π_A serving to represent the specific application. When used for switching applications, π_A is assigned a value of 0.7. The power rating of the IGBT is represented by the factor π_R, which is equal to 1 [20]. The surrounding environment factor π_E is another parameter that can impact the failure rate of IGBTs, with a value of 6 assigned to it for controlled environments [20].

2.3. MISSION PROFILE METHODOLOGY

Fig. 2.1 illustrates the half-bridge (HB) submodule (SM) integrated MMC layout. It comprises six arms in which n SMs are connected in series. Within the structure of SM, there are several components, including two power electronics switch valves, a capacitor bank, gate drives, a thyristor, and a control system [14, 17].

2.3.1. MMC MODEL

In an ideal MMC, the DC side current (I_{dc}) is evenly distributed in the three phases of the MMC. By assuming the harmonic components on the AC side are compensated, the AC side currents i_{x} (x = a, b, c) and voltage v_{x} (x = a, b, c) taking the phase a as an example, can be as follows.

$$v_{\text{a}} = V_{\text{m}} sin(\omega t) \tag{2.8}$$

$$i_{\text{a}} = I_{\text{m}} sin(\omega t - \Phi) \tag{2.9}$$

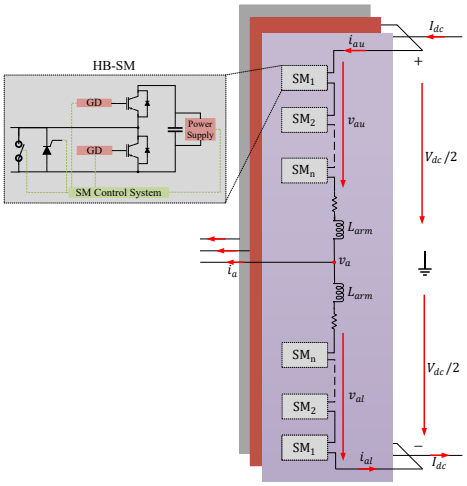

Figure 2.1: MMC layout with HB SM.

$$\omega = 2\pi f \tag{2.10}$$

where V_{m} and I_{m} are the amplitude of voltage and current, ω is the angular frequency, f is the fundamental frequency, and Φ is the power factor (PF) of the system. the upper and lower arm current can be obtained as follows.

$$i_{\mathrm{au}} = \frac{I_{\mathrm{dc}}}{3} + \frac{i_{\mathrm{a}}}{2} \tag{2.11}$$

$$i_{\mathrm{al}} = \frac{I_{\mathrm{dc}}}{3} - \frac{i_{\mathrm{a}}}{2} \tag{2.12}$$

consequently the upper and lower arm voltages ($v_{\mathrm{au}}, v_{\mathrm{al}}$) are caused by AC and DC currents. Also, according to the power balance, the AC and DC side power should be equal. Hence, power equality can ideally be written as follows:

$$P_{\mathrm{AC}} = P_{\mathrm{DC}} \rightarrow \frac{3}{2} V_{\mathrm{m}} I_{\mathrm{m}} cos\Phi = V_{\mathrm{dc}} I_{\mathrm{dc}} \tag{2.13}$$

$$m = \frac{V_{\mathrm{m}}}{V_{\mathrm{dc}}/2} \tag{2.14}$$

where m is the modulation index to link the magnitude of AC and DC side voltages, P_{AC} is the output power, and P_{DC} is the input power. By substituting the (2.14) in (2.13), I_{dc} can be written as (2.15).

$$I_{\mathrm{dc}} = \frac{3 m I_{\mathrm{m}} cos\Phi}{4} \tag{2.15}$$

Now, the voltage and current of each arm (upper, lower) can be obtained as follows.

$$\begin{cases} v_{\mathrm{au}} = \frac{V_{\mathrm{dc}}}{2}(1 - msin(\omega t)) \\ v_{\mathrm{al}} = \frac{V_{\mathrm{dc}}}{2}(1 + msin(\omega t)) \end{cases} \tag{2.16}$$

$$\begin{cases} i_{\text{au}} = \frac{I_{\text{dc}}}{3} + \frac{I_{\text{m}}}{2} sin(\omega t - \Phi) \\ i_{\text{al}} = \frac{I_{\text{dc}}}{3} - \frac{I_{\text{m}}}{2} sin(\omega t - \Phi) \end{cases} \tag{2.17}$$

in the MMC, the voltage of the upper and lower arms can be written as (2.18).

$$\begin{cases} v_{\text{au}} = n_{\text{au}} V_{\text{dc}} \\ v_{\text{al}} = n_{\text{al}} V_{\text{dc}} \end{cases} \tag{2.18}$$

where n_{au} is the duty ratio of the upper arm and n_{al} is the duty ratio of the lower arm. In MMC, the DC link voltage should always remain equal to V_{dc}, so, by substituting the (2.16) in (2.18), the duty ratio can be rewritten as follows.

$$\begin{cases} n_{\text{au}} = \frac{1}{2}(1 - msin(\omega t)) \\ n_{\text{al}} = \frac{1}{2}(1 + msin(\omega t)) \end{cases} \tag{2.19}$$

2.3.2. THERMAL MODELLING

POWER LOSSES MODEL

The current that passes through each element should be calculated individually to estimate the thermal stresses of SM's components (IGBT, diode, and capacitor). In Fig. 2.1, taking the upper arm of phase a as an example, the estimated current is shown in Fig. 2.2 working in inverter mode; hence, the current is positive for a period of $(\theta, \pi + 2\phi - \theta)$ and negative in the period of $(\pi + 2\phi - \theta, 2\pi + \theta)$.

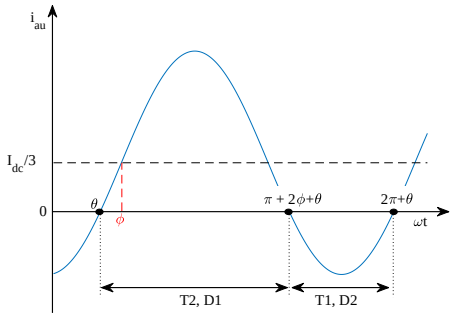

Figure 2.2: Illustration of arm current of phase a.

In Fig. 2.3, the effective working range of each component is presented. If the current is positive, T_2 or D_1 are working, while T_1 or D_2 are operational if the current is negative. Hence, the average current (i_{ave}) and RMS current (i_{RMS}) of each semiconductor is given as (2.20) where the equation variables are specified for each switch in Table 2.1.

$$\begin{cases} i_{\text{ave,x1}} = \frac{1}{2\pi} \int_{\text{a}}^{\text{b}} Y_1 \, d(\omega t) \\ i_{\text{RMS,x1}} = \sqrt{\frac{1}{2\pi} \int_{\text{a}}^{\text{b}} Y_2 \, d(\omega t)} \end{cases} \tag{2.20}$$

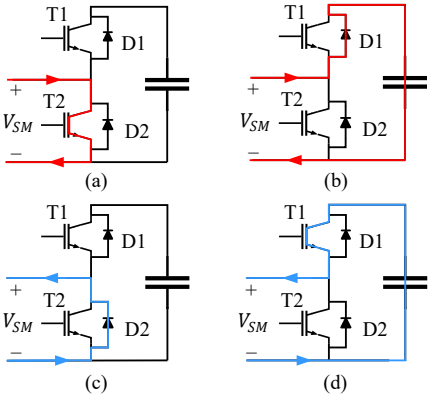

Figure 2.3: Current flow is inserted/bypassed SMs for different arm current directions, (a) positive current & SM is bypassed, (b) positive current & SM is inserted, (c) negative current & SM in bypassed, (d) negative current & SM is inserted.

Table 2.1: SPECIFICATIONS OF (2.20) FOR DIFFERENT POWER SWITCHES

x1	a	b	Y_1	Y_2
T_1	$\pi+2\phi-\theta$	$2\pi+\theta$	$n_{\text{au}}i_{\text{au}}$	$n_{\text{au}}i_{\text{au}}^2$
T_2	θ	$\pi+2\phi-\theta$	$n_{\text{al}}i_{\text{au}}$	$n_{\text{al}}i_{\text{au}}^2$
D_1	θ	$\pi+2\phi-\theta$	$n_{\text{au}}i_{\text{au}}$	$n_{\text{au}}i_{\text{au}}^2$
D_2	$\pi+2\phi-\theta$	$2\pi+\theta$	$n_{\text{al}}i_{\text{au}}$	$n_{\text{al}}i_{\text{au}}^2$

Regarding the capacitor bank, the ripple current can be obtained by (2.21).

$$\begin{aligned} i_{\text{cap}} = n_{\text{au}}i_{\text{au}} = &\frac{1}{6}(I_{\text{dc}} - \frac{3}{4}mI_{\text{m}}cos\Phi) + \frac{1}{4}I_{\text{m}}sin(\omega t - \Phi) \\ &- \frac{1}{6}mI_{\text{dc}}sin(\omega t) + \frac{1}{8}mI_{\text{m}}sin(2\omega t - \Phi) \end{aligned} \tag{2.21}$$

since the capacitor current's DC component cannot pass through, the capacitor's first term in (2.21) is equal to zero. But, the RMS current of the capacitor can be evaluated as (2.22), which is composed of 50 Hz (second and third terms of (2.21)) and 100 Hz (fourth term of (2.21)) frequency components.

$$\begin{cases} i_{\text{RMS,cap-50Hz}} = \sqrt{\frac{1}{2\pi}\int_0^{2\pi} i_{\text{cap-50Hz}}d(\omega t)} \\ i_{\text{RMS,cap-100Hz}} = \sqrt{\frac{1}{2\pi}\int_0^{2\pi} i_{\text{cap-100Hz}}d(\omega t)}. \end{cases} \tag{2.22}$$

The power losses can be estimated after calculating RMS and the average current passing through each component. The significant sources of power switch losses are conduction loss of IGBT ($P_{\text{cond,T}}$), switching loss of IGBT ($P_{\text{sw,T}}$), conduction loss of the diode ($P_{\text{cond,D}}$), and reverse recovery loss of the diode ($P_{\text{rec,D}}$). The conduction losses

of IGBT (diode) are due to the voltage drop of V_{CE} (V_D), and it depends on the on-state current (I) and junction temperature (T_j) given by 2.23.

$$\begin{cases} V_{CE} = V_T(T_j) + R_{CE}(T_j)I & \text{,IGBT} \\ V_D = V_D(T_j) + R_D(T_j)I & \text{,diode} \end{cases} \tag{2.23}$$

where V_{CE}, V_D, R_{CE}, and R_D are fitting parameters obtained from data-sheet given in Table 2.3. Therefore, The power losses of IGBT (diode) due to conduction losses can be written as (2.24).

$$\begin{cases} P_{cond,T}(T_j) = \frac{1}{T}\int_0^T V_{CE}(T_j)I\,dt \\ = V_T(T_j)|i_{ave.T}| + R_{CE}(T_j)i^2_{RMS.T} \\ P_{cond,D}(T_j) = \frac{1}{T}\int_0^T V_D(T_j)I\,dt \\ = V_D(T_j)|i_{ave.D}| + R_D(T_j)i^2_{RMS.D}. \end{cases} \tag{2.24}$$

As mentioned, the energy losses of IGBT's turn-on ($E_{sw,T}$) and the energy losses of reverse recovery of the diode ($E_{rec,D}$) are the other two major sources of losses calculated as (2.25).

$$\begin{cases} E_{sw,T}(T_j) = a_T + b_T|i_{ave,T}| + c_T {i_{RMS,T}}^2 \\ E_{rec,D}(T_j) = a_D + b_D|i_{ave,D}| + c_D {i_{RMS,D}}^2 \end{cases} \tag{2.25}$$

where a_T, a_D, b_T, b_D, c_T, and c_D (in Table 2.3) are dynamic characteristics of the power switches obtained from data-sheet by curve fitting. Moreover, the effect of the applied voltage is considered for calculating the power losses of IGBT and diode due to switch losses and reverse recovery, respectively.

$$\begin{cases} P_{sw,T}(T_j) = f_{sw}E_{sw,T}(T_j)\frac{V_{SM,ave}}{V_{nom}} \\ P_{rec,D}(T_j) = f_{sw}E_{rec,D}(T_j)\frac{V_{SM,ave}}{V_{nom}} \end{cases} \tag{2.26}$$

where V_{nom} is the nominal voltage at the test condition. The total power losses of the IGBT and diode can be obtained by summing the above losses as (2.27).

$$\begin{cases} P_T = P_{cond,T}(T_j) + P_{sw,T}(T_j) \\ P_D = P_{cond,D}(T_j) + P_{rec,D}(T_j). \end{cases} \tag{2.27}$$

For capacitor losses calculation, the equivalent series resistor (ESR) is the source of losses. Hence, the total losses of the SM's capacitor can be calculated by (2.28).

$$P_C = R_{ESR}(50\text{Hz})i^2_{RMS,cap\text{-}50Hz} + R_{ESR}(100\text{Hz})i^2_{RMS,cap\text{-}100Hz} \tag{2.28}$$

where the value of R_{ESR} is given in the data-sheet. Note that the exact value of R_{ESR} is different at different frequencies. However, this is given in some capacitor data sheets; in others, it is not. Hence, if it is not given, we can assume that $R_{ESR}(50\text{Hz})$ is equal to $R_{ESR}(100\text{Hz})$.

ELECTRIC-THERMAL MODEL

A. IGBTs

The power electronic components have switching and conduction losses, as was elaborated prior in this section. By using the information given in the IGBT's datasheet and thermal equivalent network of the IGBT shown in Fig. 2.4, the average junction temperature of the IGBT and diode can be estimated as given in (2.29).

$$\begin{cases} T_{\mathrm{j,T}} = P_{\mathrm{T}}(\sum_{i=1}^{4} R_{\mathrm{T,j\text{-}ci}} + R_{\mathrm{T,c\text{-}h}}) + T_{\mathrm{h}} \\ T_{\mathrm{j,D}} = P_{\mathrm{D}}(\sum_{i=1}^{4} R_{\mathrm{D,j\text{-}ci}} + R_{\mathrm{D,c\text{-}h}}) + T_{\mathrm{h}} \\ T_{\mathrm{h}} = (P_{\mathrm{T}} + P_{\mathrm{D}})R_{\mathrm{h\text{-}a}} + T_{\mathrm{a}}. \end{cases} \tag{2.29}$$

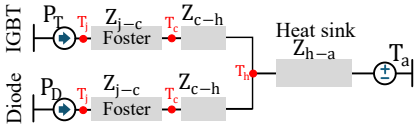

Figure 2.4: Thermal equivalent network of the IGBT module, Zj-c and Zc–h represent junction-to-case and case-to-heatsink thermal impedances, respectively, typically modeled using a Foster network to capture transient thermal behavior.

B. Capacitors

For capacitors, the equivalent series resistance R_{ES} represents the total losses in the capacitor. According to the capacitor thermal network (Fig. 2.5), the temperature of the capacitor (T_{Cap}) can be estimated as follows.

$$T_{\mathrm{Cap}} = P_{\mathrm{C}}(R_{\mathrm{hc}} + R_{\mathrm{ca}}) + T_{\mathrm{a}} \tag{2.30}$$

where, for example, $R_{\mathrm{h\text{-}c}}$ = 0.10 and $R_{\mathrm{c\text{-}a}}$ = 0.08 are thermal resistance read from the datasheet of AVX capacitors model DKTFM1#B3367.

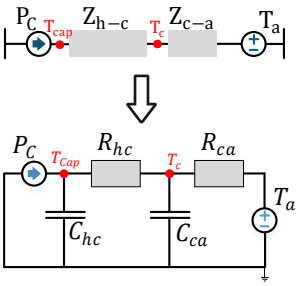

Figure 2.5: Thermal equivalent network of the capacitor.

As it can be understood, the mission profile-based reliability process has many coefficients and constant values. The data given in the datasheet of FF450R33T3E3 from

Infineon is used to guide the reader on how these values are calculated. Nevertheless, the general method given in [21] can also be followed to estimate these constants and coefficients. In Table 2.2, all the information regarding the values used for the thermal model is provided, and the details on how to read this data are shown. From Fig. 2.6, the thermal characteristics of the diode and IGBT module are given that could be used for reliability analysis in the mission profile method.

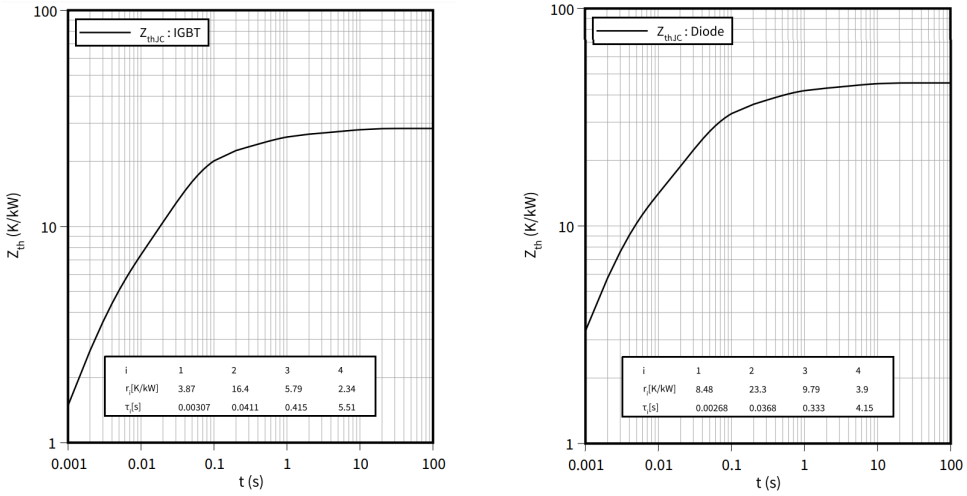

Figure 2.6: The thermal characteristics of the switch given in the datasheet of IGBT model: FF450R33T3E3 for its (a) IGBT and (b) body diode.

Table 2.2: SEMICONDUCTOR THERMAL PARAMETERS OF THE SWITCH GIVEN IN THE DATASHEET OF IGBT MODEL: FF450R33T3E3

	i	**1**	**2**	**3**	**4**
Diode	r_i (K/kW)	8.48	23.3	9.79	3.9
	$\tau_i(s)$	0.0026	0.0368	0.333	4.15
IGBT	r_i (K/kW)	3.87	16.4	5.79	2.34
	$\tau_i(s)$	0.003	0.0411	0.415	5.51

To perceive the dynamics model of the IGBT and its body diode, it is required to calculate the V_{CE}, V_D, R_{CE}, and R_D that are all fitting parameters obtained from data-sheet. Fig. 2.7 is given to guide the reader on how these parameters are calculated from the datasheet of the switch. Note that the same strategy can be applied to the body diode of the switch as well, where the characteristics are provided in the datasheet. For instance, to calculate the dynamic characteristics from the datasheet of the given switch model FF450R33T3E3, the values are obtained by curve-fitting (red dashed-line in Fig. 2.7 (a) for V_{CE}, R_{CE} and red solid-line in Fig. 2.7 (b) for a_T, b_T, c_T) where in this case the values are provided in Table 2.3 for only the IGBT. An identical method can be used for the

diode.

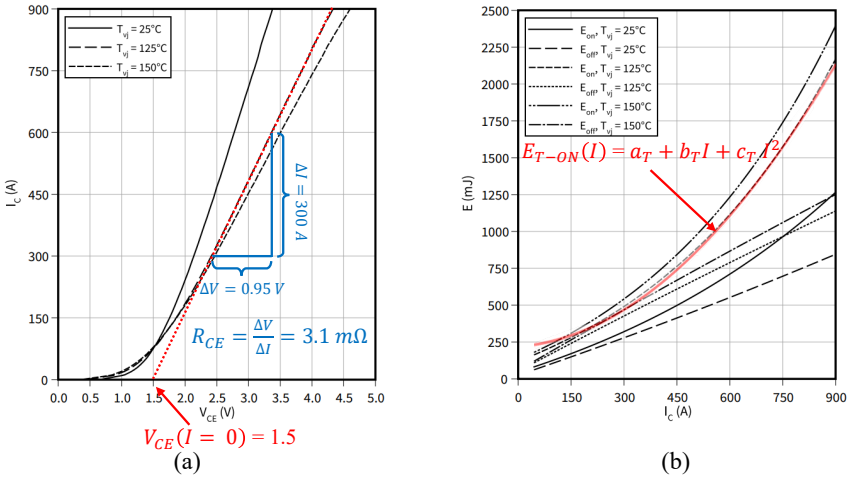

Figure 2.7: The dynamic characteristics of the switch given in datasheet of model: FF450R33T3E3 for the IGBT wherein (a) the V_{CE} and R_{CE} are estimated and in (b) the curve fitting for required energy (a_T, b_T, c_T) to turn ON the IGBT at 125^oC is shown and the values are given in Table 2.3.

Table 2.3: OBTAINED DYNAMIC CHARACTERISTICS SHOWN IN FIG. 2.7 FROM THE DATASHEET OF THE SWITCH MODEL: FF450R33T3E3

	$a_{T/D}$	$b_{T/D}$	$c_{T/D}$	$V_{CE/D}$ (V)	$R_{CE/D}$ (Ω)
IGBT	0.175	$0.372e^{-3}$	$2.005e^{-6}$	1.5	$3.1e^{-3}$
Diode	0.182	$0.978e^{-3}$	$-6.131e^{-7}$	1.5	$3.8e^{-3}$

T and CE are for IGBT, D is for diode

In mission profile methodology, different lifetime models can be applied to estimate the failure rate of the IGBT and capacitor, such as the Coffin-Manson and Bayerer models [22, 23]. Each model considers various factors that influence the lifetime of the components. For example, the Coffin-Manson model focuses on the effects of temperature variation and is utilized particularly when the primary failure mechanism in power devices is bond wire fatigue. On the other hand, the Bayerer lifetime model considers additional influential factors on device lifetime, like heating duration. This model is more appropriate when Direct Bonded Copper (DBC) solder fatigue and bond wire fatigue are the main causes of failure. The quantitative comparison of these lifetime models is examined in [24]. In this chapter, the Bayerer method is employed to estimate the end of life of the IGBT module. This method considers factors such as junction temperature (T_j), thermal cycle (ΔT_j), on-time (t_{on}), current per bond wire (I_b), voltage class, and the diameter of the bonding wire (D) all specified in [17]. To estimate the thermal cycle to failure (N_f), equation (2.31) is utilized.

$$N_{\mathrm{f}} = A\Delta T_j^{\beta_1} e^{\left(\frac{\beta_2}{T_{\mathrm{jmin}}+273}\right)} t_{\mathrm{on}}^{\beta_3} I_{\mathrm{b}}^{\beta_4} V^{\beta_5} D^{\beta_6} \tag{2.31}$$

where the values of constants A, $\beta_1 - \beta_6$, are listed in Table 2.4.

Table 2.4: PARAMETERS FOR BAYERER LIFETIME MODEL

A	β_1	β_2	β_3	β_4	β_5	β_6
9.3e14	-4.416	1285	-0.463	-0.716	-0.761	-0.5

For estimating the lifetime of the capacitor, the 10-kelvin rule obtained from Arrhenius law is applied, which is widely used as follows:

$$L = L_0 \left(\frac{V}{V_0}\right)^{-n} 2^{\frac{T_0 - T_{\mathrm{Cap}}}{10}} \tag{2.32}$$

where L_0 is the lifetime under test condition, n is between 7-9, V_0 is the rated voltage for the capacitor. In IGBTs, the thermal cycle causes damage, and the damage to the capacitor bank is estimated by summation of the consumed lifetime. Hence, the damage and lifetime are estimated in (2.33) [25].

$$\begin{cases} D = \sum_{i=1}^{N_{\mathrm{t}}} \frac{N_{\mathrm{i}}}{N_{\mathrm{f,i}}} & \text{for IGBT and diode} \\ D_{\mathrm{Cap}} = \sum_{i=1}^{N_{\mathrm{s}}} \frac{\Delta t}{L(T_{\mathrm{Cap}})} & \text{for capacitor} \end{cases} \tag{2.33}$$

The counts N_{t} and N_{s} are obtained using the rainflow algorithm, which is used to analyze the cyclic loading of the system. Considering the physical performance and concepts discussed earlier, the relationship between lifetime and degradation is transformed into reliability by fitting the Weibull Distribution to estimate the reliability of the MMC [26]. To accomplish this, Monte Carlo Simulation (MCS) is employed [27], as it allows for considering parameter deviation, such as the Bayerer coefficients. MCS is necessary to capture the stochastic nature of the system and obtain reliable estimates of the MMC's reliability.

$$\begin{cases} f(t) = \frac{\beta}{\eta}(\frac{t}{\eta})^{\beta-1} e^{-(\frac{t}{\eta})^{\beta}} \\ R_{\mathrm{MP}}(t) = 1 - \int_0^t f(t)\,dt = e^{-(\frac{t}{\eta})^{\beta}} \end{cases} \tag{2.34}$$

The failure probability density function, denoted as f(t), describes the probability of failure over time. The reliability of the SM denoted as $R_{\text{SM-MP}}(t)$, as well as the shape factor (β) and the scale factor (η), is obtained from MCS results. The SM's failure rate is determined by its components, which include two IGBTs, two diodes, and a capacitor bank. The successful operation of the SM requires that all these components remain healthy, as expressed by equation (2.35).

$$R_{\text{SM-MP}}(t) = \prod R_{\text{k-MP}}(t), \mathrm{k} = T_1, T_2, D_1, D_2, \mathrm{Cap} \tag{2.35}$$

2.4. FIDES

The FIDES method is a widely recognized standard for the calculation of the reliability of electronic components. This method considers a range of factors that can affect the reliability of electronic components, such as the conditions of manufacturing, the environment in which the component will be used, and the expected lifetime of the component [28]. By considering these factors, the FIDES method provides a more accurate and up-to-date estimation of the failure rate of electronic components than previous methods like the MIL standard [28]. In FIDES, unlike λ_{MIL}, λ_{FIDES} considers loading profile (similar to the mission profile method), the technical control over manufacturing (Π_{pm}), field operation and maintenance (Π_{process}) and physical failure ($\lambda_{\text{physical}}$) that is given by (2.36) and (2.37).

$$\lambda_{\text{FIDES-x}} = \lambda_{\text{physical}} \times \Pi_{\text{pm}} \times \Pi_{\text{process}} \rightarrow \text{x} \in (\text{IGBT}, \text{Cap}) \tag{2.36}$$

$$\lambda_{\text{physical}} = \sum_{i}^{\text{phases}} \left[\frac{t_{\text{annual}}}{8760} \right] \Pi_i \lambda_i \tag{2.37}$$

where t_{annual} represents the length of time for the i^{th} phase of the mission profile over one year. The factors Π_i (2.38) and λ_i (2.39) are associated with specific environmental and operational stresses for each phase i [6, 28]. These factors are considered when calculating the overall failure rate of electronic components. The values of Π_i and λ_i are determined by considering the conditions and stresses the electronic component will be subjected to during each phase of the mission profile. By incorporating these factors, the calculated failure rate is more accurate and representative of the actual performance of the electronic component under real-world conditions [28].

$$\Pi_{\text{i}} = (\Pi_{\text{Placement}} \Pi_{\text{App}} \Pi_{\text{Rugg}})^{0.511 ln(C_{\text{Sensitivity}})} \tag{2.38}$$

The Π factor is user-defined and application-specific, based on each mission phase's environmental and operational stresses. The second term, λ_i, includes k physical contributions for each component, as defined in equation (2.39). This considers factors such as manufacturing quality, thermal, and vibration stress to predict the overall failure rate more accurately.

$$\lambda_{\text{i}} = \sum_{k} \lambda_{0\text{k}} \Pi_{\text{acceleration (k)}} \tag{2.39}$$

the acceleration factors quantify how much physical limitations affect the component during active or inactive stages. These limitations can be caused by factors such as heat (including temperature stress), case and solder joints, humidity, and mechanical stress, and impact the failure rate λ_{i} [28]. The acceleration factor for semiconductors and capacitors can be expressed using equations (2.40) and (2.42), respectively.

$$\lambda_{\text{i-IGBT}} = \begin{pmatrix} \lambda_{0\text{TH}} \Pi_{\text{Thermal}} \\ +\lambda_{0\text{TCyCase}} \Pi_{\text{TCyCase}} \\ +\lambda_{0\text{TCySolderjoints}} \Pi_{\text{TCySolderjoints}} \\ +\lambda_{0\text{RH}} \Pi_{\text{TRH}} \\ +\lambda_{0\text{Mech}} \Pi_{\text{TMech}} \end{pmatrix}_i \tag{2.40}$$

where

$$\begin{cases} \Pi_{\text{Thermal}} = e^{11604\times 0.7\times\left[\frac{1}{293}-\frac{1}{T_{\text{mean}}+273}\right]} \\ \Pi_{\text{TCyCase}} = \left(\frac{12\times N_{\text{annual,cy}}}{t_{\text{annual}}}\right)\times\left(\frac{\Delta T_{\text{cycling}}}{20}\right)^{4} \\ \times e^{1414\times\left[\frac{1}{313}-\frac{1}{T_{\text{max,cyclying}}+273}\right]} \\ \Pi_{\text{TCySolderjoints}} = \left(\frac{12\times N_{\text{annual,cy}}}{t_{\text{annual}}}\right)\times\left(\frac{min(\Theta_{\text{cy}},2)}{2}\right)^{\frac{1}{3}} \\ \times\left(\frac{\Delta T_{\text{cycling}}}{20}\right)^{1.9}\times e^{1414\times\left[\frac{1}{313}-\frac{1}{T_{\text{max,cyclying}}+273}\right]} \\ \Pi_{\text{TRH}} = \left(\frac{RH_{\text{ambient}}}{70}\right)^{4.4}\times e^{11604\times 0.9\times\left[\frac{1}{293}-\frac{1}{T_{\text{a}}+273}\right]} \\ \Pi_{\text{TMech}} = \left(\frac{G_{\text{RMS}}}{0.5}\right)^{1.5} \end{cases} \tag{2.41}$$

in [28], the details of these parameters are specified.

$$\lambda_{\text{i-Cap}} = \lambda_{0\text{Cap}}\begin{pmatrix}\Pi_{\text{Thermo-electrical}}\\ +\Pi_{\text{TCy}}\\ +\Pi_{\text{Mechanical}}\end{pmatrix}_{i} \tag{2.42}$$

where

$$\begin{cases} \Pi_{\text{Thermo-electrical}} = \gamma_{\text{TH-EL}}\times\left(\frac{1}{S_{\text{reference}}}-\frac{V_{\text{applied}}}{V_{\text{rated}}}\right)^{3} \\ \times e^{11604\times E_{\text{a}}\times\left[\frac{1}{293}-\frac{1}{T_{\text{mean}}+273}\right]} \\ \Pi_{\text{TCy}} = \gamma_{\text{Tcy}}\times\left(\frac{12\times N_{\text{annual,cy}}}{t_{\text{annual}}}\right)\times\left(\frac{min(\Theta_{\text{cy}},2)}{2}\right)^{\frac{1}{3}} \\ \times\left(\frac{\Delta T_{\text{cycling}}}{20}\right)^{1.9}\times e^{1414\times\left[\frac{1}{313}-\frac{1}{T_{\text{max,cyclying}}+273}\right]} \\ \Pi_{\text{Mechanical}} = \gamma_{\text{Mech}}\times\left(\frac{G_{\text{RMS}}}{0.5}\right)^{1.5} \end{cases} \tag{2.43}$$

where the base failure rate $\lambda_{0\text{x}}$ and corresponding acceleration factors Π_x are specified in [28]. For calculating the reliability of the MMC using the FIDES methodology, the flowchart shown in Fig. 2.8 is applied. It starts with reading the power mission of the MMC and estimating the power losses of IGBT (switching losses, conduction losses) and losses of the capacitor. Afterward, by applying equations (2.29) and (2.30), the IGBT's junction temperature and the capacitor's core temperature can be estimated. By using the rain-flow algorithm which its description is given in section 2.5, the values of thermal cycle amplitude ($\Delta T_{\text{cycling}}$), cycle mean temperature (T_{mean}), cycle duration (Θ_{cy}), and maximum cycle temperature ($T_{\text{max,cycling}}$) are extracted. Therefore, these values are substituted in (2.41) and (2.42) to estimate the failure rate of IGBT and capacitors. By accumulating the failure rates, the total failure rate of the components can be estimated. The details on choosing the coefficients are all provided in [28] and are not repeated. Nevertheless, in the FIDES method, the selection of the constant and coefficients can greatly affect the outputs, similar to the MIL method.

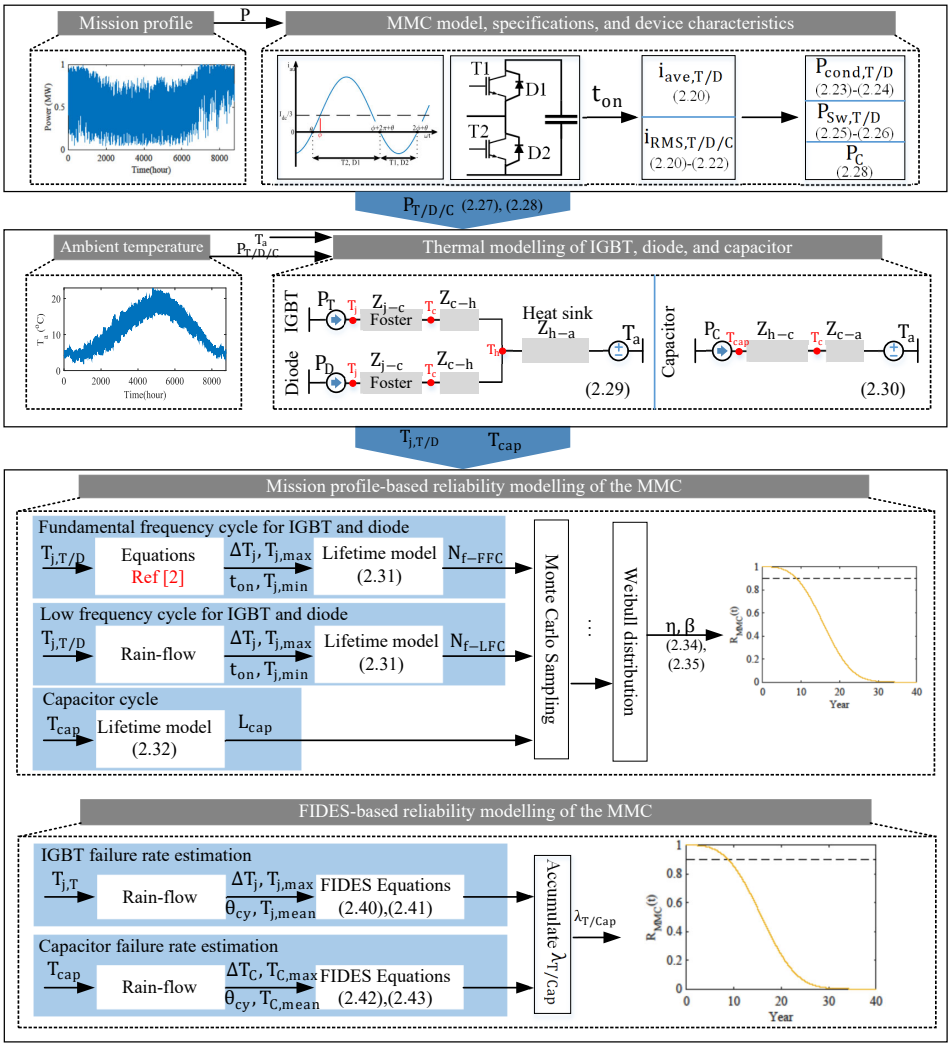

Figure 2.8: FIDES-based and Mission profile-based flowcharts for the reliability-oriented design of power devices.

2.5. CASE STUDY AND COMPARATIVE RESULTS

To compare the reliability of the MMC using these three distinctive methods, this chapter considers an MMC with characteristics given in Table 3.1. Also, the impact of redundancy is shown numerically to showcase its impacts. However, the details of applied redundancy and the considered MMC will be all given in the subsequent chapters.

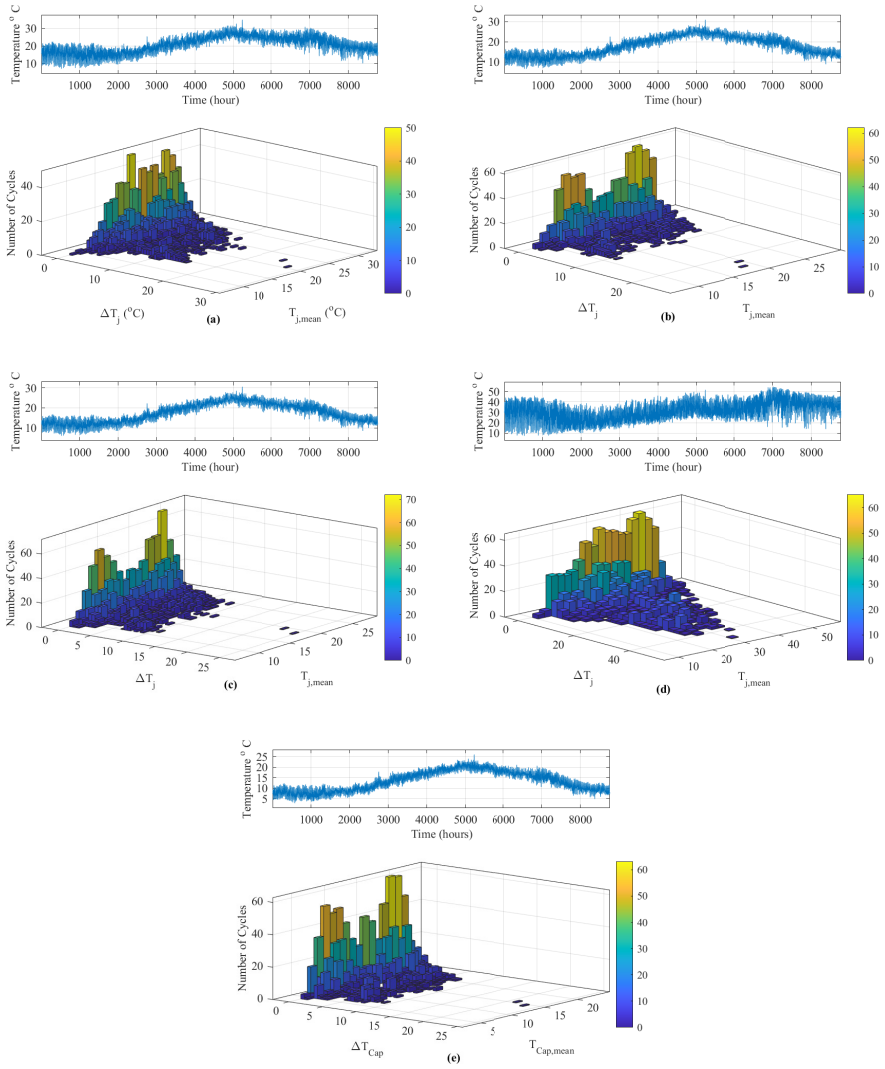

Figure 2.9: Yearly distribution of temperature by rain flow algorithm for (a) D1, (b) D2, (c) T1, (d) T2, and (e) capacitor where schematic for SM is provided in Fig. 2.3.

This chapter utilizes a mission profile adopted from [29], with an annual average loading of 57%. The modulation technique employed is Phase-Shift Carrier (PSC) Pulse Width Modulation (PWM), which is commonly used in MMC applications due to its ability to reduce harmonic distortion and improve modularity. To analyze the fatigue behavior of the components, the rainflow algorithm is employed, a widely accepted tool for cycle counting in fatigue analysis. The rainflow evaluates the reliability of MMC components by identifying and quantifying the temperature cycles experienced during operation. It calculates the mean temperature (T_{mean}) and the temperature fluctuations

(ΔT_j) for all critical components, including diodes (D_1, D_2), IGBTs (T_1, T_2), and capacitor. These outputs are essential inputs for both the mission profile and FIDES reliability assessment methodologies, as they provide the necessary parameters to predict component lifetime accurately. The rainflow analysis results for components D_1, D_2, T_1, T_2, and the capacitor are presented in Fig. 2.9.

From the rainflow analysis, it is observed that in inverter mode, component T_2 experiences the highest temperature fluctuations (ΔT_j), indicating greater thermal stress and, consequently, higher fatigue. In contrast, the temperature fluctuations across other components (D_1, D_2, T_1, and the capacitor) are relatively lower, suggesting less thermal fatigue and stress in these parts. This observation highlights T_2 as the most vulnerable component in the system, warranting further analysis. The Monte Carlo Simulation (MCS) results, presented in Fig. 2.10, provide additional insights by applying Weibull Distribution fitting to the expected lifetimes of the components. The Weibull Distribution is a statistical tool that enables reliability predictions by modeling the probability of failure over time. According to the MCS results:

- Component T_2 is predicted to have the shortest expected lifetime, approximately 63 years, due to its high-temperature fluctuations and associated fatigue.
- The expected lifetimes of components D_1, D_2, T_1, and the capacitor are significantly longer, estimated at 1714 years, 3901 years, 3730 years, and 136 years, respectively.

The shorter lifetime of T_2 underscores the need for targeted design interventions to mitigate its failure risks, such as improved thermal management or redundancy strategies. In contrast, the extended lifetimes of D_1, D_2, T_1, and the capacitor suggest these components are less likely to be critical failure points under the given mission profile.

This section aims to compare the reliability of MMCs using three distinct methodologies: MIL, FIDES, and the Mission Profile. To achieve this, the reliability of an MMC is analyzed without redundancy using all three methods, and the results are illustrated in Fig. 2.11 (a). The analysis reveals significant discrepancies between the methodologies. The MIL method estimates a B_{10} lifetime of approximately 0.2 years, substantially lower than the FIDES method, which predicts a B_{10} lifetime -the B_{10} lifetime refers to the time by which 10% of the population of the components are expected to have failed- of 0.98 years. Meanwhile, the mission profile method yields a considerably higher B_{10} lifetime of 8.5 years.

To further examine the impact of incorporating one redundant SM in each arm, the results are shown in Fig. 2.11 (b). With redundancy, the MIL method improves the B_{10} lifetime to around 1.7 years, while the FIDES method significantly enhances it to approximately 10.5 years. The mission profile method demonstrates the increasing B_{10} lifetime to 18.3 years. These variations in reliability predictions stem from several factors inherent to each methodology. First, the resolution of the mission profile plays a critical role. The mission profile method uses a 1-hour resolution in this study, which, according to [18], can underestimate the MMC's failure rate by nearly a factor of seven. A higher resolution, such as sub-hourly or even real-time data, could provide a more accurate representation of operational stresses and environmental conditions, potentially

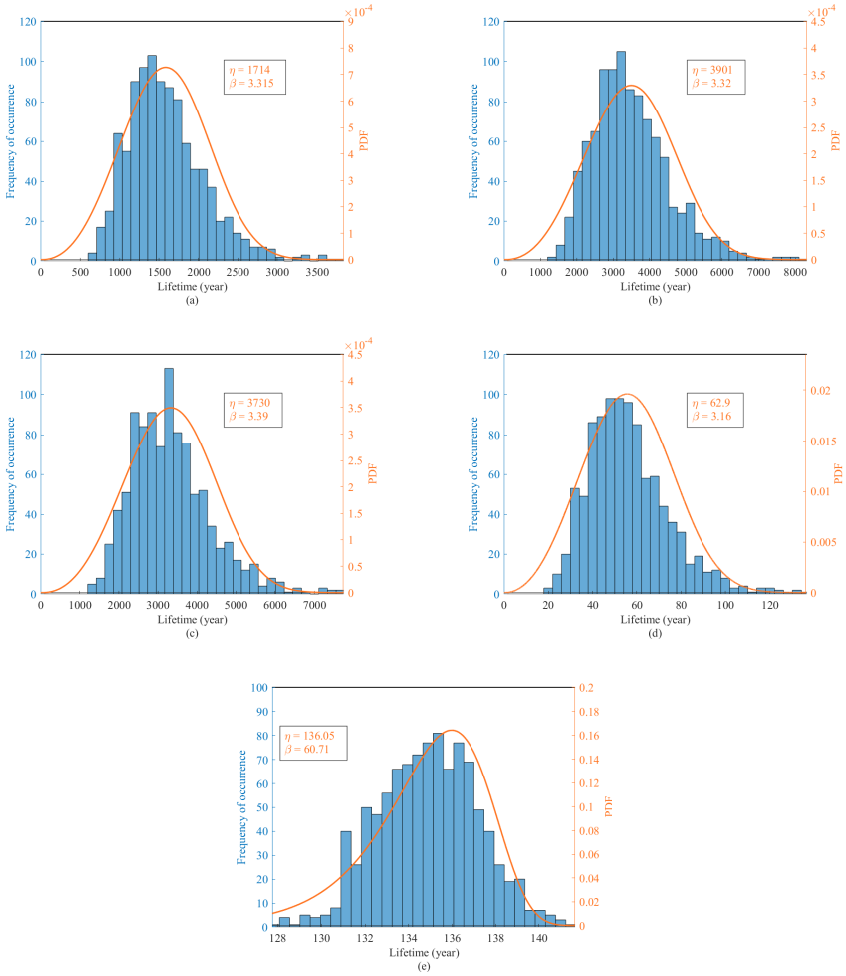

Figure 2.10: MCS results and fitting with Weibull distribution for (a) D1, (b) D2, (c) T1, (d) T2, and (e) capacitor.

altering reliability predictions significantly. Beyond resolution, the methodologies differ fundamentally in their approaches and assumptions:

1. **MIL methodology:** The MIL method relies on standardized failure rate models derived from statistical data and empirical studies. These models often assume constant failure rates and do not account for dynamic operating conditions or environmental variations. As a result, the MIL method tends to provide conservative and lower reliability estimates, especially for complex systems like MMCs operating under variable loads [20].

2. **FIDES methodology:** FIDES incorporates technical controls over design, manufacturing, and operational processes. It adjusts failure rates based on factors such as quality management and process improvements. At the same time, this method pro-

vides a more detailed assessment compared to MIL [6, 7, 28].

3. **Mission profile methodology:** The mission profile method, in contrast, models the actual operating conditions of the system, including load variations, thermal cycles, and environmental stresses. However, the accuracy of the mission profile method heavily depends on the resolution and quality of the input data. A low-resolution mission profile, such as the 1-hour resolution used in this study, averages out transient conditions and peak stresses, leading to an overestimation of reliability. High-resolution mission profiles could capture these variations more effectively, reducing the observed discrepancy between mission profiles and other methods. Other contributing factors include differences in the granularity of component-level failure data and assumptions about maintenance strategies and failure mechanisms [11–13]. The MIL and FIDES method-

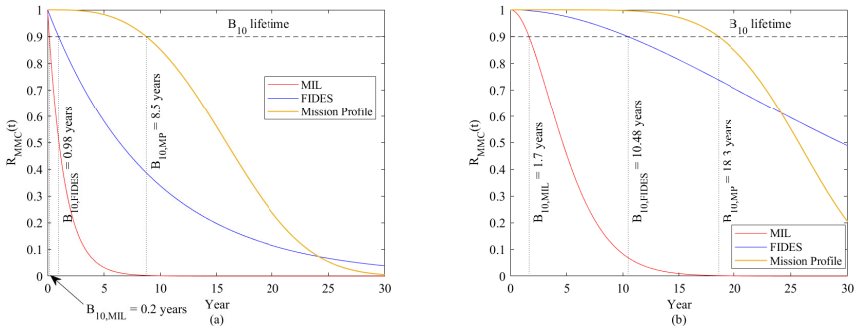

Figure 2.11: Reliability results of 10 MW 17 kV DC link MMC with the annual average of 57% loading for MIL, FIDES, and Mission Profile with (a) no redundancy and (b) 1 redundant SM in each arm.

ologies are often based on the failure rate obtained by following the criteria provided in their handbook. It is worth mentioning that the system's mission profile is used in the FIDES method, but guidance given in its handbook should still be followed. It can be said that the FIDES method is an advanced version of the MIL. In contrast, the mission profile method allows for a tailored analysis, incorporating the exact characteristics of the system and its operational context. These findings highlight the importance of carefully selecting and calibrating reliability assessment methodologies based on the application requirements and available data. The significant differences in B_{10} lifetime predictions underscore the need for caution when interpreting reliability metrics and the value of high-resolution, context-specific analyses in accurately assessing the reliability of MMCs.

2.6. CONCLUSION

This chapter has explored three distinct methodologies for assessing the reliability of MMCs: the Military Handbook, FIDES, and Mission Profile Methodology. Each method offers unique strengths and insights into the reliability assessment process. The Military Handbook provides a well-established, standardized approach that is widely recognized in military and aerospace applications. In contrast, the FIDES methodology incorporates more comprehensive factors, including manufacturing and operational controls,

offering a more nuanced reliability estimation. The Mission Profile Methodology stands out for its detailed environmental and operational modeling, making it highly suitable for applications with specific mission data. The comparative analysis indicates that each method will lead to very different absolute final results. Also, the great impact of redundancy on reliability improvements was shown regardless of the fact that which method is used for reliability evaluation.

REFERENCES

[1] M. Ahmadi, A. Shekhar, and P. Bauer, *Switch voltage rating selection considering cost-oriented redundancy and modularity-based trade-offs in modular multilevel converter,* IEEE Trans. Power Deliv. (2023), 10.1109/TPWRD.2023.3263270.

[2] P. Tu, S. Yang, and P. Wang, *Reliability- and cost-based redundancy design for modular multilevel converter,* IEEE Trans. Ind. Electron. **66**, 2333 (2019).

[3] F. Richardeau and T. T. L. Pham, *Reliability calculation of multilevel converters: Theory and applications,* IEEE Trans. Ind. Electron. (2013), 10.1109/TIE.2012.2211315.

[4] W. Liu and Y. Xu, *Reliability model of mmc-based flexible interconnection switch considering the effect of loading state uncertainty,* IET Power Electronics **12**, 358 (2019), https://ietresearch.onlinelibrary.wiley.com/doi/pdf/10.1049/iet-pel.2018.5262 .

[5] H. Li, X. Xie, A. McDonald, Z. Chai, T. Yang, Y. Wu, and W. Yang, *Cost and reliability optimization of modular multilevel converter with hybrid submodule for offshore dc wind turbine,* International Journal of Electrical Power Energy Systems **120**, 105994 (2020).

[6] J. Marin and R. Pollard, *Experience report on the fides reliability prediction method,* in *Annual Reliability and Maintainability Symposium, 2005. Proceedings.* (2005) pp. 8–13.

[7] P. I. Prodanov and D. D. Dankov, *Comparison of failure rates and reliability of power semiconductors in power electronic devices using methodologies mil-hdbk-217f and fides,* in *2021 17th Conference on Electrical Machines, Drives and Power Systems (ELMA)* (2021) pp. 1–5.

[8] S. E. De León-Aldaco, H. Calleja, and J. Aguayo Alquicira, *Reliability and mission profiles of photovoltaic systems: A fides approach,* IEEE Trans. on Power Electronics **30**, 2578 (2015).

[9] S. de Leon, H. Calleja, and J. Mina, *Reliability of photovoltaic systems using seasonal mission profiles and the fides methodology,* Microelectronics Reliability **58**, 95 (2016).

[10] S. Peyghami, Z. Wang, and F. Blaabjerg, *A guideline for reliability prediction in power electronic converters,* IEEE Trans. on Power Electronics **35**, 10958 (2020).

[11] G. Lv, W. Lei, M. Wang, C. Lv, and J. Zhao, *Reliability analysis and design of mmc based on mission profile for the components degradation,* IEEE Access **8**, 149940 (2020).

[12] Y. Yang, W. Wang, and K. Ma, *Mission-profile-based testing scheme for sub-modules in modular multilevel converter,* IEEJ Journal of Industry Applications **9**, 219 (2020).

[13] Y. Zhang, H. Wang, Z. Wang, F. Blaabjerg, and M. Saeedifard, *Mission profile-based system-level reliability prediction method for modular multilevel converters,* IEEE Transactions on Power Electronics **35**, 6916 (2020).

[14] H. Liu, K. Ma, Z. Qin, P. C. Loh, and F. Blaabjerg, *Lifetime estimation of mmc for offshores wind power hvdc application,* IEEE Journal of Emerging and Selected Topics in Power Electronics (2016), 10.1109/JESTPE.2015.2477109.

[15] C. Zhan, L. Zhu, W. Wang, Y. Zhang, S. Ji, and F. Iannuzzo, *Multidimensional mission-profile-based lifetime estimation approach for igbt modules in mmc–hvdc application considering bidirectional power transfer,* IEEE Trans. Ind. Electron. (2023), 10.1109/TIE.2022.3203768.

[16] J. V. M. Farias, A. F. Cupertino, V. d. N. Ferreira, H. A. Pereira, S. I. Seleme, and R. Teodorescu, *Reliability-oriented design of modular multilevel converters for medium-voltage statcom,* IEEE Trans. Ind. Electron. **67**, 6206 (2020).

[17] J. Xu, L. Wang, Y. Li, Z. Zhang, G. Wang, and C. Hong, *A unified mmc reliability evaluation based on physics-of-failure and sm lifetime correlation,* International Journal of Electrical Power Energy Systems **106**, 158 (2019).

[18] Y. Zhang, H. Wang, Z. Wang, Y. Yang, and F. Blaabjerg, *The impact of mission profile models on the predicted lifetime of igbt modules in the modular multilevel converter,* in *IECON 2017* (2017).

[19] L. Wang, J. Xu, G. Wang, and Z. Zhang, *Lifetime estimation of igbt modules for mmc-hvdc application,* Microelectronics Reliability **82**, 90 (2018).

[20] *Reliability Prediction of Electronic Equipment: MIL-HDBK-217D.*, Military standardization handbook (Department of Defense, 1983).

[21] J. E. Huber and J. W. Kolar, *Optimum number of cascaded cells for high-power medium-voltage ac–dc converters,* IEEE Journal of Emerging and Selected Topics in Power Electronics **5**, 213 (2017).

[22] M. Held, P. Jacob, G. Nicoletti, P. Scacco, and M. Poech, *Fast power cycling test of igbt modules in traction application,* in *Proceedings of Second International Conference on Power Electronics and Drive Systems*, Vol. 1 (Singapore, 1997) pp. 425–430.

[23] R. Bayerer, T. Herrmann, T. Licht, J. Lutz, and M. Feller, *Model for power cycling lifetime of igbt modules - various factors influencing lifetime,* in *5th International Conference on Integrated Power Electronics Systems* (Germany, 2008) pp. 1–6.

[24] F. Kardan, A. Shekhar, and P. Bauer, *Quantitative comparison of the empirical lifetime models for power electronic devices in ev fast charging application,* in *2023 International Power Electronics Conference (ICPE-Jeju 2023- ECCE Asia)* (2023).

[25] M. A. Miner, *Cumulative damage in fatigue,* Journal of Applied Mechanics **12**, 159–164 (1945).

[26] W. Weibull, *Statistical distribution function of wide applicability,* ASME Journal of Applied Mechanics **18**, 293 (1951).

[27] J. McPherson, *Reliability Physics and Engineering*, 2nd ed. (Springer International, Switzerland, 2013).

[28] *Fides guide 2009 edition a, "reliability methodology for electronic system", fides group, france, 2004.* .

[29] A. Shekhar, T. B. Soeiro, Y. Wu, and P. Bauer, *Optimal power flow control in parallel operating ac and dc distribution links,* IEEE Trans. Ind. Electron. **68** (2021), 10.1109/TIE.2020.2970675.

3

RELIABILITY ASSESSMENT FOR MMCS USING MONTE CARLO SIMULATIONS

This chapter introduces the reliability assessment methods for MMCs using Monte Carlo Simulations (MCS). MCS is particularly valuable for considering the uncertainty of reliability indices and validating theoretical outputs. This chapter shows how the MCS is a strong tool for evaluating different reliability aspects of the system, which can be challenging when analytical methods are used.

This chapter is based on:

- M. Ahmadi, A. Shekhar, P. Bauer, "Reliability Assessment for Modular Multilevel Converters using Monte Carlo Simulations," in International Journal of Electrical Power & Energy Systems, 2025.

3.1. INTRODUCTION

Component failures within the MMC can lead to significant impacts in terms of cost and overall system safety [1]. Hence, it becomes imperative to evaluate MMC reliability during the design and development phase [2]. RMR is explored to enhance the reliability of grid-connected MMC systems, as will be detailed in subsequent chapters. As shown in chapter 2, various methodologies are employed to assess MMC reliability, including the mission profile, FIDES, and MIL methods. The mission profile method is rooted in the physics of a specific failure mechanism, focusing on time-to-failure or cycle-to-failure within the system's mission profile [3]. The latter methodology involves analytical formulations, utilizing standards such as the FIDES Guide and Military Handbook (MIL-HDBK) [4] to gauge system reliability [5]. Another valuable tool for reliability analysis is Monte Carlo Simulation (MCS), which could help consider the uncertainty of reliability indices [6, 7]. MCS converges to a specific value as the number of trials increases, settling within the tolerance level range [8].

MCS finds diverse applications, serving as both a validation tool and a means to account for parameter variations. In the context of [9], MCS is employed to validate theoretical outputs. The study demonstrates that with 10,000 trials, MCS outputs align closely with analytical results over a 40-year lifespan. However, specific details regarding the implementation of MCS are not provided. Additionally, MCS is utilized to validate the reliability of MMC, considering two redundancy strategies.

In [10], the authors focus on estimating the reliability of the DC/DC converter due to electrothermal stresses on power electronic switches and capacitors. The MCS accounts for variations in defined parameters. The study reveals that introducing redundancy in such a converter can extend its lifetime from 4.5 to 7.5 years. Another instance of MCS application is highlighted in [11], where vehicle behavior is simulated using MCS to compare the service capacities and earnings of electric vehicle (EV) charging and battery swapping.

In [12], three distinct MCS methods—static, semi-dynamic, and dynamic MCSs—are introduced to evaluate the reliability of power electronics based on the mission profile. However, MCS is primarily utilized to account for variations in applied parameters. The study reveals that the static MCS exhibits the fastest calculation time. From an accuracy perspective, it is concluded that if the number of trials exceeds 1000, there is no discernible difference among the outputs of various MCS strategies. In [5], MCS is employed to investigate the reliability of a photovoltaic (PV) power plant. The study derives an estimation of failure rates from FIDES Guide standards, utilizing MCS to obtain the probability of system failure. Moreover, in [13, 14], a reliability-based design method is proposed for MMC. MCS is applied to consider a 5% variation in applied parameters by acknowledging potential deviations in statistical analysis from actual values.

This chapter aims to establish MCS as a methodology for evaluating the reliability of MMC across various redundancy strategies. MCS provides the flexibility to account for improbable system effects that may not be captured by analytical approaches [15]. It's worth noting that this part of the thesis doesn't prioritize a specific reliability methodology (MIL, FIDES, or mission profile) for measuring component failure rates. Nevertheless, MCS is a valuable and highly accurate tool for estimating the converter's failure rate. Unlike much of the existing literature, which primarily focuses on parameter deviation

[16], this chapter broadens the scope of MCS application [17]. The key contributions are summarized as follows:

- Propose the approach for applying MCS to assess the reliability of the MMC employing all available redundancy strategies, as detailed in Section 3.3.
- Compare the MCS outputs with analytical equations to validate the effectiveness of applying MCS (Section 3.3/3.2).
- Estimating the MMC's reliability by applying the mission profile method where the results are unavailable with two redundancy strategies (Section 3.4).
- Demonstrating the application of MCS in dynamic preventive maintenance (Section 3.4).
- Compute the required time for performing MCS with different system configurations (Section 3.5).

3.2. REDUNDANCY STRATEGIES OF MMC

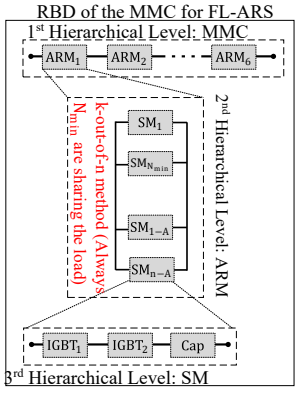

Figure 3.1: RBD model of MMC with FL-ARS.

The configuration of MMC is presented in Fig 2.1. MMC has three phases, and each phase has two arms in which SMs are connected in series to reach the desired voltage and power rating. As shown in Fig 2.1, SM comprises an IGBT module, capacitor bank, and auxiliary components [18]. The minimum number of the required series connection of SMs is determined based on the required DC-link voltage and the IGBT rating given by (1.1)[19, 20]. However, to increase reliability, extra SMs are used that enhance the MMC reliability and availability time [21]. Redundant SMs can be implemented in various ways, that are as follows:

3.2.1. FIXED-LEVEL ACTIVE REDUNDANCY STRATEGY (FL-ARS)

In FL-ARS, only $N_{\min}$ SMs are operational while the redundant SMs are energized and operate. But, in FL-ARS, the triggering signal is only sent to $N_{\min}$ random SMs. Hence,

all SMs will take turns to be triggered and operating. Note that operating SMs can be either from original SMs or redundant SMs. All SMs will have constant voltage stress throughout the MMC operation in this redundancy strategy. Based on the Reliability Block Diagram (RBD) model of FL-ARS in [22], also shown in Fig. 3.1. The reliability of an arm is obtained by the k-out-of-n probability model, in which $N_{\min}$ SMs out of n SMs are required for the arm's success. In LS-ARS, the reliability of an arm is given by (3.1).

$$R_{\text{arm-FL}}(t) = \sum_{i=N_{\min}}^{n} C_n^i R_{\text{SM}}(t)^i (1 - R_{\text{SM}}(t))^{n-i} \tag{3.1}$$

$$R_{\text{SM}}(t) = e^{-\lambda_{\text{SM}} t} \tag{3.2}$$

where R_{SM} is the reliability of the SM, λ_{SM} is the total failure rate of the SM that is composed of power switches, capacitor banks, power supply, gate drive, and bypass switch. As mentioned, these components' failure rates could be estimated by applying different reliability methods. However, this chapter does not focus on calculating these failure rates or which components should be considered [23]. So, it is assumed that these assumptions are set and the failure rates are estimated with acceptable accuracy.

3.2.2. STANDBY REDUNDANCY STRATEGY (SRS)

In SRS, the number of operating SMs is always $N_{\min}$, and the redundant SMs are in idle mode. In case of an SM failure, the failed SM is bypassed, and the first redundant SM starts to operate. The redundant SMs are bypassed in SRS, so their failure rate is assumed to be zero. In SRS, the voltage stress across the operational SMs is similar to FL-ARS. Based on the RBD model of SRS shown in Fig. 3.2 [9]. The reliability of an arm is obtained by applying the Homogeneous Poisson Process with a constant failure rate of λ_s where it is the arm failure rate with $N_{\min}$ a minimum number of required SMs per arm. The reliability of an arm follows the Poisson Distribution, which can be obtained as (3.3) and (3.4).

$$R_{\text{arm-SRS}}(t) = P[N(t) \leq (n - N_{\min})] = \sum_{i=0}^{n-N_{\min}} \frac{(\lambda_{\text{s}} t)^i}{i!} e^{-\lambda_{\text{s}} t} \tag{3.3}$$

$$\lambda_{\text{s}} = \lambda_{\text{SM}} \times N_{\min} \tag{3.4}$$

3.2.3. LOAD-SHARING ACTIVE REDUNDANCY STRATEGY (LS-ARS)

In LS-ARS, all the n SMs, including redundant SMs within the arm, are operational and share the load in normal conditions. Therefore, compared to the SRS and FL-ARS, the voltage across the SMs will be lower, decreasing the risk of SM failure. In LS-ARS, if an SM fails, the faulty SM will be bypassed, and the remaining SMs will continue to operate. Nevertheless, in case of SMs failure in LS-ARS, the voltage across the operational SMs will increase, consequently changing the SM's failure rate. This fact is essential to be considered. The RBD model of the MMC with applied LS-ARS is shown in Fig 3.3.

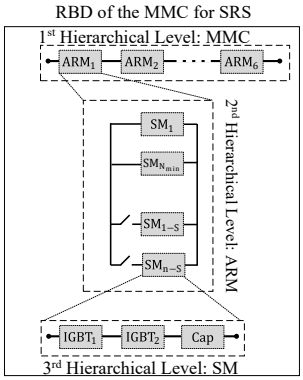

Figure 3.2: RBD model of MMC with SRS.

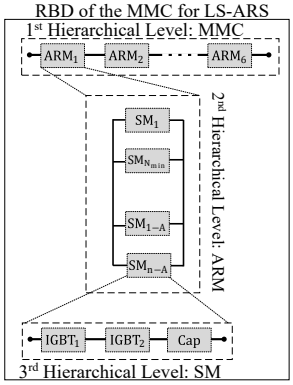

Figure 3.3: RBD model of MMC with active load-sharing redundancy.

According to the RBD model and the fact that in LS-ARS, the voltage across the SMs changes in case of SM failure, the Markov Chain is used for calculating the reliability of MMC's arm shown in Fig 3.4.

In the Markov Chain shown in Fig. 3.4, state 0 is the initial state in which all the n SMs are sharing the load, whereas state n-$N_{\min}$+1 is representative of the fail state in which more than $N_{\min}$ minimum required SMs failed. The differential equations obtained by Markov Chain are as (3.5).

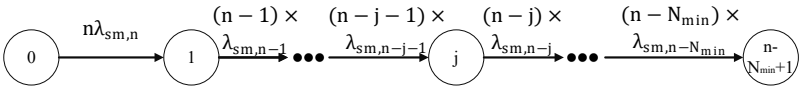

Figure 3.4: Markov chain for an arm in LS-ARS mode.

$$
\begin{aligned}
\frac{dP_0(t)}{dt} &= -n\lambda_{\mathrm{SM,n}}P_0(t)\\
&\vdots\\
\frac{dP_{\mathrm{j}}(t)}{dt} &= (n-j-1)\lambda_{\mathrm{SM,n\text{-}j\text{-}1}}P_{\mathrm{j\text{-}1}}(t)\\
&\quad -(n-j)\lambda_{\mathrm{SM,n\text{-}j}}P_{\mathrm{j}}(t)\\
&\vdots\\
\frac{dP_{\mathrm{n}\text{-}N_{\min}+1}(t)}{dt} &= N_{\min}\lambda_{\mathrm{SM,n}\text{-}N_{\min}}P_{\mathrm{n}\text{-}N_{\min}}(t)
\end{aligned}
\tag{3.5}
$$

In which $P_{\mathrm{j}}(t)$ is the state j, $\lambda_{SM,n-j-1}$ is the failure rate of SM upon the condition that n-j SMs are operational. The Laplace transform of (1.5) and then the inverse transform will result in (1.6) as follows:

$$
\begin{aligned}
P_0(t) &= e^{-n\lambda_{\mathrm{SM,n}}t}\\
&\vdots\\
P_{\mathrm{j}}(t) &= \int_0^t (n-j-1)\lambda_{\mathrm{SM,n\text{-}j\text{-}1}}e^{-(n-j)\lambda_{\mathrm{SM,n\text{-}j}}\tau}P_{\mathrm{j\text{-}1}}(t-\tau)d\tau\\
&\vdots\\
P_{\mathrm{n}\text{-}N_{\min}+1}(t) &= \int_0^t N_{\min}\lambda_{\mathrm{SM,n}\text{-}N_{\min}}P_{\mathrm{n}\text{-}N_{\min}}(\tau)d\tau
\end{aligned}
\tag{3.6}
$$

In the Markov Chain, if state 0 is the initial state in which all the n = $N_{\min}$ + N_{red} SMs are sharing the load, whereas state n-$N_{\min}$+1 is representative of the fail state in which more than $N_{\min}$ minimum required SMs failed. So, the successful operation of the arm can be obtained by summing successful states as in (3.7)

$$
R_{\text{arm-LS}}(t) = \sum_{j=0}^{N_{\mathrm{red}}} P_{\mathrm{j}}(t) \tag{3.7}
$$

after calculating the arm's reliability considering various redundancy strategies, the reliability of the MMC can be calculated as (3.8):

$$R_{\text{MMC-x}}(t) = (R_{\text{arm-x}}(t))^6 \rightarrow x \in \text{FL-ARS, SRS, LS-ARS} \tag{3.8}$$

3.3. MONTE CARLO MODELS OF MMC UNDER VARIOUS REDUNDANCY STRATEGIES

MCS is a tool that assesses the reliability of a system by simulating its realistic functions and random behaviors. In MCS, experiments (trials) are conducted to estimate the probability of system failure or success. In contrast, analytical approaches describe the system using mathematical equations, which are sometimes simplified. There are two methods of applying MCS: time-independent (random) and time-dependent (sequential). The selected approach depends on the characteristics of the system. If the time intervals in MCS impact the subsequent intervals, time-dependent MCS should be employed. In time-dependent MCS, uniform numbers between 0-1 should be converted into the time distribution. As given in (3.2), the exponential distribution can be transformed using the inverse transform method, outlined as follows [24]:

$$R_{\text{SM}}(t) = e^{-\lambda_{\text{SM}} t}, (\lambda_{\text{SM}} > 0, t \geq 0) \tag{3.9}$$

so the unreliability function can be obtained as (3.10).

$$U_{\text{SM}}(t) = 1 - R_{\text{SM}}(t) \rightarrow e^{-\lambda_{\text{SM}} t} = 1 - U_{\text{SM}}(t) \tag{3.10}$$

by applying the inverse transform function:

$$t = -\frac{1}{\lambda_{\text{SM}}} ln(1 - U_{\text{SM}}(t)) \tag{3.11}$$

where $1 - U_{\text{SM}}(t)$ is uniformly distributed over the interval [0, 1]. Therefore, the time interval distribution for each SM can be determined. It's crucial to emphasize that even if the failure rate of the SM is estimated using the Weibull Distribution, which considers the wear-out period and component degradation in the mission profile reliability method, MCS remains applicable. However, when considering the wear-out period, the inverse transform function for MCS can be derived, as expressed in (3.12).

$$t = \eta \times \sqrt[\beta]{-ln(1 - U_{\text{SM}}(t))} \tag{3.12}$$

where $1 - U_{\text{SM}}(t)$ is uniformly distributed over the interval [0, 1], with β and η representing the shape and scale parameters derived from the mission profile results. This will be more elaborated in section 3.4 A. Throughout the remainder of this chapter, the methodology applied for MCS is demonstrated based on a single trial and by applying the failure rate achieved according to the MIL method. Nevertheless, the same method applies to mission profiles, which will be explained in section 3.5. However, it is imperative to repeat these trials to obtain results with acceptable accuracy by conducting 1000 trials. Additionally, t_{M} denotes the mission time, ranging from 0 to a specified time interval (30 years in this chapter) with specific time steps (0.05 years in this chapter). In each trial, all

SMs ($SM_1, SM_2, SM_3, ...$) will have random operational intervals ($t_1, t_2, t_3, ...$), respectively obtained from (3.11). Subsequently, the mission time is compared with the random operational interval of each SM, indicated by the marker ×. Each marker × shown in Fig. 3.6 is achieved through the repetition of these trials (number of simulations) at that specific time.

This chapter assesses an MMC with the characteristics outlined in Table 3.1 across various redundancy strategies. The configuration includes a minimum required number of SMs in each arm, denoted as $N_{min} = 9$. The base failure rates for the capacitor and IGBT are provided in Table 3.1. To account for voltage stress and other factors, the equations from [25], initially derived from MIL-HDBK (detailed in chapter 2) [4], are implemented. The methodology for applying MCS to the MMC with different redundancy schemes is further elaborated below.

Table 3.1: MMC CHARACTERISTICS AND FAILURE RATES

Symbols	Item	Value
N_{min}	Minimum number of SMs	9
V_{dc}	Pole-to-pole DC voltage	17 kV
S_{MMC}	Rated power	10 MVA
V_{IGBT}	Rated IGBT Voltage	3300 V
k_{max}	Capacitors voltage ripple	10%
S_f	Safety factor of IGBT	0.6
C_{SM}	SM capacitance	3.3 mF
f_{sw}	Switching frequency	313 Hz
N_{red}	Redundant per arm	1
IGBT	FF450R33T3E3(Infineon)	-
Capacitor	DKTFM1*#B3367(AVX)	-
$\lambda_{base\text{-}IGBT}$	IGBT base failure rate (MIL)	100 FIT† [9]
$\lambda_{base\text{-}Cap}$	DC capacitor base failure rate (MIL)	100 FIT† [9]

†FIT (Failure In Time) is a reliability metric that indicates the number of expected failures in one billion (10^9) hours of operation.

3.3.1. FL-ARS MCS

Each arm is configured with 10 SMs to assess the MMC with FL-ARS. The assumption is made that the minimum required number of SMs per arm is $N_{min} = 9$, and $N_{red} = 1$ represents the number of redundant SMs in each arm. The operational cycle of an arm utilizing FL-ARS is illustrated in Fig. 3.5 (a).

In Fig. 3.5 (a), the FL-ARS involves the operation of all n SMs, where only 9 out of 10 SMs are necessary for an arm to succeed. In this stochastic trial, at failure time (T_s), the second failure occurs, and T_s is equal to t_1 of SM_1. Consequently, if mission time (t_M) is less than T_s, it is considered a successful mission; otherwise, it is deemed a failed mission. This experiment should be repeated, and the total number of successes (or failures) divided by the total number of trials yields the success (or failure) probability, as depicted in Fig. 3.6 (a). This representation demonstrates that the applied methodology

of FL-ARS MCS output with 1000 simulations aligns with the output results of analytical equations (3.1) used for calculating the reliability of MMC with FL-ARS. Note that 1000 trials are selected to show the sporadic distribution of trials. With a higher number of trials, the MCS will exactly match the analytical outputs.

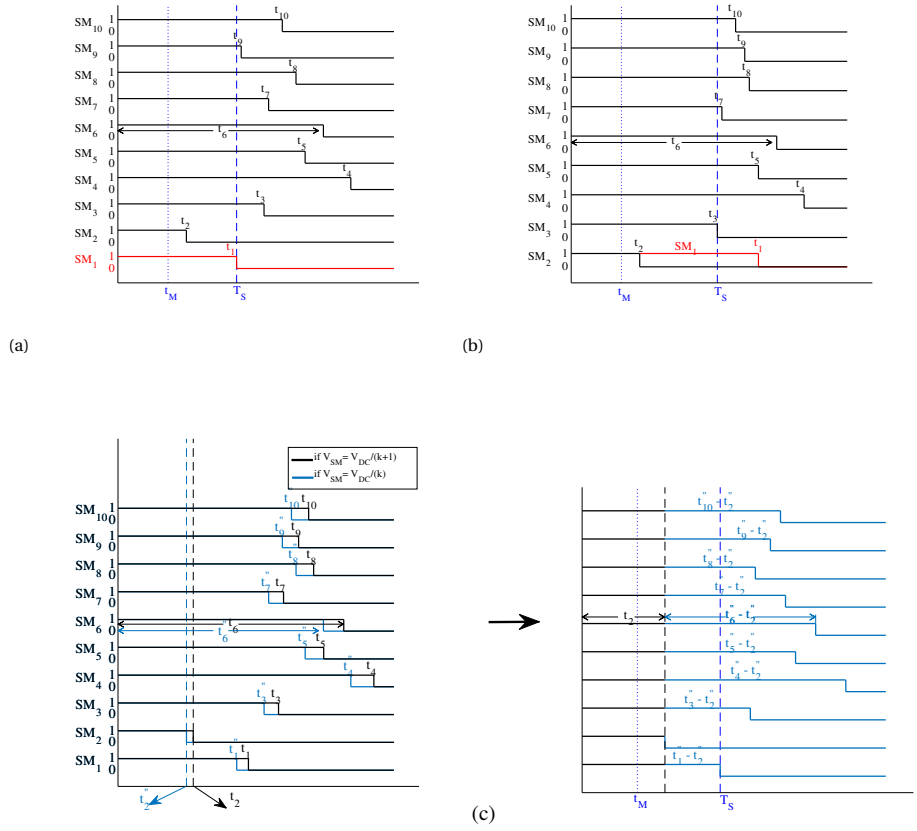

Figure 3.5: Operating cycle of an arm of MMC with (a) FL-ARS; (b) SRS; and (c) LS-ARS.

3.3.2. SRS MCS

In the case of the MMC arm employing SRS, the same number of SMs is utilized. The operating cycle of an arm with SRS is presented in Fig. 3.5 (b). As illustrated, the number of operating SMs equals $N_{\min}$, and the redundant SM (SM_1) remains in idle mode. In this stochastic trial, the first failure occurs at t_2 (in SM_2), prompting the redundant SM_1 to start operating at t_2. Consequently, at least nine operating SMs are required for the arm to succeed. However, the second failure occurs in SM_3 at t_3, leading to the arm being considered failed beyond that time. Therefore, in this trial, T_s is equal to t_3, and if t_M is less than T_s, that trial is counted as a success. As previously mentioned, this trial should

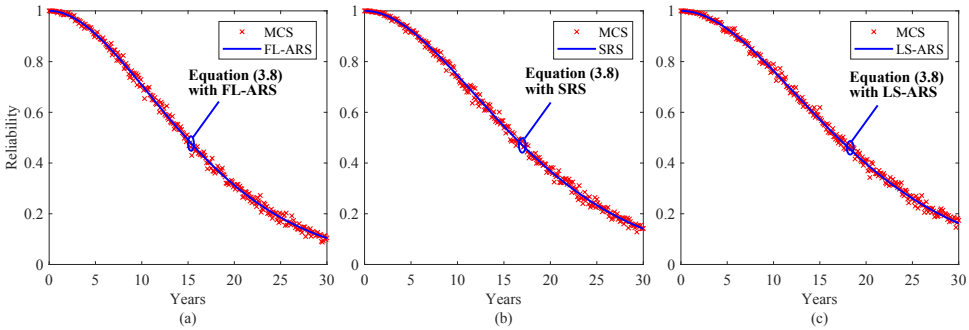

Figure 3.6: MMC reliability applying analytical and MCS methods (1000 trials) for (a) FL-ARS; (b) SRS; and (c) LS-ARS.

be repeated. The ratio between the number of successful missions and the total number of trials yields the success probability, as shown in Fig. 3.6 (b). The results presented in Fig. 3.6 (b) validate the effectiveness of applying the SRS MCS methodology, as the analytical and MCS (1000 trials) outputs align.

3.3.3. LS-ARS MCS

Fig. 3.5 (c) illustrates the operational cycle of an arm in the MMC employing LS-ARS. In LS-ARS, the number of operating SMs includes the redundant SM, and unlike FL-ARS and SRS, all SMs share the load. Consequently, the voltage stress is lower than both SRS and FL-ARS. However, in LS-ARS, the voltage across operating SMs in healthy conditions increases after each SM failure, leading to higher voltage stress over time. This factor is crucial to consider. As shown in Fig. 3.5 (c) on the left side, if the voltage across each SM is $V_{\mathrm{SM}} = \frac{V_{\mathrm{dc}}}{N_{\mathrm{min}}+N_{\mathrm{red}}}$, the voltage stress is lower than the case where the voltage across each SM is equal to $V_{\mathrm{SM}} = \frac{V_{\mathrm{dc}}}{N_{\mathrm{min}}}$. Therefore, in this stochastic trial, the operational time of SMs in the former case $(t_1, t_2, ..., t_{10})$ will be higher than in the latter case $(t_1^{"}, t_2^{"}, ..., t_{10}^{"})$.

After calculating the first step, the second step for evaluating the MCS of an arm under LS-ARS is presented in Fig. 3.5 (c) on the right-hand side. At time 0, all the SMs are operational and share the load. When at t_2, SM_2 fails, the remaining SMs operate with higher voltage stress. Hence, the remaining SMs' lifetime reduction can be calculated, as shown in Fig. 3.5 (c) on the right-hand side, such as for SM_6 where the operational lifetime is equal to $t_2 + (t_6^{"} - t_2^{"})$. Then T_{s} is calculated, since at t_1, SM_1 fails in this stochastic trial, $T_{\mathrm{s}} = t_2 + (t_1^{"} - t_2^{"})$. After obtaining the operation cycle of MMC under LS-ARS, t_{M} is compared with T_{s}.

3.3.4. ERROR ASSESSMENT: MCS VS. ANALYTICAL METHODS

This section assesses the difference between MCS and analytical methods given by (3.13). The outcomes of this evaluation are visually depicted in Fig. 3.7, which indicates that if the number of trials exceeds 10,000, it can be inferred that the error between analytical and MCS results is approximately 1%, which can be neglected.

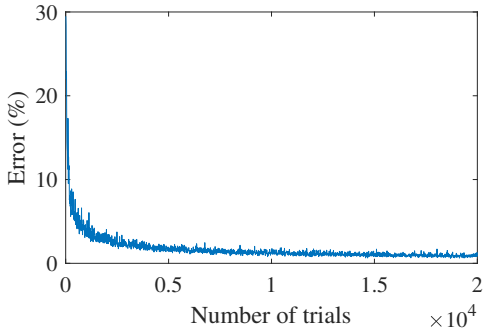

Figure 3.7: Examining uncertainty of MCS results compared to analytical methods.

$$\text{Error}(\%) = \left| \frac{R_{\text{MMC-MCS}} - R_{\text{MMC-analytical}}}{R_{\text{MMC-analytical}}} \right| \times 100 \tag{3.13}$$

3.4. IMPLEMENTATION OF MCS IN GRID SPECIFIC APPLICATIONS

This section will explain how the MCS solves several problems where providing an analytical solution is challenging or unavailable in the literature.

3.4.1. REDUNDANCY STRATEGIES FOR MISSION PROFILE METHOD

Conventional reliability evaluation methods for MMCs have analytical solutions when considering diverse redundancy strategies and applying MIL methods. The mission profile methods struggled to accommodate the complexity of different redundancy strategies beyond FL-ARS. Specifically, the mission profile method restricted evaluation to FL-ARS due to analytical constraints, leaving the reliability of MMCs with SRS and LS-ARS unaddressed. This gap in methodology hindered a comprehensive assessment of MMC reliability under varying operating conditions. To achieve this, the applicability of the MCS is assessed through FL-ARS, and the MMC's reliability is assessed without redundancy. Then, the MCS outputs for FL-ARS and without redundancy are compared with existing analytical equations (equation (3.1)) to validate the MCS's effectiveness in applying the mission profile method. Then, the MCS is extended for SRS and LS-ARS, where no analytical approach is provided.

Table 3.2: SHAPE AND SCALE FACTOR PARAMETERS [26]

		T_1	T_2	D_1	D_2	Cap
n=N_{min}	η	5.1e3	110	3.1e3	5.5e3	147
	β	3.38	3.15	3.43	3.37	58
n=N_{min}+N_{red}	η	5.2e3	117.1	3.2e3	5.6e3	309
	β	3.36	3.15	3.38	3.37	42.2

Considering the MMC with the given characteristic in Table 3.1. The mission profile method is well-established and has not been repeated here [7, 16, 26, 27]. The second row of the Table 3.2 is added for LS-ARS. If one redundant SM is used, the output parameters improve because the voltage stress decreases across all the SMs validated in Table 3.2. To evaluate the system-level reliability of the MMC, these numbers should be converted into failure probability density function as well as reliability outputs as follows:

$$\begin{cases} f(t) = \frac{\beta}{\eta}(\frac{t}{\eta})^{\beta-1} e^{-(\frac{t}{\eta})^{\beta}} \\ R(t) = 1 - \int_0^t f(t)dt = e^{-(\frac{t}{\eta})^{\beta}} \end{cases} \tag{3.14}$$

where f(t) is the failure probability density function, and R(t) is the reliability of the components. Within the structure of the HB-SM, there are five components, including two IGBTs (T_1 and T_2), two body diodes for semiconductors (D_1 and D_2), and a capacitor bank (Cap). The successful operation of the SM requires that all these components remain healthy, as expressed by equation (3.15).

$$R_{\mathrm{SM}}(t) = \prod R_{\mathrm{k}}(t), \mathrm{k} = \mathrm{T_1}, \mathrm{T_2}, \mathrm{D_1}, \mathrm{D_2}, \mathrm{Cap} \tag{3.15}$$

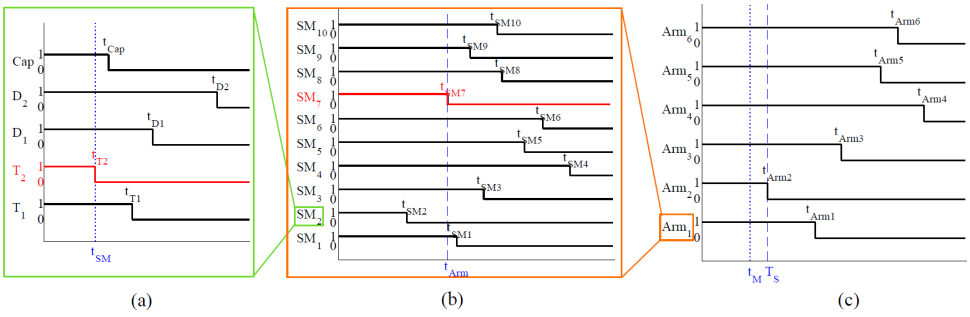

Figure 3.8: Operating cycle of MMC with FL-ARS applying mission profile method at (a) SM, (b) Arm, and (c) MMC levels.

The methodology of applying MCS for the mission profile method in the case of FL-ARS at arm level is presented in Fig. 3.8. As shown in Fig. 3.8 (a), by applying the equation (3.12) using the data in Table 3.2, each component that fails faster (in this case T2), it is considered as the lifetime of that SM. Then, assuming that FL-ARS is the arm-level redundancy type shown in Fig. 3.8 (b), where there are 10 SMs, the second failure (in this case, SM_7) is the lifetime of that arm, and the same strategy for the MMC shown in Fig. 3.8 (c) where t_M is compared with T_s to estimate the reliability of the MMC.

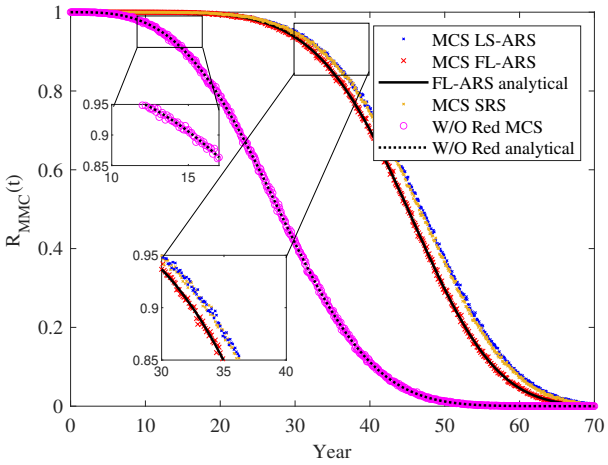

Figure 3.9: MCS results (10,000 trials) compared to analytical methods for mission profile method.

In Fig. 3.9, the reliability of the MMC using the mission profile method with different redundancy strategies is presented by applying MCS. The analytical equations for the MMC without redundancy (dashed-black line) and FL-ARS (solid-black line) are available to validate the MCS's effectiveness. Analytical equations for LS-ARS and SRS that apply the mission profile method are unaddressed due to mathematical challenges. However, by applying the MCS technique, the reliability of the MMC can be estimated. Besides the validation by analytical equations for FL-ARS and without redundancy, note that in the MIL method, the superiority of the redundancy strategies is consequently LS-ARS, SRS, and FL-ARS. The same trend can be seen in the case of the mission profile MCS outputs.

3.4.2. MAINTENANCE CONSIDERING AGING EFFECTS IN HVDC

To assess the advantage of MCS over analytical equations, this part is designed to simulate real-life scenarios in the context of HVDC-MMC. In HVDC-MMC, operations and maintenance (O&M) are crucial for ensuring continuous functionality. This involves replacing faulty SMs with new ones. However, after each maintenance cycle, a combination of SMs operated without failure, and new SMs replaced the faulty ones. Analytically evaluating the reliability of MMC under such circumstances is challenging. Therefore, MCS emerges as a potent solution. Through MCS, it becomes feasible to determine the optimal number of redundant SMs required in each arm, ensuring uninterrupted MMC operation. Moreover, the MCS methodology empowers us to estimate the annual frequency of maintenance, the number of faulty SMs, and how often staff intervention is needed.

This study adopts a dynamic preventive maintenance strategy based on the number of active SMs in each arm of the system. For this purpose, the hot-reserved redundancy is detailed in sections 3.2 A and 3.4 A. Also, for maintenance applications, aging effects are considered by applying a variable failure rate outlined in section 3.3 (mission-profile

equation (3.12)). In dynamic preventive maintenance, If there is only one active SM in an arm, replacement should be initiated after the first failure occurs in that specific arm. Maintenance should be performed after the second failure when two redundant SMs are in each arm. It's crucial to note that if faulty SMs are present in other arms, they should also be replaced. Similarly, when each arm contains three redundant SMs, maintenance should be conducted after the third failure, along with replacing faulty SMs in other arms. This maintenance approach ensures the operational continuity of the MMC, as there will always be at least a minimum number (N_{min}) of operational SMs available.

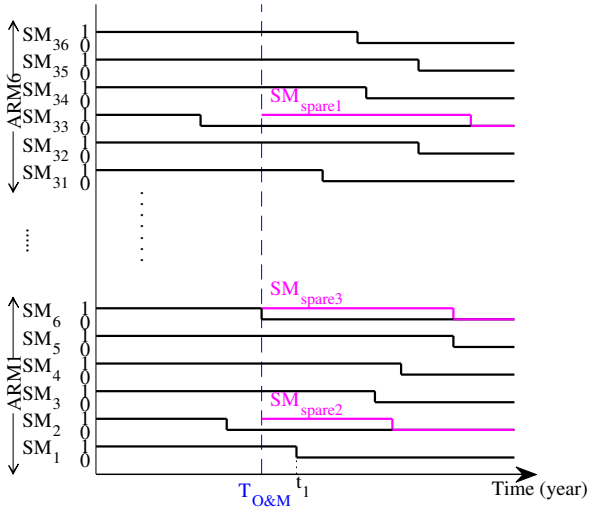

Figure 3.10: Operating cycle of the MMC considering dynamic maintenance with 6 SMs in each arm, including two active redundant SMs (N_{min} = 4, N_{red} = 2).

To enhance understanding of MCS working principles, Fig. 3.10 is included in this study. For simplicity, the figure considers an MMC configuration with six SMs in each arm, of which two are redundant. The results illustrated in Fig. 3.10 depict a trial scenario where the initial two failures occurred in arm 1, and arm six had previously encountered one failure (assuming no failures in other arms). Consequently, maintenance will be conducted shortly after the second failure in arm 1, replacing three faulty SMs with spare ones. It's essential to emphasize that this trial should be repeated multiple times to ensure statistically reliable results. Taking an example of the MMC in [27] with

Table 3.3: SHAPE AND SCALE FACTOR PARAMETERS [27]

	T_1	T_2	D_1	D_2	Cap
η	836	37.2	495	378	63.6
β	2.58	2.42	2.57	2.54	14.7

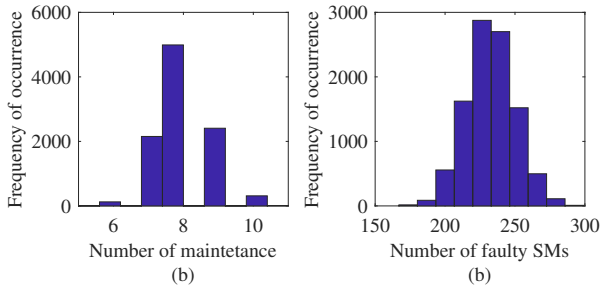

Figure 3.11: MCS results (10,000 trials) for MMC with $N_{\text{min}} = 200$ and $N_{\text{red}} = 8$ (in 20 years) (a) the distribution of the estimated number of required O&M with $\mu = 8$ and $\sigma = 0.798$ (b) the distribution of the estimated number of SMs that will be replaced with $\mu = 233$ and $\sigma = 17.43$.

$N_{\text{min}} = 200$ and $N_{\text{red}} = 8$, the MCS results are presented in Fig. 3.11. The data (such as β and η for each component) used for this evaluation are all adopted from [27] given in Table 3.3. In Fig. 3.11 (a), it is estimated that within 20 years of operation, eight times of maintenance is required for this particular MMC. Furthermore, Fig. 3.11 (b) shows that the estimated number of potential SM failures that will be replaced with new SMs within the same period is around 233 SMs.

3.5. COMPUTATION TIME

Fig. 3.12 presents the computation time of MCS concerning the number of trials compared to the analytical solution for different redundancy strategies for the MMC. The results indicate that SRS has a higher computation time compared to FL-ARS, and this difference grows as the number of trials increases.

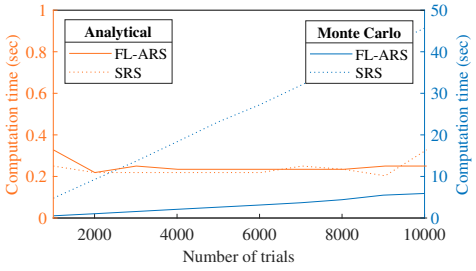

Figure 3.12: Analytical and MCS computation time outputs for SRS and FL-ARS with varying trials.

Fig. 3.13a shows that MCS has comparable computation time independent of N_{min} for FL-ARS and $N_{\text{min}} > 20$ for SRS. On the other hand, Fig. 3.13b shows that a higher level of redundancy results in increased MCS computation time.

In our study, we compared the computation time of MCS using two different computers, Computer 1 (Laptop) and Computer 2 (PC). Computer 1 had a standard configuration with an 11th Gen Intel(R) Core(TM) i7-1185G7 @ 1.80 GHz, 16 GB RAM, and a

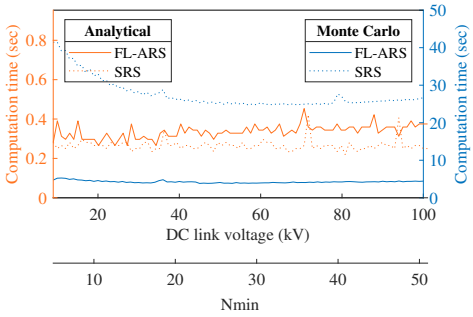

(a)

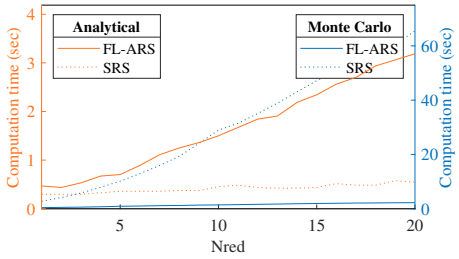

(b)

Figure 3.13: Analytical and MCS computation time outputs for SRS and FL-ARS with (a) varying number of levels for 10000 trials, (b) varying number of redundancy ($N_{\text{min}} = 51$).

512 GB SSD, while Computer 2 had an upgraded configuration with 12th Gen Intel(R) Core(TM) i5-12500 @ 3.00GHz, 8 GB RAM, and a 512 GB SSD. We ran the same Monte Carlo Simulation on both computers, and the results clearly demonstrated that Computer 2 showed significantly better performance in terms of computation time. The upgraded configuration of Computer 2, with a faster processor, allowed it to process the simulation faster, resulting in 35 % reduced computation time compared to Computer 1.

Table 3.4: MCS COMPUTATION TIME OF SRS AND FL-ARS FOR 10000 TRIALS WITH DIFFERENT COMPUTER

	Computer 1 (sec)	**Computer 2 (sec)**
SRS	45.672	27.89
FL-ARS	5.906	4.25

3.6. CONCLUSION

This chapter proposed a detailed procedure for applying MCS with different redundancy strategies for MMC. MCS is particularly useful for MMC maintenance, where analytical methods fall short—because after each maintenance, the system consists of a mix

of aged and new components, making it difficult to model failure behavior analytically. Also, the reliability of the MMC with SRS and LS-ARS using the mission profile method, which was unaddressed, can be easily estimated by applying MCS. Additionally, the error in applying MCS is found to be less than 1% when the number of trials exceeds 10,000. The results of the MCS are compared with the analytical method to validate the derived reliability assessment methods. MCS with FL-ARS took significantly lower computation time than SRS, particularly for more trials. For example, for 10,000 trials, it took approximately 45 s for SRS while only about 6 s for FL-ARS with $N_{\min} = 5$. It is interesting to observe that MCS for MMC with more SMs has comparable computation time, particularly when N>20. For example, it still takes approximately 6 s for FL-ARS with 10 times higher SMs ($N_{\min} = 50$ for 10,000 trials). While an increase in redundancy results in a higher computation time, particularly for SRS. Overall, the proposed MCS approach provides a valuable tool for analyzing the performance of MMC systems. It can help engineers optimize the reliability-based design by digitizing such systems and plan application-dependent preventive maintenance, which is impossible with analytical equations.

REFERENCES

[1] A. Sangwongwanich and F. Blaabjerg, *Monte carlo simulation with incremental damage for reliability assessment of power electronics,* IEEE Transactions on Power Electronics **36** (2021).

[2] H. Wang, M. Liserre, and F. Blaabjerg, *Toward reliable power electronics: Challenges, design tools, and opportunities,* IEEE Industrial Electronics Magazine **7**, 17 (2013).

[3] H. Huang and P. A. Mawby, *A lifetime estimation technique for voltage source inverters,* IEEE Transactions on Power Electronics **28**, 4113 (2013).

[4] *Reliability Prediction of Electronic Equipment: MIL-HDBK-217D.*, Military standardization handbook (Department of Defense, 1983).

[5] N. Shahidirad, M. Niroomand, and R.-A. Hooshmand, *Investigation of pv power plant structures based on monte carlo reliability and economic analysis,* IEEE Journal of Photovoltaics **8** (2018).

[6] A. S. Nazmul Huda and R. Živanović, *Study effect of components availability on distribution system reliability through multilevel monte carlo method,* IEEE Transactions on Industrial Informatics **15**, 3133 (2019).

[7] L. Wang, J. Xu, G. Wang, and Z. Zhang, *Lifetime estimation of igbt modules for mmc-hvdc application,* Microelectronics Reliability **82**, 90 (2018).

[8] P. Jirutitijaroen and C. Singh, *Comparison of simulation methods for power system reliability indexes and their distributions,* IEEE Transactions on Power Systems **23**, 486 (2008).

[9] P. Tu, S. Yang, and P. Wang, *Reliability- and cost-based redundancy design for modular multilevel converter,* IEEE Transactions on Industrial Electronics **66**, 2333 (2019).

[10] D. Zhou, H. Wang, and F. Blaabjerg, *Mission profile based system-level reliability analysis of dc/dc converters for a backup power application,* IEEE Transactions on Power Electronics **33** (2018).

[11] T. Zhang, X. Chen, Z. Yu, X. Zhu, and D. Shi, *A monte carlo simulation approach to evaluate service capacities of ev charging and battery swapping stations,* IEEE Transactions on Industrial Informatics **14**, 3914 (2018).

[12] M. Novak, A. Sangwongwanich, and F. Blaabjerg, *Monte carlo based reliability estimation methods in power electronics,* in *IEEE 21st Workshop on Control and Modeling for Power Electronics* (2020).

[13] J. V. M. Farias, A. F. Cupertino, V. d. N. Ferreira, H. A. Pereira, S. I. Seleme, and R. Teodorescu, *Reliability-oriented design of modular multilevel converters for medium-voltage statcom,* IEEE Transactions on Industrial Electronics **67**, 6206 (2020).

[14] Y. Zhang, H. Wang, Z. Wang, F. Blaabjerg, and M. Saeedifard, *Mission profile-based system-level reliability prediction method for modular multilevel converters,* IEEE Transactions on Power Electronics **35**, 6916 (2020).

[15] R. Billinton and R. Karki, *Application of monte carlo simulation to generating system well-being analysis,* IEEE Transactions on Power Systems **14**, 1172 (1999).

[16] R. K. Gatla, W. Chen, G. Zhu, D. Zeng, and R. Nirudi, *Lifetime estimation of modular cascaded h-bridge mlpvi for grid-connected pv systems considering mission profile,* Microelectronics Reliability **88-90**, 1051 (2018).

[17] H. Liu, K. Ma, Z. Qin, P. C. Loh, and F. Blaabjerg, *Lifetime estimation of mmc for offshore wind power hvdc application,* IEEE Journal of Emerging and Selected Topics in Power Electronics **4**, 504 (2016).

[18] X. Xie, H. Li, A. McDonald, H. Tan, Y. Wu, T. Yang, and W. Yang, *Reliability modeling and analysis of hybrid mmcs under different redundancy schemes,* IEEE Transactions on Power Delivery **36**, 1390 (2021).

[19] G. Abeynayake, G. Li, T. Joseph, J. Liang, and W. Ming, *Reliability and cost-oriented analysis, comparison and selection of multi-level mvdc converters,* IEEE Transactions on Power Delivery **36**, 3945 (2021).

[20] M. Ahmadi, A. Shekhar, and P. Bauer, *Switch voltage rating selection considering cost-oriented redundancy and modularity-based trade-offs in modular multilevel converter,* IEEE Transactions on Power Delivery , 1 (2023).

[21] J. Xu, H. Jing, and C. Zhao, *Reliability modeling of mmcs considering correlations of the requisite and redundant submodules,* IEEE Transactions on Power Delivery **33**, 1213 (2018).

[22] J. E. Huber and J. W. Kolar, *Optimum number of cascaded cells for high-power medium-voltage ac–dc converters,* IEEE Journal of Emerging and Selected Topics in Power Electronics **5**, 213 (2017).

[23] M. Ahmadi, A. Shekhar, and P. Bauer, *Impact of the various components consideration on choosing optimal redundancy strategy in mmc,* in *2022 IEEE 20th International Power Electronics and Motion Control Conference (PEMC)* (2022) pp. 21–26.

[24] R. Billinton and R. N. Allan, *Reliability evaluation of engineering systems: concepts and techniques,* (1992).

[25] J. Guo, X. Wang, J. Liang, H. Pang, and J. Gonçalves, *Reliability modeling and evaluation of mmcs under different redundancy schemes,* IEEE Transactions on Power Delivery **33** (2018).

[26] M. Ahmadi, F. Kardan, A. Shekhar, and P. Bauer, *Reliability assessment of modular multilevel converters: A comparative study of mil and mission profile methods,* in *13th International Conference on Integrated Power Electronics Systems* (2024).

[27] J. Xu, L. Wang, Y. Li, Z. Zhang, G. Wang, and C. Hong, *A unified mmc reliability evaluation based on physics-of-failure and sm lifetime correlation,* International Journal of Electrical Power Energy Systems **106**, 158 (2019).

4

COST-ORIENTED REDUNDANCY AND MODULARITY-BASED DESIGN OF MMC

This chapter introduces methods for designing MMCs by considering cost-oriented redundancy and modularity-based trade-offs. MMCs are favored for medium to high-voltage applications due to their modularity, scalability, high efficiency, and superior harmonic performance. However, higher modularity increases the risk of failure. Therefore, cost-effective design for reliability by balancing modularity and redundancy is crucial. This chapter reviews existing literature and proposes a comprehensive methodology to optimize switch voltage ratings, considering capital investment, operational losses, and reliability.

This chapter is based on:

- M. Ahmadi, A. Shekhar and P. Bauer, "Switch Voltage Rating Selection Considering Cost-Oriented Redundancy and Modularity-based Trade-offs in Modular Multilevel Converter," in IEEE Transactions on Power Delivery, 2023.

4.1. INTRODUCTION

The extensive interconnection of power electronics-based systems into power grids affects the system's reliability. MMC is a promising candidate due to its modularity, scalability, high efficiency, and superior harmonic performance [1]. However, higher modularity consequently increases the number of components in the system, thereby influencing the risk of failure [2]. Therefore, the cost-effective design for reliability by considering the trade-off between modularity and redundancy is important [3].

For the MMC design, reliability and cost-based methods by only considering redundancy are reported in [4–7]. In [4], the cost-based model of the MMC with two redundancy strategies is evaluated, and it is presented that standby redundancy has a lower cost than active redundancy. Authors in [5] present an optimization method by considering the cost and redundancy aspects of the MMC with hybrid SMs. In [6], a method is proposed that provides reliability indices to plan periodic preventive maintenance for the MMC in off-shore applications. In [7], three converter topologies, including 2-level, 3-level neutral-point-clamped (NPC) and MMC with fixed switch voltage rating of 4.5 kV are compared for Medium Voltage (MV) applications. Analysis of [7] shows that using 3-level NPC is the most economical when the rated current is below 400 A and DC link voltage is below 56 kV. If the rated current is in the range of 500 A-700 A and DC link voltage is above 46 kV, MMC is the most cost-efficient choice. Likewise, for the current rated above 700 A, regardless of DC link voltage, MMC is the most cost-efficient converter. The design of the MMC that only focuses on redundancy are well-explored in [8–12], where the system reliability is improved by applying different redundancy strategies. For instance, in [9], a redundancy strategy is proposed where the redundant SMs can be shared among all arms. It is presented that with this redundancy strategy, the number of required redundant SM is decreased by 33 % compared to the conventional redundancy strategies.

Modularity (switch voltage rating) is another factor in the MMC that can play an important role in the reliability and cost (initial investment and operational loss) aspects. Few works [13–16] have reported on the design of the MMC by considering modularity aspects of the MMC. In [13], a mission profile method is proposed to design the 17 MW 28 kV DC link MMC with the focus on modularity to suggest that SM with switches of 3.3 kV voltage rating are the most reliable and cost-efficient choice as compared to other market available ratings. The impact of redundancy is considered in [14], and it is suggested that 3.3 kV switch is the optimal choice for line-to-line AC side voltages between 22 kV and 58 kV in an MV cascaded H-bridge AC-DC converter. In [15], the reliability of the MMC by applying individual IGBT SM using Hipak style IGBTs, and series valve SM using press-pack IGBT are compared. It is shown that using Hipak style IGBTs has the lowest conduction losses, while for the first few operational years, presspack IGBTs are more effective in preventing the arm's voltage from decreasing, and the need for installing redundant SMs decreases. [16] compares the semiconductor with different rated voltages to find the optimum choice based on SM utilization and losses for HVDC applications. Authors conclude that HVDC in the power range below 900 MW, 4.5 kV switch is optimal. For the power range between 900 and 1000 MW, both switches with rating voltage of 4.5 kV and 6.5 kV have similar performance, while the switch with a rating voltage of 6.5 kV is optimal for power range above 1000 MW.

Table 4.1 summarizes and compares the existing literature with the proposed method.

Table 4.1: COMPARISON OF THE EXISTING LITERATURE AND PROPOSED STUDY FOR MMC DESIGN

Reference	Mod†	Red‡	Cost	Varying DC link vol	Varying loading
[13]	✓		✓		✓
[14]	✓	✓		✓	
[7]		✓	✓	✓	✓
[16]	✓	✓	✓		
[4–6]		✓	✓		
[8–12]		✓			
Current study	✓	✓	✓	✓	✓

† Modularity ‡ Redundancy

In this chapter, both concepts of redundancy and modularity, which are two aspects of reliability in the MMC, are combined to suggest the optimum voltage rating of the switch. Concerning costs, the insights of [13] are extended by considering the costs associated with redundancy and its corresponding sensitivity to different system parameters such as DC link voltage, average converter loading, required lifetime, and energy price. This chapter aims to quantitatively establish the trade-off between the impact of higher modularity on converter reliability corresponding to the redundancy costs for the given lifetime requirements while considering the operational efficiency. The key contributions of this chapter are as follows:

- Quantify the MMC's trade-off between modularity and redundancy by varying the SM switch rating and suggesting the optimal number of levels for the given DC link voltage and operating power considering the capital cost, efficiency, and reliability.
- Derive a generalized insight on selecting the optimal switch rating considering the above trade-off with varying DC link voltage, power rating, average loading, required lifetime, failure rate (FR), components cost, and energy price.
- It also investigates the influence of using two different methodologies (Military Handbook (MIL-HDBK) and FIDES) for calculating the FR of components and the effect of various current ratings.

The remainder of the chapter is organized as follows. Section 4.2 gives the system's characteristics and the method for analyzing the MMC reliability. Section 4.3 defines a case study and evaluates the system's cost, reliability, and efficiency. Sensitivity analysis is carried out in Section 4.4. In Section 4.5, the general application proposed in this chapter is recommended, and the conclusions are given in Section 4.6.

4.2. SYSTEM DESCRIPTION AND RELIABILITY DESIGN

This section provides a system description and the methodology for evaluating the reliability.

4.2.1. MODULARITY DESIGN

The general configuration of the MMC with half-bridge (HB) SM is presented in Fig. 2.1. In this chapter, as an example, the considered MMC system has rated power (S_n) of 10 MVA with line voltage (V_g) of 8.16 kV. The DC link voltage (V_{dc}) can be estimated by [14]:

$$V_{dc} = \frac{2\sqrt{2} \times V_s}{\sqrt{3} \times m} \tag{4.1}$$

where m is the modulation index and it is equal to 0.96, V_s is the RMS of line-to-line voltage equal to $\sqrt{3}/\sqrt{2}\ V_g$. As it was defined in (1.1), the minimum number of required SMs (N_{min}) in each arm depends on the selected power switch rating. Besides this, the maximum value of SM capacitors voltage ripple k_{max} needs to be considered (which in this study is equal to 10 %).

In this chapter, the safety factor equals 0.65, which is in the range of maximum steady state voltage of IGBT [16]. A design element that plays a crucial role in the cost, reliability, and operation of MMC is the SM capacitor. The time-average stored energy and peak value of capacitor voltage are needed to determine the SM's capacitor. According to [17], the required capacitor is given by:

$$C_{SM} = \frac{N_{min} \times S_n \times W_{MMC}}{3(k_{max} V_{dc})^2} \tag{4.2}$$

where W_{MMC} is the required energy storage per MVA that is approximately 40 kJ/MVA as defined in [18].

The operating switching frequency (f_{sw}) is chosen in this study such that the effective frequency ($f_{eff} = N_{min} \times f_{sw} \approx 3$ kHz) is constant for the chosen switch rating with the given DC link voltage. This ensures that the harmonic performance of the designed converter is compliant with IEEE 519 with similar power quality for the same arm/filter inductance when different switch ratings and hence the number of levels are selected [19]. Correspondingly, the varying switching and conduction losses for various operating frequencies and the number of levels can be calculated while ensuring that harmonic performance is the same for the given DC link voltage. Table 4.2 summarizes the number of SMs per arm, SM capacitance, and switching frequency, which are all defined based on the withstand voltage of the IGBT module (V_{IGBT}).

Table 4.2: MMC PARAMETERS FOR FIVE DIFFERENT SWITCHES RATING

V_{IGBT} (kV)	V_{dc} **(kV)** (4.1)	N_{min} (1.1)	f_{sw} **(Hz)**	C_{SM} **(mF)** (4.2)	$V_{SM,av}$ **(kV)** (4.3)	$S_{f,act}$ (4.4)
1.2	17	24	125	9.2	0.71	0.650
1.7	17	17	177	6.5	1.00	0.647
3.3	17	9	334	3.4	1.89	0.629
4.5	17	7	429	2.7	2.43	0.594
6.5	17	5	600	1.9	3.40	0.575

Herein, N_{min} is given by (1.1) and the average operating SM voltage ($V_{SM,ave}$) is given

by (4.3).

$$V_{\text{SM,ave}} = \frac{V_{\text{dc}}}{N_{\text{min}}} \tag{4.3}$$

Consequently, the actual operating safety factor ($S_{\text{f,act}}$) associated with maximum SM voltage is given by (4.4),

$$S_{\text{f,act}} = \frac{k_{\text{max}} V_{\text{SM,ave}}}{V_{\text{IGBT}}} \tag{4.4}$$

As observed, $S_{\text{f,act}}$ is closer to the initial design value S_{f} for a lower switch rating due to the impact of ceiling function in (1.1). Consequently, it results in a slightly lower switch utilization and SM FR with higher switch ratings. This effect is reduced when a second ceiling function is applied with redundancy requirements for the given B_{10} lifetime, as discussed in the subsequent section. Furthermore, the difference in switch utilization in trade-off with reliability is further reduced for higher DC link voltages as shown in Fig. 4.1.

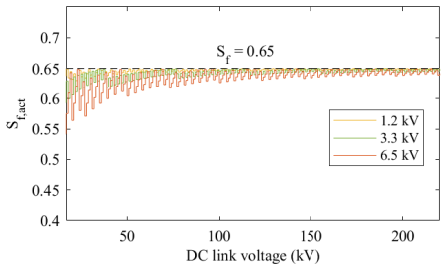

Figure 4.1: The actual safety factor value with varying DC link voltage.

4.2.2. RELIABILITY DESIGN

The FR of the MMC components within the MMC needs to be evaluated for reliability analysis. Also, redundancy as a fault-tolerant strategy is applied to increase the MMC reliability [20]. The following scrutinizes the FR of power components and the redundancy effect.

FR CALCULATION

In MMC, SMs construct the arms; its configuration is shown in Fig. 2.1. The SM comprises two IGBTs, a capacitor bank, and auxiliary components [8]. The FR of the switches and capacitor can be calculated as given in chapter 2 section 2.2 by using equations from the MIL-HDBK [21].

In this chapter, it is assumed if the MMC is not operating (0% loading), the junction temperature of the capacitor and IGBT is equal to the ambient temperature (25^o C), and If it operates at full load (100% loading), the junction temperature is 100^o C. So, the junction temperature can be estimated at any chosen loading by using the thermal model and mission profile, which relate power losses to temperature rise based on the load-dependent switching and conduction losses over time. $V_{\text{operating}}$ and V_{rated} are the actual and nominal voltage across the capacitor, respectively.

REDUNDANCY EVALUATION

Redundancy as a fault-tolerant strategy is applied to have a normal post-fault operation without degradation [22]. Different redundancy strategies are explored in chapter 3, and the optimal redundancy choice depends on many factors such as efficiency, dynamics, and economics. This chapter applies the fixed-level active redundancy strategy (FL-ARS) [4, 7, 14]. In this redundancy strategy, the number of operating SMs within the arm always equals $N_{\min}$ to recall FL-ARS working mode. However, in this operating mode, all the SMs (n) are energized, but the triggering signal is only sent to random $N_{\min}$ SMs. Hence, all the SMs take turns operating. In this redundancy strategy, triggered SMs could be either original or redundant [14]. In the FL-ARS operational state, if N_{red} = n-$N_{\min}$ is the number of redundant SMs in each arm, the reliability of the arm can be calculated by applying k-out-of-n given in chapter 3 [23].

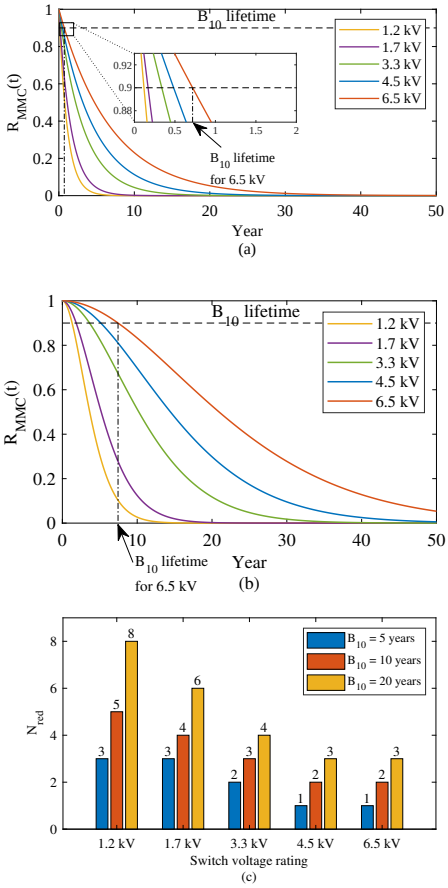

Figure 4.2: Reliability results of 10 MW 17 kV DC link MMC with 57% loading, (a) reliability output for different switch voltage rating with no redundancy, (b) reliability output for different switch voltage rating with one redundant SM in each arm, and (c) number of required redundant SM in each arm to meet B_{10} lifetime requirement of 10 years.

RELIABILITY INDEX

In this study, the percentage of the lifetime B_α is used, which determines what percentage of devices fail at the time as (4.5):

$$F_{\text{MMC}}(B_\alpha) = 1 - R_{\text{MMC}}(B_\alpha) = \frac{\alpha}{100} \tag{4.5}$$

where unreliability function F_{MMC} represents the proportion of population failure. B_{10} lifetime is expressed as the required time to reach 90% of the system's reliability (or 10% of devices fails). Hence, the number of redundant SMs is selected in the design process to reach the required B_{10} lifetime. Table 4.3 shows the B_{10} lifetime of the MMC without redundancy and having one redundant SM in each arm with different switch ratings (obtained from Fig. 4.2 (a) and (b) respectively). According to [4, 7, 24, 25], the required

Table 4.3: OBTAINED B_{10} LIFETIME IN YEARS (FIG. 4.2 (A) AND (B)) FOR 10 MW 17 KV DC LINK MMC WITH DIFFERENT SWITCH RATINGS

Switch ratings		**1.2 kV**	**1.7 kV**	**3.3 kV**	**4.5 kV**	**6.5 kV**
B_{10} lifetime	No red*	0.12	0.17	0.34	0.48	0.72
	One red	1.31	1.85	3.63	5.14	7.44

*red: redundancy

lifetime of power electronic systems can vary from 2 years to more than 30 years. Still, the necessary lifetime in most applications falls between 5 to 20 years. Hence, this work considers B_{10} lifetime of 10 years as the reliability index for determining the number of redundant SMs in each arm. Additionally, the sensitivity analysis will be carried out in the case if the required B_{10} lifetime is 5 and 20 years.

Fig. 4.2 (a) and (b) show the reliability of the MMC with different switch voltage ratings at 57% loading with no redundancy and only one redundant SM in each arm, respectively. It can be seen from Fig. 4.2 (a) and (b) that the inclusion of one redundant SM in the MMC with a higher switch rating improves the reliability much more than the case where a switch with a lower rating is used. However, it is essential to remember that the cost of one redundant SM, for example, for a 6.5 kV switch is higher than a 1.2 kV switch. Hence, there is a trade-off between modularity, redundancy, and cost of the MMC. The MMC's B_{10} lifetime without redundancy and one redundant SM in each arm, as shown in Table 4.3, is less than 10 years. In order to reach the required lifetime of 10 years, more redundant SMs are needed. Fig. 4.2 (c) shows the number of redundant SMs required in each arm for the MMC with various switch voltage ratings to meet the 10-year lifetime requirement at 57% loading.

4.3. CASE-STUDIES FOR COST, RELIABILITY, AND EFFICIENCY-BASED OPTIMAL SWITCH SELECTION

Concerning the total cost of the MMC, the capital investment (CI) and operational losses are considered, which are explained in the following.

4.3.1. CAPITAL INVESTMENT

Major components' costs are considered for calculating the CI of the MMC, where the dominant components are power electronics components (semiconductors, control system, power supply) and capacitor cost. Hence, the estimated CI of the power electronics components CI_{PE} is formulated as follows [13]:

$$CI_{\mathrm{PE}} = K_{\mathrm{PE}} N_{\mathrm{semi}} V_{\mathrm{IGBT}} I_{\mathrm{nominal}} \tag{4.6}$$

where I_{nominal} is the nominal or rated current of the IGBT, which in this study is calculated and equals to 480 A, N_{semi} is the total number of IGBT switches in the MMC that is equal to $N_{\mathrm{semi}} = 6 \times 2 \times n$, where n is the total number of SMs in each arm including the redundant SMs, K_{PE} is the estimated price of installed power that is equal to 3.5 €/kVA [26]. The estimated CI of capacitance (CI_{Cap}) can also be calculated from (4.7) - (4.9):

$$CI_{\mathrm{Cap}} = K_{\mathrm{Cap}} E_{\mathrm{Cap}} \tag{4.7}$$

$$E_{\mathrm{Cap}} = 6 \times n \times E_{\mathrm{Cell}} \tag{4.8}$$

$$E_{\mathrm{Cell}} = \frac{1}{2} C_{\mathrm{SM}} V_{\mathrm{SM}}^2 \tag{4.9}$$

where K_{Cap} is the estimated price of the installed capacitor equal to 150 €/kJ. Hence, the CI of the MMC can be estimated by adding the CI of installed capacitance and power electronics switches. In Fig. 4.3 (a), the CI of the MMC with different switch ratings for varying DC link voltage at 57% loading is presented. As shown in Fig. 4.3 (a), switch rating of 1.2 kV is the most economical option from the only CI point of view throughout the varying DC link voltage. The normalized price can be obtained from (4.10).

$$\text{Normalized CI}(/\,€\text{kVA}) = \frac{CI_{\mathrm{total}}}{S_{\mathrm{n}}}, (S_n \text{ in kVA}). \tag{4.10}$$

As mentioned in section 4.2, redundancy is applied to increase the MMC reliability with various modularity (Fig. 4.2 (b)). However, the cost of using redundancy and CI of the MMC differs for different switch ratings; hence, cost aspects are a determining factor in selecting the cost-efficient switch rating while the reliability requirements are met. Fig. 4.3 (b) presents the ratio of redundancy costs concerning the total CI of the MMC. As shown from Fig. 4.3 (b), applying redundancy has a lower price for higher DC link voltage ranges, while it is more costly for lower DC link voltage ranges. Also, it can be realized that the cost of applying redundancy for the MMC with higher switch voltage rating is more.

4.3.2. OPERATIONAL LOSSES

The model developed in [27] is applied to obtain the MMC's operational efficiency with various modularity levels. The physics-based methodology explained in [14] is used to estimate the switching and conduction losses of IGBTs. Also, switching and conduction losses are evaluated for varying loading. For calculating the annual energy losses (E_l) with different modularity levels, (4.11) is applied as follows:

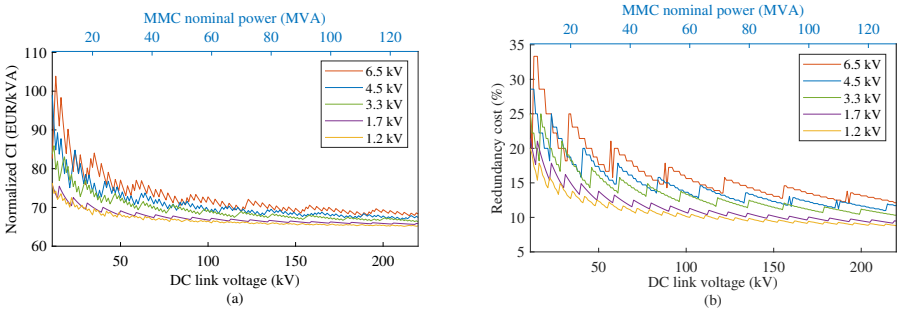

Figure 4.3: Cost results of the MMC with 57% loading, (a) normalized CI of the MMC with different switch voltage rating, (b) redundancy percentage of total CI with B_{10} = 10 years.

4

$$E_l = \int (100 - \eta(t_i)) \times P_{\text{MMC}} \tag{4.11}$$

where $\eta(t_i)$ is the efficiency of the MMC at time t_i and P_{MMC} is the MMC rated power in MW.

4.3.3. CASE STUDY FOR OPERATIONAL LOSSES

Fig. 4.4 (a) and (b) show the histogram of two Mission Profiles (MPs) used in this study based on the hourly data adapted from [28]. The average power demand (P_{ave}) of MP I and MP II is 38 % and 57 %, respectively. Fig. 4.5 presents the cumulative yearly energy

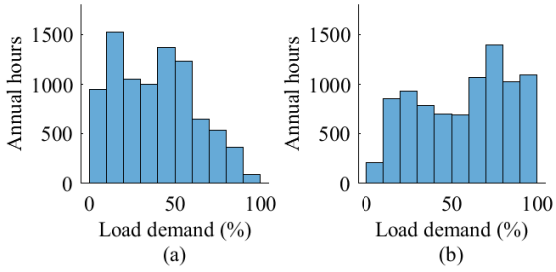

Figure 4.4: Histogram of hourly annual power demand for (a) MP I and (b) MP II.

losses for MMC with different switch ratings according to the daily power demand for two cases shown in Fig. 4.4.

Likewise, these calculations can be repeated for varying DC link voltage other than 17 kV considered. For this evaluation, the phase current is kept constant, and the DC link voltage is changing (as well as the rated power of the MMC). Since the rated current is kept constant, the same switch rating with the same character can be applied, but the number of levels, operational losses, reliability, and CI will change. In Fig. 4.6, the conduction and switching losses of the MMC are presented. Switching loss is dominant for

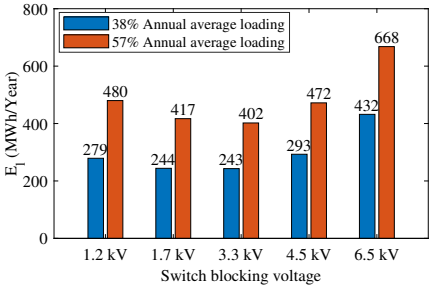

Figure 4.5: Cumulative yearly energy losses E_l for 10 MW 17 kV MMC.

4

low DC link voltages, while conduction loss is becoming the dominant factor in higher DC link voltages. Fig. 4.7 shows the total losses of the MMC for the annual loading shown in Fig. 4.4 for varying DC link voltage (with 1 kV resolution).

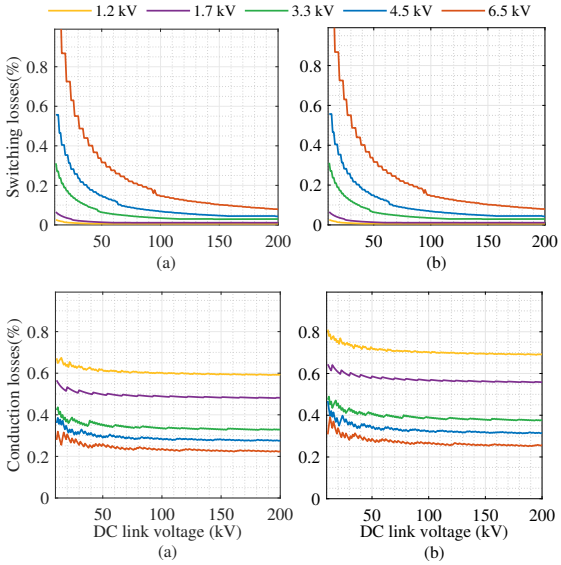

Figure 4.6: Losses of the MMC due to (a) switching losses in MP I (b) switching losses in MP II (c) conduction losses in MP I (d) conduction losses in MP II.

To better clarify the importance of annual loading, two points as P_1 and P_2 are considered from Fig 4.7. For MP I, the switch with a rated voltage of 4.5 kV is the most efficient for the DC link voltage range between $P_1 \approx 65$ kV to $P_2 \approx 157$ kV. However, this range is $P_1' \approx 62$ kV to $P_2' \approx 138$ kV when higher average loading corresponding to MP II is considered.

To generalize the scenarios mentioned in this sub-section for two different annual loading, an average annual loading point is considered, which can change from 1 % to

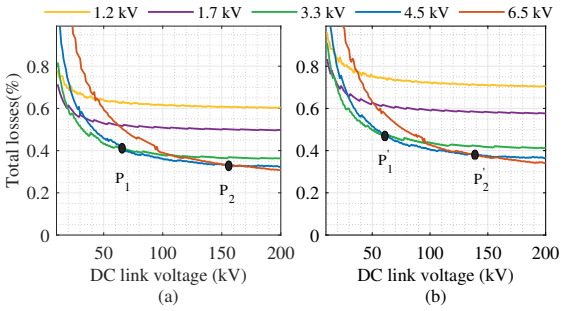

Figure 4.7: Total losses of the MMC for varying DC link voltage, (a) MP I and (b) MP II.

100 %. Fig. 4.8 shows the heat map of the most efficient switch for varying DC link voltage and annual average loading. As shown in Fig. 4.8, for a DC link voltage higher than

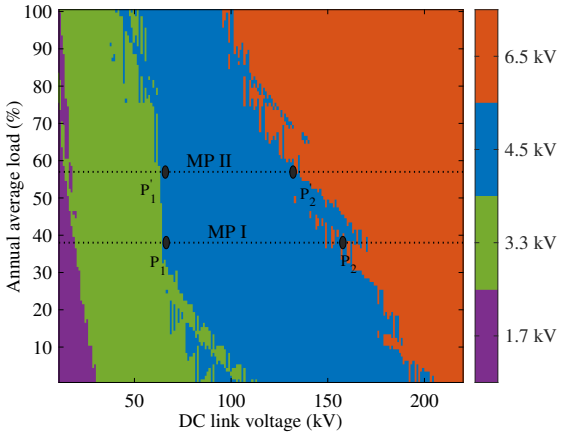

Figure 4.8: Optimal switch voltage rating choice map based on the efficiency of the MMC under various annual average loading with varying DC link voltage.

200 kV, a switch with 6.5 kV rating voltage is the most efficient choice regardless of the average loading of the converter. For lower DC link voltages, there is a trend between an optimal switch dependent on the MMC's annual average loading. From Fig. 4.8, it can be seen that higher DC link voltage leads to a shift in preference towards higher rated voltage of switch for the same average yearly loading. Likewise, for the same DC link voltage, a higher annual load leads to a shift in preference toward a higher switch voltage rating. Please note that the energy savings obtained from constant average annual loading slightly differ when MMC's hourly power demand is considered. This is shown in Fig. 4.8 as points P_1, P_2, P_1', and P_2' obtained originally from hourly power demand in Fig. 4.7. As can be seen, the points are not exactly on the boundary between switches

with 4.5 kV and 6.5 kV ratings, which is slightly different.

4.4. SENSITIVITY ANALYSIS FOR GENERALIZED SWITCH VOLTAGE RATING SELECTION

As presented, many variables are needed to determine the most economical switch for every specific DC link voltage and annual average loading. Fig. 4.9 summarizes the characteristic comparison of the MMC for three switches with rated voltage of 1.2, 3.3, and 6.5 kV. The trend shown in Fig. 4.9 is valid for all DC link voltages and annual average loading. Nevertheless, combining all these characteristics defines the most economically viable choice for the rated voltage of the switch.

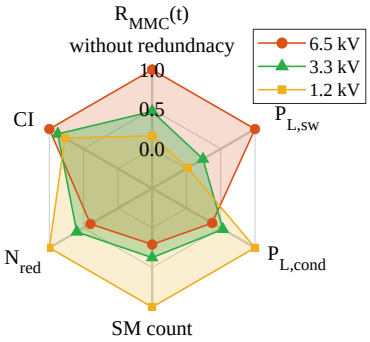

Figure 4.9: Overview of the trade-offs for 10 MW 17 kV DC link MMC affected by switch voltage rating.

A financial index must be defined to compare different rated voltages of switches and find the economic viability range of each switch in terms of DC link voltage and annual average loading. This study considers payback as the economic index for determining the most economical switch choice. Payback helps make a financial decision based on how long it takes to get profit from extra invested money. The CI and savings of the various switch choices are compared to calculate the payback as follows:

$$\text{Payback (PB)} = \frac{\Delta CI}{S_\text{i}} \tag{4.12}$$

$$S_\text{i} = \int \Delta E_i \times P_\text{t} \tag{4.13}$$

where ΔCI is the difference of CI between different switch ratings, S_i is the difference in cost saving due to efficiency, ΔE_i (kWh) is the energy saving difference, Pt is the price for electricity that in The Netherlands is equal to 0.190 €/kWh. In this study, the economic viability boundary is defined based on a considered payback time of 10 years. The steps given in the flowchart in Fig. 4.10 can be followed to find the optimum rated voltage of the switch in the MMC with specified characteristics (DC link voltage and annual load demand). The methodology for finding the cost-efficient switch rating is shown in Fig.

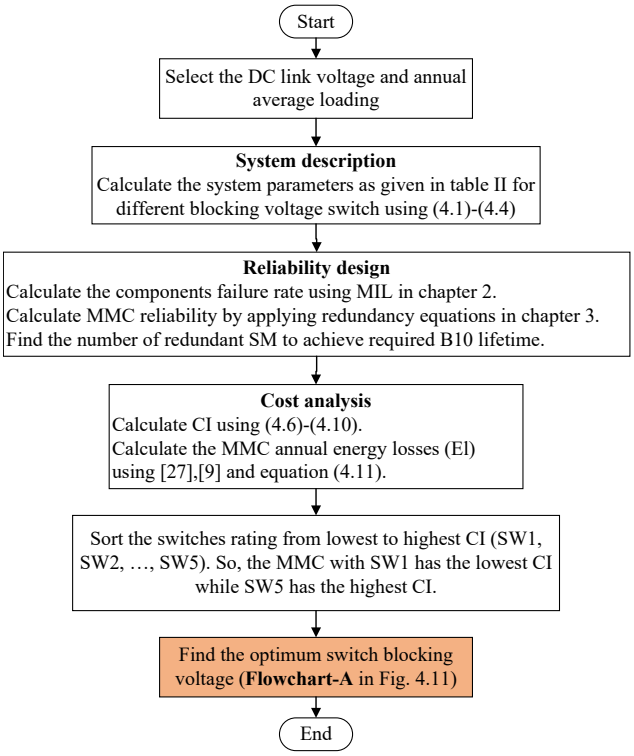

Figure 4.10: Flowchart of the proposed methodology for finding the optimum rated voltage of the switch.

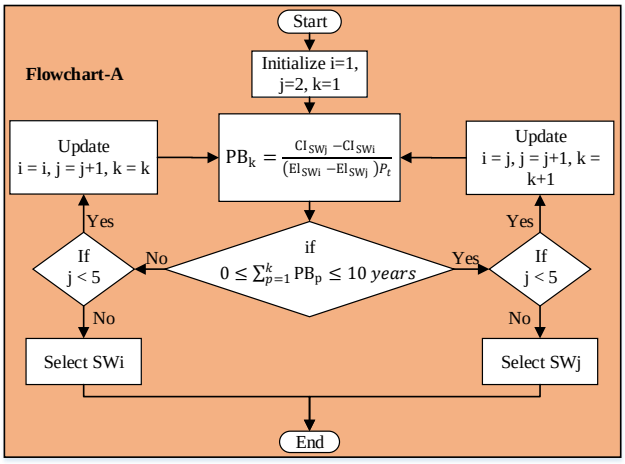

Figure 4.11: Algorithm for finding the optimum switch voltage rating among five options.

4.11. This algorithm evaluates if investing extra money in the MMC with the lowest CI to use other switch ratings could have a payback of 10 years or less.

Fig. 4.12 presents the economic viability regions among various rated voltage of switches for $B_{10} = 10$ years with varying DC link voltage and annual average loading considering a 10-year payback. Similar to the obtained heat map of efficiency, the current and voltage rating of the switches are fixed. A comparison is performed among different rated voltage of switches. Fig. 4.12 suggests that each rated voltage of the switches is more economically viable for a specific DC link voltage and loading. As presented in Fig. 4.3 (a), the MMC with a rating voltage of 1.2 kV has the lowest CI, and Fig. 4.12 shows if extra money invested in the MMC with higher switch voltage rating has a payback of 10 years or less. For instance, Fig. 4.12 suggests that if the DC link voltage is 50 kV and the expected annual loading is 50 %, extra investment in the MMC that uses a switch with a rating voltage of 3.3 kV (instead of 1.2 kV and 1.7 kV) will have a payback of 10 years or less.

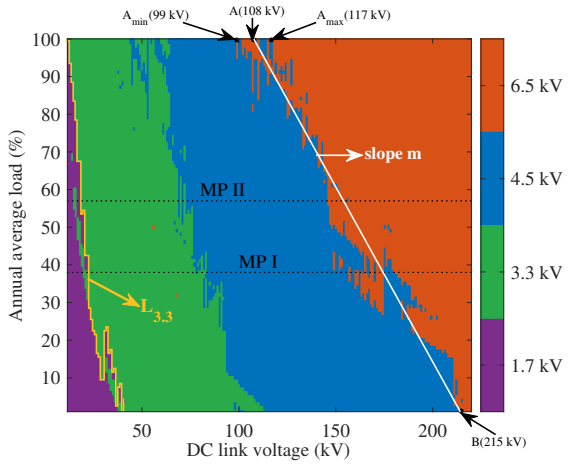

Figure 4.12: Economic viability region for different switch voltage rating with variation in MMC loading and DC link voltage considering a payback of 10 years and a required $B_{10} = 10$ years ($L_{3.3}$ is the boundary line between 1.7 kV and 3.3 kV switches).

The two considered case studies are shown with dashed black lines in which fixed load is representative of annual average loading. From Fig. 4.12 can be seen that in the case of MP II, the switch with a rated voltage of 1.7 kV is the most economical for the range of 10-22 kV DC link voltage. Regarding the case with MP I, 1.7 kV switch is economically viable for DC link voltages between 10 kV and 27 kV. Regarding extra investment in the switch with 3.3 kV rated voltage for MP II, the economically viable DC link voltage is estimated to be between 22 kV and 72 kV. For MP I, the estimated range is 27 kV to 83 kV. The same economically viable DC link range can be estimated for the switches with rated voltage of 4.5 kV and 6.5 kV. Another example is 10 MW 17 kV DC link MMC in which the switch rating of 1.7 kV is the best choice, as shown in Fig. 4.12. If the lifetime requirement is 10 years, using a switch with a 1.2 kV rating voltage results in a lower initial cost (according to Fig. 4.3). But, choosing a 1.7 kV switch leads to a 15% reduction in

operational losses (according to Fig. 4.7). Hence, in this case, the switch with the rated voltage of 1.7 kV is selected because the extra investment will have a payback of less than 10 years, and it is due to the higher efficiency.

4.4.1. SENSITIVITY ANALYSIS FOR DIFFERENT FR, B_{10} LIFETIME REQUIREMENT, COMPONENTS COST AND ENERGY PRICE

The sensitivity of the switch regions' payback to different B_{10} lifetime requirements, FR, component cost, and energy price is shown in Fig. 4.13. The boundary line ($L_{3.3}$) between economic regions of 1.7 kV and 3.3 kV switches is considered since the same trend is valid for other boundary lines between other regions.

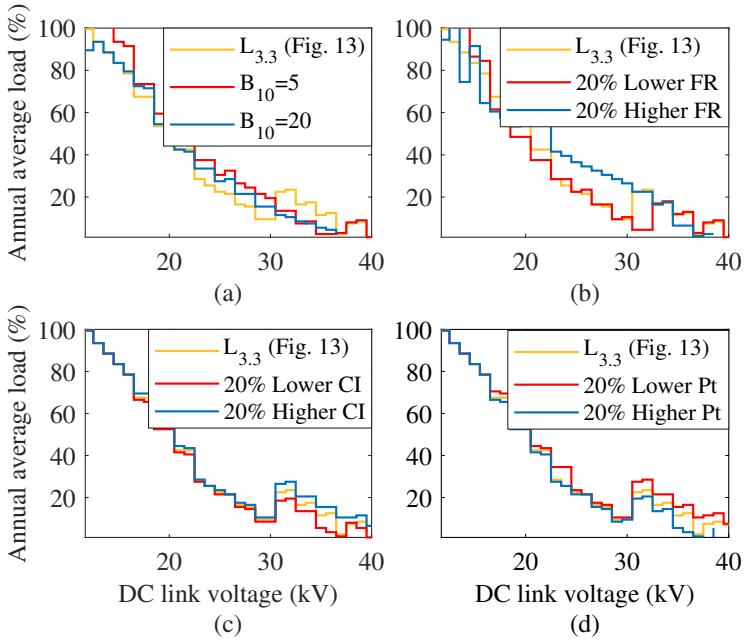

Figure 4.13: Shift in $L_{3.3}$ with change in (a) B_{10} lifetime; (b) FR; (c) capital investment (CI), and (d) electricity price (Pt).

The required B_{10} lifetime can vary from 5 to 20 years. hence, the effect of higher or lower required B_{10} lifetime is shown in Fig. 4.13 (a). As can be seen, there is no specific trend with an increase or decrease in the required B_{10} lifetime. As explained in Section 4.2 B, the methodology in MIL is used to estimate the FR of the IGBT and capacitor. However, the obtained values might not be precise as many environmental factors (π_x) can change the SM's actual FR. Moreover, there are other components within the structure of the SM, such as gate drives, control systems, and power supply, which might experience random failure. Therefore, for sensitivity analysis, the SM's FR's exact value is 20% higher and lower than the obtained values. It can be observed from Fig. 4.13 (b) that the boundary line between regions of 1.7 kV and 3.3 kV switches has a limited dependence on the FR variation.

Considering the component's cost, the dependence of the boundary line on CI is shown in Fig. 4.13 (c). It can be realized that if components are more expensive, the boundary line ($L_{3.3}$) moves upwards quite trivially, and the economic viability region of the switch with 1.7 kV rated voltage (purple) increases. However, an increase in energy price has a reverse effect on the boundary line compared to the CI presented in Fig. 4.13 (d), which is negligible.

4.4.2. SENSITIVITY ANALYSIS BY USING MIL AND FIDES

In this section, a more recent FIDES method [29] to calculate the FR of components (λ_{FIDES}) is compared with λ_{MIL} used thus far in the chapter. Unlike λ_{MIL}, λ_{FIDES} considers the technical control over manufacturing (Π_{pm}), field operation and maintenance (Π_{process}) and physical failure ($\lambda_{\text{physical}}$) that is given by (4.14) and (4.15).

$$\lambda_{\text{FIDES}} = \lambda_{\text{physical}} \times \Pi_{\text{pm}} \times \Pi_{\text{process}} \tag{4.14}$$

$$\lambda_{\text{physical}} = \sum_{i}^{\text{phases}} \left[\frac{t_{\text{annual}}}{8760} \right] \Pi_i \lambda_i \tag{4.15}$$

where t_{annual} denotes the duration of the i^{th} phase of the mission profile for one year. Π_i and λ_i are associated with environmental and operation stress-specific factors for each phase i. The complete methodology for FIDES is described in [29] and not repeated here for conciseness. Under assumptions corresponding to similar operating and environmental conditions, the estimated λ_{FIDES} compared with λ_{MIL} for the two mission profiles is shown in Table 4.4.

Table 4.4: FR OF THE CAPACITOR AND IGBT CONSIDERING MIL AND FIDES

Components	**MP**	**FR (occ/year)**	
		FIDES	**MIL**
IGBT	I	0.00052	0.0017
	II	0.00086	0.0022
Capacitor	I	0.00042	0.0009
	II	0.00068	0.0012

The sensitivity analysis is carried out to evaluate the impact of FIDES and MIL methods on the boundary line (i.e., $L_{3.3}$ in Fig. 4.12). Table 4.4 shows that the FIDES method estimates the FR of components to be lower than MIL. Therefore, the shift in the boundary line ($L_{3.3}$) between regions of 1.7 kV and 3.3 kV switches can be seen in Fig. 4.14. The sensitivity analysis represents that if the FIDES method is used for estimating the FR, the economic viability region of 1.7 kV switch expands for annual average loading of more than 30%.

4.4.3. IMPACT OF CONVERTER POWER CAPACITY

The selection of switch voltage rating for various DC link voltage and loading at a fixed rated capacity has been discussed. In this section, further evaluation is carried out to determine the most economically viable switch rating with variation in current rating and

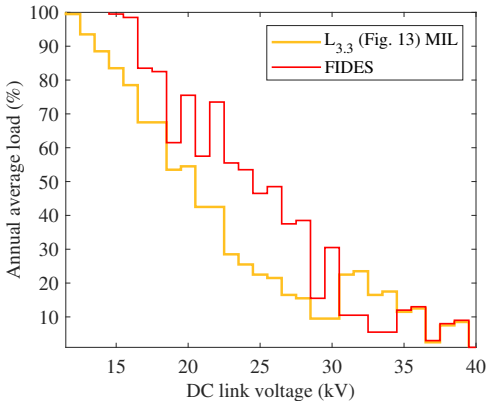

Figure 4.14: Shift in $L_{3.3}$ using FIDES and MIL to estimate the component's FR.

varying DC link voltage at 100% loading. As shown in Fig. 4.15, the MMC-rated current is changed from 480 A to 1025 A, corresponding to the converter power rating from about 6.5 MVA to 275 MVA. From Fig. 4.15, it can be observed that the switch rating selection is independent of rated current and only depends on loading and DC link voltage.

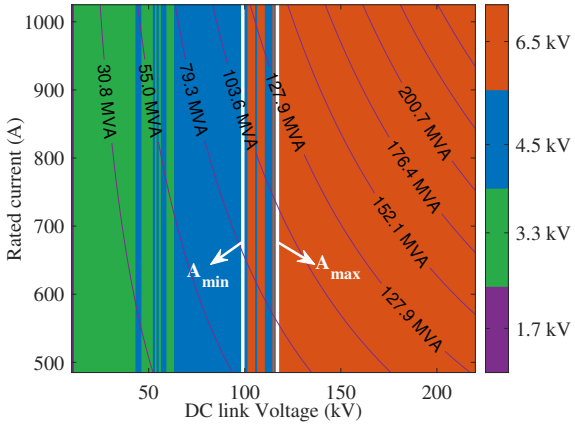

Figure 4.15: Economic viability region for different switch voltage rating with variation in MMC current rating and DC link voltage at 100% loading (i.e., 480 A, given in Fig. 4.12) considering a payback of 10 years and a required $B_{10} = 10$ years.

4.5. APPLICATION SPECIFIC RECOMMENDATIONS

MMC can be applied for different applications having different DC link voltage and current ratings [30]. The most economical switch voltage rating in these applications depends on the selected DC link voltage and loading. In this context, to generalize the

Table 4.5: THE SPECIFICATIONS OF EQUATION (4.16)

Transition	$1.7 \leftrightarrow 3.3$ kV	$3.3 \leftrightarrow 4.5$ kV	$4.5 \leftrightarrow 6.5$ kV
m	3.3×10^{-5}	2×10^{-5}	9×10^{-6}
V_{ref}	40 kV	110 kV	220 kV
Voltage range(kV)	$10 \leq V \leq 50$	$50 < V \leq 110$	$110 > V$

proposed method, equation (4.16) is derived from Fig. 4.12.

$$\begin{cases} \text{if } \frac{\text{L}}{100} + \text{m}(V - V_{\text{ref}}) \geq 0, & \text{Select the higher switch rating} \\ \text{else,} & \text{Select the lower switch rating} \end{cases} \tag{4.16}$$

4

where L is the annual average loading of the MMC in percentage, m and V_{ref} are introduced indices specified in Table 4.5, and V is the considered DC link voltage. In Fig. 4.12, a line with slope m connects two points (A, B) on boundaries between different switch ratings at 100 % and 1% loading. For instance, to find these two points between 4.5 kV and 6.5 kV switches at 100 % loading, the voltage rating is 108 kV. This voltage rating is calculated by taking the average of A_{min} and A_{max}, as shown in Fig. 4.12. Thus, points A and B coordinate (108 kV, 100%) and (215 kV, 1%), respectively. Hence, the slope m can be calculated by having these two points.

For example, in [7], the DC link voltage is 54 kV, and the annual average loading is about 60 %. Since the DC link voltage is within the range of the second column of Table 4.5, the second column values are used. After putting these values in (4.16), it suggests that the most economical rated voltage of the switch is 3.3 kV. However, 4.5 kV switch is used in [7], which is overrated and can impact the cost and efficiency of the system. Table 4.6 summarizes some of the MMC applications found in the literature and shows the optimal rated voltage of the switch using the proposed method.

Table 4.6: OPTIMAL SWITCH VOLTAGE RATINGS FOR DIFFERENT APPLICATIONS

[Ref]	**Application**	$\mathbf{V_{dc}}$	$\mathbf{S_n}$	$\mathbf{P_{l,ave}}$	$\mathbf{V_{IGBT}}$ (kV)	
		kV	MVA	%	Used	Optimal
[7]	MVDC Grid	±27	30	60	4.5	3.3
[4]	MVDC Grid	10	3	30	1.7	1.7
[5]	Wind	17	10	10-100 †	4.5	1.7/3.3
[28]	MVDC Grid	17	10	38 & 57	3.3	1.7
[13]	STATCOM	28	17	25-100 †	3.3	1.7/3.3
[15]	HVDC	±320	1000	-	4.5	6.5
[31]	Wind-HVDC	32	18	0-100 †	6.5	1.7/3.3
[32]	Wind-HVDC	160	320	-	3.3	4.5/6.5

† Variable power

4.6. CONCLUSION

This chapter presents cost-oriented reliability and modularity-based trade-offs to select an optimal rated voltage of the switch for MMC. The steps involved in the proposed method are explained through flowcharts, and a heat map is provided for varying DC link voltage and yearly loading of the MMC. It is presented that the system's modularity increases when a lower switch voltage rating is selected for the MMC SMs. For example, in a 10 MW MMC with a DC link voltage of 17 kV, a switch rating of 1.7 kV is optimal for both case studies. Higher modularity can be achieved with 1.2 kV rated voltage with a lower CI for a B_{10} lifetime of 10 years. But, when 1.7 kV switch is selected instead of 1.2 kV switch, the operational losses are approximately 15 % lower in both cases (MP I and MP II), leading to payback of less than 10 years. Higher DC link voltage leads to a shift in preference towards a higher switch rating for the same average loading. For example, the optimal choice of switch-rated voltage changes from 1.7 kV to 3.3 kV in both case studies (MP I and MP II) if the given DC link voltage is increased from 17 kV to 50 kV. Transitions between preferred switch ratings with variation in DC voltages between 10-220 kV are shown for different average loading. The sensitivity analysis shows that the preference's boundary changes from 1.7 kV to 3.3 kV switch rating shifts downward slightly with lower CI and higher energy price. However, the preferred switch choices show limited sensitivity to variation in required B_{10} lifetime and assumed FR of individual components. Also, the preference's boundary from 1.7 kV to 3.3 kV shifts downward if FIDES methodology is used for estimating the components FR.

In conclusion, this chapter proposed selection regions for the optimum rated voltage of the switch in the MMC for varying DC link voltage and yearly load demand. Sensitivity analysis shows that for MMC with fixed-level active redundancy, the variation among switches' regions has limited dependence on the precise FR value and required B_{10} lifetime. Also, it was observed that changes in CI and energy prices have a negligible effect. However, using the methodology proposed in FIDES for calculating the FR can affect the region as a specific trend was realized for annual loading higher than 30%. The potential savings of applying the method proposed in this chapter is demonstrated by presenting a generalized version of it and applying it in published works.

REFERENCES

[1] S. Du, B. Wu, and N. Zargari, *Common-mode voltage minimization for grid-tied modular multilevel converter,* IEEE Transactions on Industrial Electronics **66**, 7480 (2019).

[2] S. Yang, A. T. Bryant, P. Mawby, D. Xiang, L. Ran, and P. J. Tavner, *An industry-based survey of reliability in power electronic converters,* IEEE Transactions on Industry Applications **47**, 1441 (2011).

[3] V. de Nazareth Ferreira, A. Fagner Cupertino, H. Augusto Pereira, A. Vagner Rocha, S. Isaac Seleme, and B. de Jesus Cardoso Filho, *Design and selection of high reliability converters for mission critical industrial applications: A rolling mill case study,* IEEE Transactions on Industry Applications **54**, 4938 (2018).

[4] P. Tu, S. Yang, and P. Wang, *Reliability- and cost-based redundancy design for modular multilevel converter,* IEEE Transactions on Industrial Electronics **66**, 2333 (2019).

[5] H. Li, X. Xie, A. McDonald, Z. Chai, T. Yang, Y. Wu, and W. Yang, *Cost and reliability optimization of modular multilevel converter with hybrid submodule for offshore dc wind turbine,* International Journal of Electrical Power & Energy Systems **120**, 105994 (2020).

[6] B. Wang, X. Wang, Z. Bie, P. D. Judge, X. Wang, and T. C. Green, *Reliability model of mmc considering periodic preventive maintenance,* IEEE Transactions on Power Delivery **32**, 1535 (2017).

[7] G. Abeynayake, G. Li, T. Joseph, J. Liang, and W. Ming, *Reliability and cost-oriented analysis, comparison and selection of multi-level mvdc converters,* IEEE Transactions on Power Delivery **36**, 3945 (2021).

[8] X. Xie, H. Li, A. McDonald, H. Tan, Y. Wu, T. Yang, and W. Yang, *Reliability modeling and analysis of hybrid mmcs under different redundancy schemes,* IEEE Transactions on Power Delivery **36**, 1390 (2021).

[9] J. Guo, X. Wang, J. Liang, H. Pang, and J. Gonçalves, *Reliability modeling and evaluation of mmcs under different redundancy schemes,* IEEE Transactions on Power Delivery **33**, 2087 (2018).

[10] J. Xu, H. Jing, and C. Zhao, *Reliability modeling of mmcs considering correlations of the requisite and redundant submodules,* IEEE Transactions on Power Delivery **33**, 1213 (2018).

[11] J. Xu, P. Zhao, and C. Zhao, *Reliability analysis and redundancy configuration of mmc with hybrid submodule topologies,* IEEE Transactions on Power Electronics **31**, 2720 (2016).

[12] J. Xu, L. Wang, D. Wu, H. Jing, and C. Zhao, *Reliability modeling and redundancy design of hybrid mmc considering decoupled sub-module correlation,* International Journal of Electrical Power & Energy Systems **105**, 690 (2019).

[13] J. V. M. Farias, A. F. Cupertino, V. d. N. Ferreira, H. A. Pereira, S. I. Seleme, and R. Teodorescu, *Reliability-oriented design of modular multilevel converters for medium-voltage statcom,* IEEE Transactions on Industrial Electronics **67**, 6206 (2020).

[14] J. E. Huber and J. W. Kolar, *Optimum number of cascaded cells for high-power medium-voltage ac–dc converters,* IEEE Journal of Emerging and Selected Topics in Power Electronics **5**, 213 (2017).

[15] J. Guo, J. Liang, X. Zhang, P. D. Judge, X. Wang, and T. C. Green, *Reliability analysis of mmcs considering submodule designs with individual or series-operated igbts,* IEEE Transactions on Power Delivery **32**, 666 (2017).

[16] R. Alvarez, M. Wahle, H. Gambach, and J. Dorn, *Optimum semiconductor voltage level for mmc submodules in hvdc applications,* in *2016 18th European Conference on Power Electronics and Applications (EPE'16 ECCE Europe)* (2016) pp. 1–9.

[17] K. Ilves, S. Norrga, L. Harnefors, and H.-P. Nee, *On energy storage requirements in modular multilevel converters,* IEEE Transactions on Power Electronics **29**, 77 (2014).

[18] J. V. M. Farias, A. F. Cupertino, H. A. Pereira, S. I. S. Junior, and R. Teodorescu, *On the redundancy strategies of modular multilevel converters,* IEEE Transactions on Power Delivery **33**, 851 (2018).

[19] A. Shekhar, L. B. Larumbe, T. B. Soeiro, Y. Wu, and P. Bauer, *Number of levels, arm inductance and modulation trade-offs for high power medium voltage grid-connected modular multilevel converters,* in *2019 10th International Conference on Power Electronics and ECCE Asia (ICPE 2019 - ECCE Asia)* (2019) pp. 1–8.

[20] J. He, Q. Yang, and Z. Wang, *On-line fault diagnosis and fault-tolerant operation of modular multilevel converters — a comprehensive review,* CES Transactions on Electrical Machines and Systems **4**, 360 (2020).

[21] *Reliability Prediction of Electronic Equipment: MIL-HDBK-217D.*, Military standardization handbook (Department of Defense, 1983).

[22] K. Hu, Z. Liu, Y. Yang, F. Iannuzzo, and F. Blaabjerg, *Ensuring a reliable operation of two-level igbt-based power converters: A review of monitoring and fault-tolerant approaches,* IEEE Access **8**, 89988 (2020).

[23] R. Billinton and R. N. Allan, *Reliability evaluation of engineering systems : concepts and techniques,* (1992).

[24] J. Falck, C. Felgemacher, A. Rojko, M. Liserre, and P. Zacharias, *Reliability of power electronic systems: An industry perspective,* IEEE Industrial Electronics Magazine **12**, 24 (2018).

[25] Y. Zhang, H. Wang, Z. Wang, Y. Yang, and F. Blaabjerg, *Impact of lifetime model selections on the reliability prediction of igbt modules in modular multilevel converters,* in *2017 IEEE Energy Conversion Congress and Exposition (ECCE)* (2017) pp. 4202–4207.

[26] H. Abu Bakar Siddique, A. R. Lakshminarasimhan, C. I. Odeh, and R. W. De Doncker, *Comparison of modular multilevel and neutral-point-clamped converters for medium-voltage grid-connected applications,* in *2016 IEEE International Conference on Renewable Energy Research and Applications (ICRERA)* (2016) pp. 297–304.

[27] A. Shekhar, T. B. Soeiro, Z. Qin, L. Ramírez-Elizondo, and P. Bauer, *Suitable submodule switch rating for medium voltage modular multilevel converter design,* in *2018 IEEE Energy Conversion Congress and Exposition (ECCE)* (2018) pp. 3980–3987.

[28] A. Shekhar, T. B. Soeiro, L. Ramírez-Elizondo, and P. Bauer, *Offline reconfigurability based substation converter sizing for hybrid ac–dc distribution links,* IEEE Transactions on Power Delivery **35**, 2342 (2020).

[29] *Fides guide 2009 edition a, "reliability methodology for electronic system", fides group, france, 2004.* .

[30] M. Priya, P. Pathipooranam, and M. Kola, *Modular multilevel converter topologies and applications - a review,* IET Power Electronics **12** (2019), 10.1049/iet-pel.2018.5301.

[31] H. Liu, K. Ma, Z. Qin, P. C. Loh, and F. Blaabjerg, *Lifetime estimation of mmc for offshore wind power hvdc application,* IEEE Journal of Emerging and Selected Topics in Power Electronics **4**, 504 (2016).

[32] G. Guo, H. Wang, Q. Song, J. Zhang, T. Wang, B. Ren, and Z. Wang, *Hb and fb mmc based onshore converter in series-connected offshore wind farm,* IEEE Transactions on Power Electronics **35**, 2646 (2020).

5

MIXED REDUNDANCY STRATEGY

This chapter introduces a Mixed Redundancy Strategy (MRS). The MRS incorporates both active and spare redundant SMs, optimizing their number based on maintenance frequency and system characteristics such as DC-link voltage and loading. The chapter also addresses the economic viability of MRS, assessing investment costs, operational losses, and reliability through sensitivity analyses and Monte Carlo Simulations.

This chapter is based on:

- M. Ahmadi, A. Shekhar, and P. Bauer, "Mixed Redundancy Strategy for Modular Multilevel Converters in High-Power Applications," in IEEE Open Journal of the Industrial Electronics Society, 2024.

5.1. INTRODUCTION

Extensive research relevant to MMC's control, modeling, configuration, and protection strategies have been carried out [1, 2]. In grid-connected power electronic converters, reliability evaluation is mostly carried out by focusing on three distinctive levels, namely component [3, 4], converter, and power system, to enhance reliability. At the component level, the mission profile and physics of the components (power switches and capacitors) are targeted to improve reliability. At the converter level, RMR can be used to enhance reliability [5]. At the power system level [6–8], reliability improvement is achieved by applying different methods, such as protection and n-1 contingency design.

Safe and seamless operation of the MMC system is paramount and represents the primary focus of reliability studies. To address this concern, redundancy concepts, as outlined in various references [9–14], have been established as effective methods for ensuring normal post-operation when SMs encounter failures. It's crucial to acknowledge that implementing redundancy involves additional upfront investment and potential operational losses, comprehensively addressed in chapter 3 and 4 [15–18]. For example, in [10], a reliability model is presented for MMCs, comparing two SMs and a Reduced Nominal Voltage (RNV) mode, concluding that the individual device SM is most efficient for converter reliability and power loss. Authors in [11] introduce a reliability analysis model for hybrid MMCs and propose Equal Reliability Incremental Principles (ERIP) to optimize the design of redundant SMs, ultimately enhancing overall system reliability. Authors in [13] give detailed reliability models for hybrid MMCs in MV and HVDC applications, including active and passive redundancy schemes. In [15], a systematic criterion for selecting multi-level Voltage Source Converters (VSCs) is outlined for MV applications, considering reliability, redundancy, efficiency, and cost factors.

Table 5.1: REVIEW OF EXISTING RELIABILITY-RELATED DESIGN OF MMC

Reference	Red†	Mod‡	Maintenance	Cost	Gen§
[10–14]	✓				
[15]	✓			✓	✓
[16–18]	✓			✓	
[19]	✓	✓			✓
[20]		✓		✓	
[21]	✓	✓		✓	✓
[22–24]	✓		✓	✓	
[25]	✓		✓		
This chapter	✓	✓	✓	✓	✓

† Redundancy ‡ Modularity § Generalization (various MMC characteristics)

Modularity, as highlighted in chapter 4 [19–21], represents another critical concept that significantly influences the reliability, efficiency, and overall cost considerations of the MMC. Chapter 4 presents a methodology for selecting the optimal switch voltage in MMCs based on cost and reliability trade-offs, showing that it depends on factors like DC link voltage, average loading, and component reliability estimation methods. Reference [19] discusses selecting the number of cascaded cells in a cascaded H-bridge con-

verter (CHB) for MV applications, considering trade-offs in efficiency, power density, and reliability. Redundancy options are also explored, providing a comprehensive perspective for designing high-power MV converter systems. In [20], a reliability-focused design methodology is proposed using a case study of a 17 MVA/13.8 kV MMC. It demonstrates that 3.3 kV devices offer the best trade-off.

The maintenance concept [22–25] for MMC is crucial to avoid unscheduled outages. It encompasses preventive, periodic, and protective maintenance. Planned maintenance involves replacing faulty SMs within the MMC structure. However, this maintenance necessitates a system shutdown, incurring substantial costs and requiring thorough planning. In [22], a reliability-centered maintenance approach is elaborated for MMC with dual redundancy, optimizing maintenance intervals based on dynamic operation states. This model aids in choosing redundancy strategies and maintenance decisions for MMCs. In [23], a reliability model for MMC incorporates preventive maintenance. The model evaluates reliability indices, maintenance intervals, and cost considerations, indicating the choice between SRS and LS-ARS. Authors in [24] introduce a dynamic preventive maintenance strategy for MMC in wind power systems, optimizing redundancy and maintenance intervals to reduce costs while maintaining reliability. Table 5.1 presents an overview of previous research endeavors documented in the literature. In this chapter, a comprehensive examination of MMC design is undertaken by applying a new redundancy strategy, encompassing facets like redundancy, modularity, maintenance, cost considerations, and generalization, which includes the consideration of MMCs operating with different DC-link voltage and loading scenarios.

This chapter introduces the Mixed Redundancy Strategy (MRS) for MMC, and section 5.2 provides a comprehensive explanation of its operational principles. In the MRS operational mode, two important parameters come into play: n_A which signifies the number of active redundant SMs within each arm, and n_S which represents the quantity of spare redundant SMs available for the MMC. During maintenance procedures, these spare SMs can substitute any faulty SMs across all arms. The MRS suits various MMC applications, including those with different maintenance planning, DC-link voltage, and annual average loading. MRS determines the optimal number of n_A in each arm and accurately estimates n_S the number of spare SMs slated for replacement during maintenance. This allows for consideration during the initial phases of MMC design, enabling a more accurate estimation of the capital cost, encompassing MMC cost, redundancy expenses, and the number of spare SMs designated for replacement. Therefore, based on the characteristics of the MMC, such as defined DC-link voltage, loading, and maintenance schedule, MRS ensures an optimized selection. It allows for the minimization of n_A based on the maintenance frequency, resulting in reduced capital costs, operational losses, and control simplicity (achieved by utilizing fewer SMs).

This work presents the following key contributions:

- Develop a reliability assessment method for the proposed MRS scheme and validate it using Monte-Carlo method (Section 5.2).

- Establish the economic viability boundary for the proposed MRS with varying V_{dc} and average annual loading by investigating the trade-off between investment cost, operational losses and reliability (Section 5.3).

Table 5.2: MMC CHARACTERISTICS AND FAILURE RATES

Symbols	Item	Value
N_{min}	Minimum number of SMs	—†
V_{dc}	DC link voltage	10 - 400 kV
S_{MMC}	Rated power	5.9 - 235.3 MVA
V_{IGBT}	IGBT Rated Voltage	1.2, 1.7, 3.3, 4.5, 6.5 kV‡
S_f	Safety factor of IGBT	0.65
$\lambda_{base\text{-}IGBT}$	IGBT base failure rate	100 FIT [18]
$\lambda_{base\text{-}Cap}$	Capacitor base failure rate	100 FIT [18]

† Changes based on the selected IGBT rated voltage
‡ Switch models are given in Appendix

- Define generalized viability boundary for MRS using sensitivity to changes in B_{10} lifetime requirement, component failure rate (FR), cost, and power capacity (Section 5.4).

- Recommend the optimal arm-level redundancy, maintenance frequency, and replacement criteria for the proposed scheme considering different scenarios (Section 5.5).

The main conclusions of the chapter 5 are presented in Section 5.6.

5.2. METHODOLOGY

5.2.1. SYSTEM DESCRIPTION AND ASSUMPTIONS

In Table 5.2, the characteristic of the considered system is shown. The minimum number of half-bridge SMs (N_{min}) that are required for each arm is estimated as given in (1.1). IGBTs and capacitors are the main high-power SM components that play a key role in the converter's operation and are relatively more prone to failure while contributing significantly to the cost and size of the system. For the cost evaluation, the system considered in [26] is used in which the IGBT module from Infineon Technologies, FF450R33T3E3BPSA1-ND, with a withstand voltage of 3.3 kV is used. The capacitor of KEMET, ALS71C133QT500-ND with 500 V and 13 mF is considered to provide a SM capacitance of approximately 3.3 mF in accordance to the MMC designed in [27] based on the method presented in [28].

In the MMC operational lifespan, the failure rate of IGBT and capacitors depends on the temperature and voltage across them. Hence, these limitations need to be considered in the failure rate formula of the IGBT and capacitors [29] that are detailed in [21] and are not repeated here. The failure rate of other auxiliary devices, including fuses, low voltage power supply, gate drive, cooling, and control system, also influences the converter life. These impacts are explored in Section 5.4 employing sensitivity of derived results to the higher failure rate.

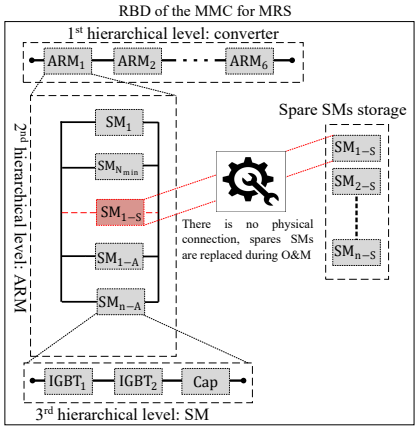

Figure 5.1: RBD of MMC's arm with MRS working mode.

5

5.2.2. WORKING PRINCIPLE OF MRS

The MMC arm's Reliability Block Diagram (RBD) in MRS working mode is shown in Fig. 5.1. In the MRS scheme, spare SMs (n_S) are not physically connected to the arms, and active redundant SMs in arms are operating identically to LS-ARS, eliminating any added complexity to the system. However, this scheme aims to minimize the number of n_A in each arm. During maintenance, the spare SMs replace faulty SMs, as illustrated in Fig. 5.1. The maintenance frequency in MRS is determined by the count of active redundant SMs in each arm (n_A). For instance, if $n_A = 1$, maintenance is scheduled upon the failure of a single SM in any arm. This strategy ensures continuous operation since there are still N_{min} SMs in the arm, allowing for timely maintenance planning.

In HV applications, where higher modularity and less frequent maintenance (e.g., 5 times in 10 years) are prevalent, the MRS scheme estimates that more active redundant SMs (n_A) in each arm are required. However, n_A remains significantly lower than conventional redundancy strategies. For instance, with $n_A = 3$, maintenance occurs after the third failure in any arm, providing a planned operational period with N_{min} SMs until maintenance. Simultaneously, other faulty SMs in different arms are also replaced by spare SMs n_S during maintenance.

So, there can be different combinations of active per arm (n_A) with spare (n_S) redundant SMs at the converter level in the MRS which will be determined based on the planned maintenance frequency and number of the levels explored in section 5.4. The MRS procedure for $n_A = 1$ and $n_S = 4$ is shown in Fig. 5.2 where only one arm is shown but spare SMs can be used in other five arms which are not shown. The arm initially will work with ($N_{min} + n_A$) level (a). When there is one SM failure (b), the maintenance will be performed shortly (c), and this chain of process (d) - (f) continues until there is no spare SM in the storage (g). Hence, the arm will always be working with ($N_{min} + n_A$) level until there is no spare SM in the storage (a) - (g). After that, if another SM fails (h) in an arm, the arm's operation level will be N_{min} (i). Ultimately, with one more SM failure in the N_{min} level operating arm (j), the converter will need to be shut down, and the converter will be out of operation (l).

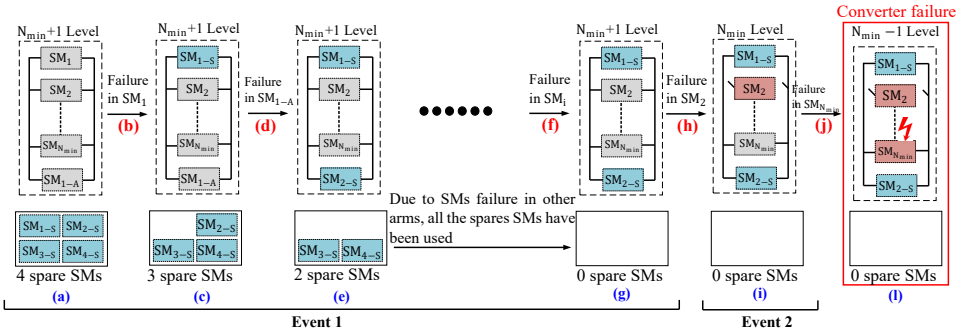

Figure 5.2: Steps of implementing MRS in one arm of the MMC .

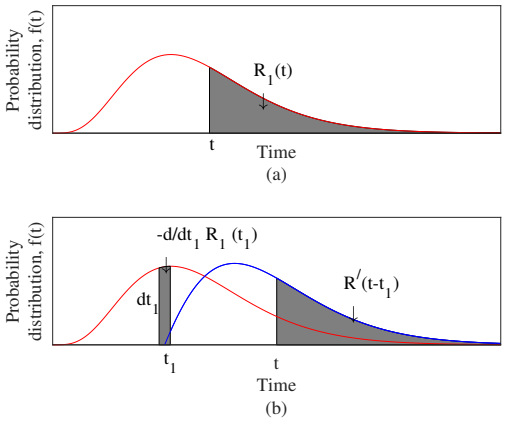

Figure 5.3: Graphical representation for reliability functions (a) $R_1(t)$ corresponding to event 1 (b) $R_2(t)$ corresponding to event 2.

5.2.3. RELIABILITY ASSESSMENT OF MRS

The reliability is estimated based on an instantaneous changeover similar to the methodology followed in [14, 18]. The concept of standby systems in [15, 30] can be applied to model the system behavior in MRS. According to the RBD model of the MRS shown in Fig. 5.1 and the assumptions regarding the proposed MRS's working principle, the MMC's reliability can be calculated by applying the joint failure density approach. 5.2, and they are as follows: Therefore, by considering that all the events that lead to system success are mutually exclusive, the expression for the reliability of the MMC under MRS working mode can be calculated by adding the mutually exclusive events. Considering the MMC in MRS mode, two events lead to the system success shown in Fig. 5.3.

1. Event 1: the MMC is operational for the time interval of 0 to t with $N_{\min} + n_{\mathrm{A}}$ level, and by each SM failure, one spare SM is substituted in a short time.

2. Event 2: at time t_1, the last spare SM has been substituted, and there is no spare

SM left, so there are only $N_{\min} + n_A$ SMs left in each arm and the MMC operates with n_A active redundant SM for time interval t_1 to t.

Fig. 5.3 (a) and (b) show the graphically represented reliability functions $R_1(t)$ and $R_2(t)$ for event 1 and event 2, respectively.

$R_1(t)$ is mathematically given by (5.1) using the Poisson distribution for MMC with n_s spare redundant SMs.

$$R_1(t) = P[N(t) \leq n_s] = \sum_{i=0}^{n_s} \frac{(\lambda_{sc} t)^i}{i!} e^{-\lambda_{sc} t} \tag{5.1}$$

$$\lambda_{sc} = (\lambda_{IGBT1} + \lambda_{IGBT2} + \lambda_{cap}) \times 6 \times (N_{\min} + n_A) \tag{5.2}$$

Note that (5.1) is also used to estimate the arm's reliability with SRS by substituting (5.2) with (5.3) as follows:

$$\lambda_{sc} = (\lambda_{IGBT1} + \lambda_{IGBT2} + \lambda_{cap}) \times N_{\min} \tag{5.3}$$

The derivative of $R_1(t)$ at t_1 gives the probability of n_s failures, with which the reliability function $R'(t-t_1)$ for MMC with active-only modules without any remaining spares SMs is weighted to estimate $R_2(t)$ as given in (5.4).

$$R_2(t) = \int_{t_1=0}^{t} -\frac{d}{dt_1} R_1(t_1) \times R'(t-t_1) dt_1 \tag{5.4}$$

Note that with $t_1 = 0$, $R'(t)$ can be estimated using the Markov Chain method from [14] to calculate the reliability of the MMC with LS-ARS. Since the two events $R_1(t)$ and $R_2(t)$ are mutually exclusive, the reliability of the MMC with MRS (R_{MRS}) can be calculated as (5.5).

$$R_{MRS}(t) = R_1(t) + R_2(t) \tag{5.5}$$

5.2.4. VALIDATION OF MRS USING MCS

An analytical method has been developed to assess the reliability of the MMC employing the MRS. Due to the absence of comparable methods in the current literature, MCS is employed to validate the obtained results. The outcomes are visually presented in Fig. 5.4 for 1,000 and 10,000 trials, respectively. It demonstrates the efficacy of the proposed analytical equation for calculating the reliability of the MMC by applying MRS.

5.2.5. OPTIMAL COMBINATION OF ACTIVE REDUNDANT AND SPARE SMS IN MRS

In MRS, different combinations can be selected between the number of active redundant and spare SMs. In the base MMC with 10 MVA, and 17 kV V_{dc}, results for three combinations are presented in Fig. 5.5. It can be seen that having one active redundant SM in each arm and storing the rest as spare SMs shows the best reliability outputs. For instance, if the required B_{10} lifetime is 20 years, this requirement can be met with 15, 18, and 20 SMs with n_A equal to 1, 2, and 3. This is because, with only one active redundant SM, more spare SMs can be shared among the MMC arms.

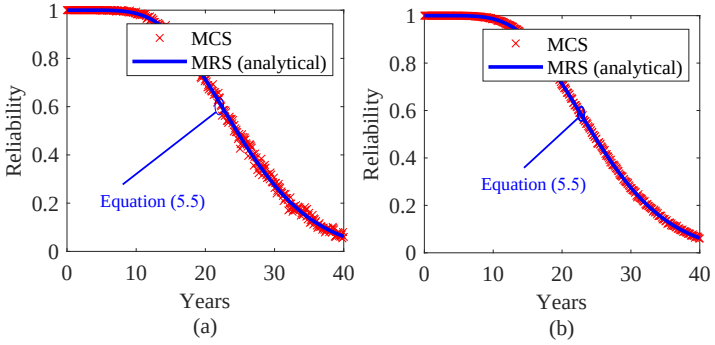

Figure 5.4: Validation of proposed MRS scheme using MCS with (a) 1,000 trials and (b) 10,000 trials.

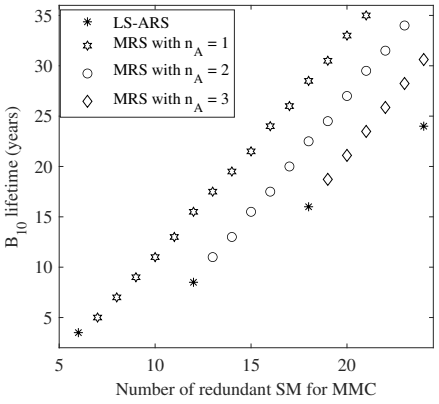

Figure 5.5: B_{10} lifetime of the MMC with various combinations of active and spare redundant SMs in MRS.

For the MMCs with very high levels, more than one redundant SMs can be active in each arm. In such cases, the optimal combination can be found based on various indicators such as preventive maintenance plans and requirements. In the subsequent section, the reliability of the considered MMC is compared for LS-ARS, SRS, FL-ARS, and MRS.

5.3. CASE-STUDIES FOR COST AND OPERATIONAL EFFICIENCY TRADE-OFFS

In this chapter, the aim is to validate the applicability of the MRS in both MV and HV applications. Two systems documented in existing literature [26, 31] are considered to achieve this. Details for each system are provided in Table 5.3.

Table 5.3: CHARACTERISTICS OF TWO CASE STUDIES.

Item	MV	HV
V_{dc} (kV)	17	320
V_{IGBT} (kV)	3.3	3.3
N_{min}	9	200
Redundant per arm	2	16
Switching frequency (Hz)	313	150

5.3.1. RELIABILITY OUTPUTS

Taking the MMCs given in Table 5.3, Fig. 5.6 shows the reliability results with different redundancy strategies. The MV system implements redundancy with two redundant SMs per arm, totaling 12 SMs. In the FL-ARS, LS-ARS, and SRS, both redundant SMs are present in each arm. Conversely, in MRS, parameters are set as $n_A = 1$ and $n_S = 6$. In the HV scenario, conventional redundancy strategies entail 16 redundant SMs in each arm. However, the MRS scheme specifies $n_A = 4$ and $n_S = 12 \times 6 = 72$. that will be scrutinized in section 5.5.

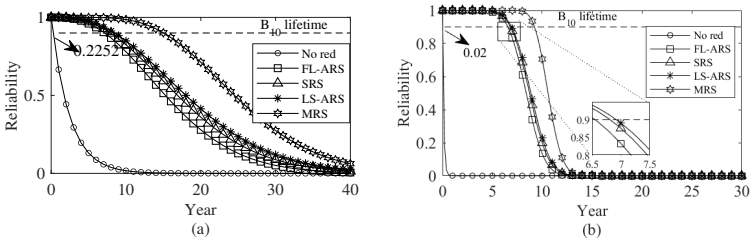

Figure 5.6: Reliability outputs for two considered MMCs with DC link voltage of (a) MV and (b) HV.

From Fig. 5.6 (a), it can be observed that B_{10} lifetime corresponding to 90 % reliability (dashed black) increases from 0.2 years (no redundancy, circle marker) to approximately 10 years when two redundant SMs are considered per arm with FL-ARS (square), SRS (triangle), and LS-ARS (asterisk). This value almost doubles when the proposed MRS (hexagon) is employed with the same number of redundant SMs in the MV system. Fig. 5.6 (b) shows that applying the MRS scheme with the same number of redundant SMs as conventional redundancy strategies will boost the lifetime corresponding to 90 % reliability from 6.5 to 9.2 years.

Fig. 5.7 shows the increase in achieved B_{10} lifetime with the increasing number of redundant SMs for different strategies in both cases of MV and HV systems. The higher impact of MRS is visible from the higher slope of the B_{10} lifetime as a function of redundancy. Since the number of redundant SMs can only be a multiple of six for LS-ARS, FL-ARS, and SRS, the flexibility of choosing the redundancy level in meeting the required reliability targets can be an advantage with the proposed MRS.

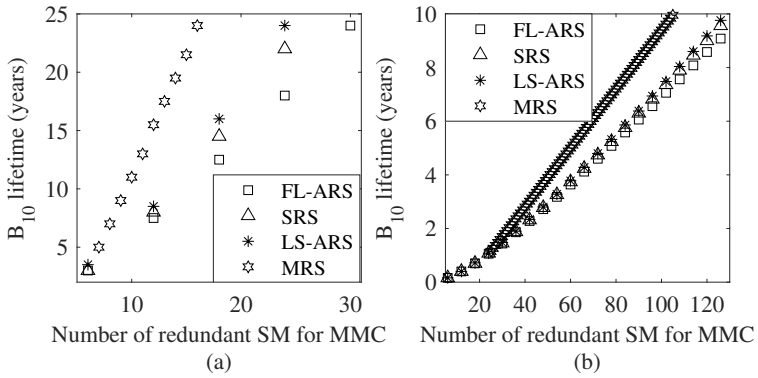

Figure 5.7: B_{10} lifetime of the MMC with various redundancy schemes for (a) MV and (b) HV.

5.3.2. OPERATIONAL EFFICIENCY

In this part, the operational efficiency of different redundancies is compared by using the normalized loading profile that is adapted based on the available hourly data of a substation in The Netherlands [32] shown in Fig. 5.8. The yearly energy losses of MMCs (E_{l_X}) in kWh with various applied redundancies can be calculated as (5.6).

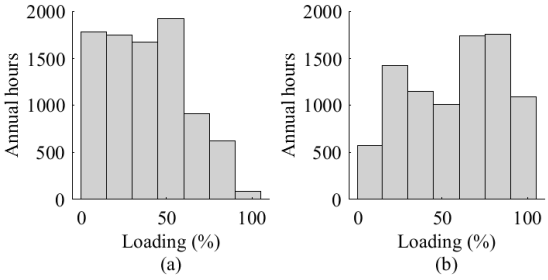

Figure 5.8: Yearly power demand for annual average loading (P_{ave}) of (a) 38 % and (b) 57 % [32].

$$E_{l_X} = \int (100 - \eta(t_i)) \times P_{\text{MMC}} \tag{5.6}$$

where $\eta(t_i)$ is the efficiency, X specifies the redundancy type, and P_{MMC} is the power rating in MW.

Fig. 5.9 (a) presents normalized switching and conduction losses for different redundancy strategies for the corresponding loading in the MV system. The efficiency of the MV system is presented in Fig. 5.9 (b), where SRS has the lowest losses compared to other redundancy strategies. The same results are shown for HV system in Fig. 5.9 (c) and (d). E_l of various redundancy schemes concerning both case studies of annual loading (Fig. 5.8) are given in Table 5.4 for B_{10} = 10 years. The information gleaned from Fig. 5.9 and Table 5.4 indicates that the MRS has lower losses in comparison to the ARS, primarily due to its utilization of a reduced number of n_{A} in each arm. Notably, the efficiency

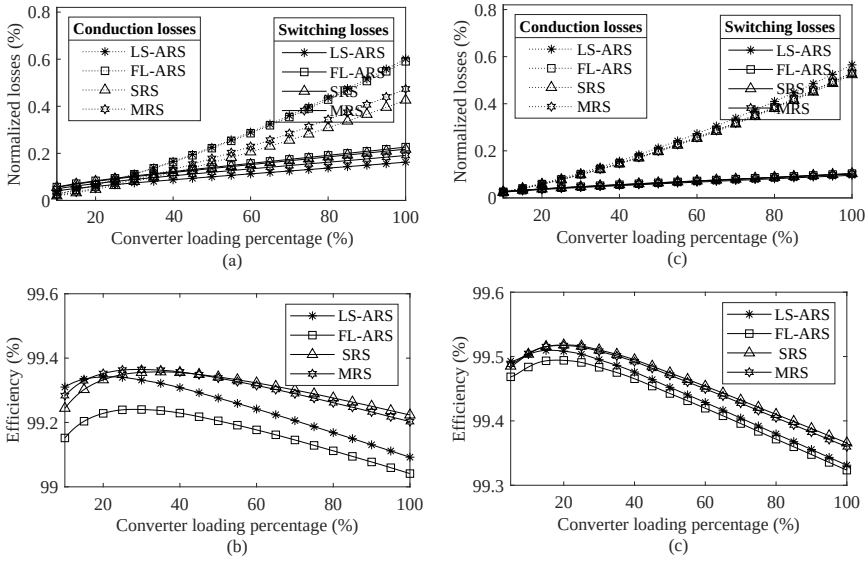

Figure 5.9: Operational losses of the MMC for (a) switching and conduction losses in MV; (b) Efficiency in MV; (c) switching and conduction losses in HV; and (d) Efficiency in HV; under various redundancy modes and loading.

Table 5.4: ANNUAL LOSSES (E_l) IN MWH (B_{10} = 10 YEARS)

Type	Annual P_{ave}	LS-ARS	FL-ARS	SRS	MRS
MV	38 %	252.24	265.36	231.42	231.94
MV	57 %	400.64	443.67	355.54	360.37
HV	38 %	3508.55	3532.81	3377.12	3397.54
HV	57 %	4901.44	4926.25	4791.02	4803.52

of the MMC tends to be higher when the SRS is employed. For applications considering the use of SRS, the efficiency aspect becomes significant. The applicability of the MRS in such scenarios is examined in Section 5.4.

The energy savings slightly differ when a fixed MMC loading represents the yearly average of the hourly demand variation of the two case studies. For example, in the MV system, 5.76 MWh annual savings are estimated when SRS is used instead of MRS with a fixed loading of 57 %, as compared to 4.83 MWh from Table 5.4 where hourly annual load profile is considered. The former is used in the subsequent section to simplify the computation effort required for the sensitivity analysis in defining the economic viability boundaries of the proposed scheme.

5.3.3. CAPITAL INVESTMENT (CI)

The capital investment (CI), design cost, and operation & maintenance (O&M) costs are relevant factors for selecting a proper redundancy scheme. Since different switches are used for various loading and V_{dc}, the cost (€/kVA) is firstly estimated for the base MMC

and by using the price of the switch voltage rating of 3.3 kV. Then it will be used for estimating the MMC price with various switches. The most recent price of components of the MMC with 3.3 kV rated switch to calculate the CI is as follows. The IGBT price is €1584.12 per unit, the gate drive price is €180.32 per unit, and the capacitor price is €108.33 per unit. Table 5.5 summarizes MMC's CI without considering redundancy. Furthermore, the design cost price is around 30 % of the total cost. In order to estimate the

Table 5.5: *CI* IN EURO OF 10 MVA 17 KV MMC WITHOUT REDUNDANCY

Components	**Total cost**
IGBT	85542.4
Gate Drive	9737.82
Heat Sink	9409.66
Total Capacitance	23399.28
Power Supply	5731.34
Sensors	2038
Control Board	1670
(O&M)	10%
Design cost	30%
CI_{WoR}	192539.9

total CI of the MMC, including redundancy, and other switch ratings, the following steps can be followed.

$$CI_{\text{N-WoR}} = \frac{CI_{\text{WoR}}}{S_{\text{MMC}}(\text{kVA})} \tag{5.7}$$

$$CI_{\text{N-WR-x}} = \frac{CI_{\text{N-WOR}}}{N_{\text{min,x}} \times 6} \times (N_{\text{min,x}} \times 6 + N_{\text{T-red}}) \tag{5.8}$$

$$N_{\text{T-red}} = \begin{cases} N_{\text{red}} \times 6 & \text{, for FL, SRS, LS} \\ 6 \times n_{\text{A}} + n_{\text{S}} & \text{, for MRS} \end{cases} \tag{5.9}$$

where CI_{WoR} is the total CI of the MMC without redundancy obtained from Table 5.5, $CI_{\text{N-WoR}}$ is the normalized price of the MMC per kVA, $CI_{\text{N-WR-x}}$ is the normalized price with redundancy for various switches (x $\in$ {1.2, 1.7, 3.3, 4.5, 6.5 kV}), $N_{\text{min,x}}$ is the minimum number of required SM for different switch ratings, and $N_{\text{T-red}}$ is the total of redundant SM in the MMC for different redundancy strategies defined in (5.9). Hence, the normalized price of the MMC, including redundancy, can be obtained. The cost of MMC with MRS is lower than the other three redundancy schemes due to the MMC's lower number of redundant SMs.

5.3.4. PAYBACK

To evaluate the simple payback, the CI and the saving of various redundancies are compared to select the most economical redundancy strategy. using (5.10) and (5.11).

$$\text{Payback} = \frac{\Delta CI}{S_{\text{i}}} \tag{5.10}$$

$$S_{\mathrm{i}} = \int \Delta E_i \times P_{\mathrm{t}} \tag{5.11}$$

where ΔCI represents the variation in capital investment between redundancy strategies, S_{i} indicates the difference in cost savings between redundancy strategies, ΔE_i (kWh) signifies the disparity in energy savings between redundancy strategies, and Pt denotes the electricity price equivalent to 0.190 €/kWh.

5.4. VIABILITY BOUNDARIES OF THE PROPOSED MRS

As highlighted in Section 5.3, in scenarios where the application of the SRS is feasible, the efficiency advantage of SRS over the MRS is acknowledged. Consequently, the suitability of MRS is evaluated. Also, it's crucial to note that this comparison is made between SRS and MRS because Table 5.5, Table 5.4, Fig. 5.6, and Fig. 5.7 suggest that LS-ARS and FL-ARS are less economically viable than MRS with the considered assumptions. When the ARS is the chosen redundancy scheme, MRS consistently emerges as the optimal choice due to its lower CI and higher efficiency. Fig. 5.10 shows the boundary of economic viability (L_{boundary}) between SRS and MRS for B_{10} = 10 years as a function of V_{dc} (10-400 kV) and loading (1-100%) considering a 10-year payback. Notably, within the 10-100 kV range, other VSC options like two-level (2L) VSC and three-level neutral-point-clamped converter (3L-NPC) can rival the MMC. However, this study exclusively delves into MMC, and for a comprehensive comparison, [15] gives detailed findings. The optimal switch selected for each voltage level differs based on chapter 4. For example, 1.7 kV switch is used for low loading below 50 kV DC link, while 3.3 kV is used in the 50-100 kV and 6.5 kV is used above about 200 kV. The current and voltage rating of each IGBT and capacitor is kept fixed. The right-side region of L_{boundary} (dash-dotted line blue) indicates the operating conditions where the MRS is more economically viable. The left-side region of L_{boundary} (solid line red) corresponds to the extra investment for SRS. It has a payback of 10 years due to better efficiency than MRS for the given DC link voltage and average annual loading.

A linearized general equation defined based on the two points of A and B for L_{boundary} is shown in Fig. 5.10, given by (5.12).

$$\begin{cases} \text{if } \frac{\text{Loading}}{100} - m(V_{\mathrm{dc}} - V_{\mathrm{ref}}) \geq 0, & \text{Select SRS} \\ \text{else,} & \text{Select MRS} \end{cases} \tag{5.12}$$

The parameters m and V_{ref} provided in Table 5.6.

Table 5.6: THE SPECIFICATIONS OF EQUATION (5.12)

	$L_{\mathbf{boundary}}$	$B_{\mathbf{10}}$ (years)		FR		CI (or Pt)		O&M of MRS	
		5	20	+20%	-20%	+20% (-20%)	-20% (+20%)	+20%	-20%
m (μ)	8.13	9.3	16.7	7.8	50	10.9	12	5	14.7
V_{ref}(kV)	10	110	0	10	123	0	104	117	0

5.4.1. SENSITIVITY ANALYSIS

Sensitivity analysis describing the shift in this defined L_{boundary} with respect to different B_{10} lifetime requirements, FR, CI (P_{t}), and O&M is presented in Fig. 5.11(a)-(d), re-

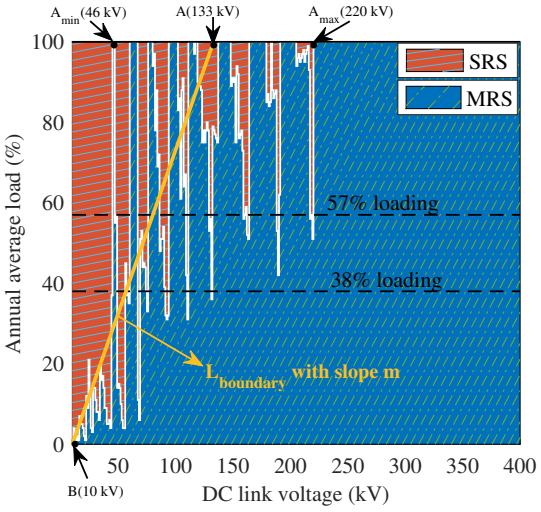

Figure 5.10: Feasibility boundary for SRS and MRS as a function of yearly average loading and V_{dc} (payback = 10 years, B_{10} = 10 years).

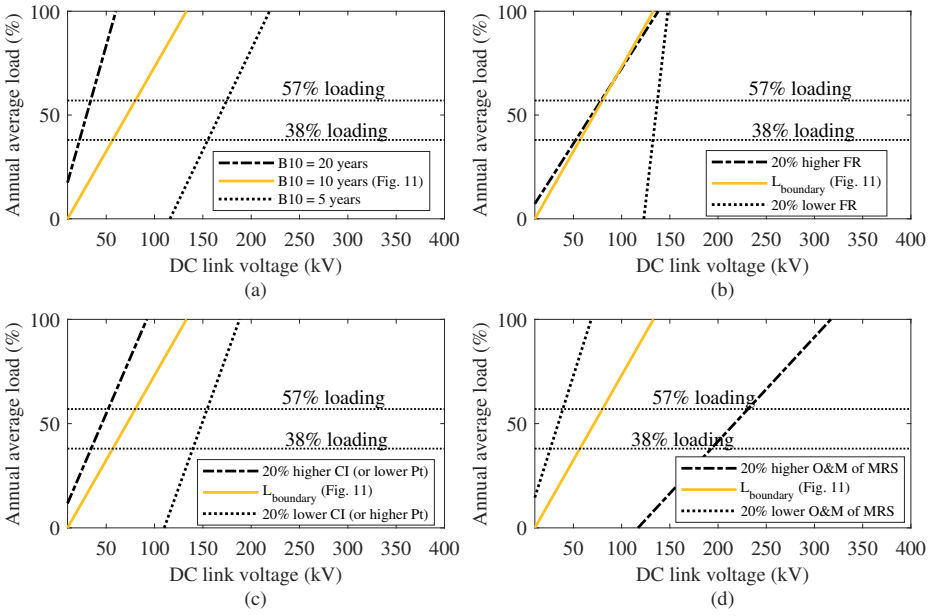

Figure 5.11: Displacement of $L_{boundary}$ as a function of yearly loading and V_{dc} (10-year payback) with a variation of (a) B_{10} (b) FR (c) CI, and (d) O&M of MRS.

spectively. In Fig. 5.11 (a), it can be observed that the proposed MRS becomes more economically viable with the increase in B_{10} lifetime requirements. For example, SRS is preferred for both 38 % and 57 % loading with a 40 kV V_{dc} if the required B_{10} lifetime is 5 and 10 years, while MRS is viable when the required B_{10} lifetime is increased to 20 years. Fig. 5.11 (b) suggests that there is a limited dependence of the $L_{boundary}$ on the MMC loading when a higher FR is considered. However, the $L_{boundary}$ shift becomes loading dependent with lower FR. Fig. 5.11 (c) shows that the proposed MRS will become more economically viable if the power electronic components are more expensive as compared to the reference converter costs considered in Table 5.5. For example, MRS is preferred over SRS for the two considered case studies with 40 kV DC link only when considered component costs are 20 % higher. Finally, Fig. 5.11 (d) suggests that if the O&M cost of the MRS is higher, it will become less viable. Since O&M in practical scenarios is important, this aspect is explored more in detail in the section 5.5.

5.4.2. SENSITIVITY TO CONVERTER POWER CAPACITY

In this section, the impact of the higher power rating of the MMC is evaluated. Initially, a fixed current rating of 480A is employed, and the power of the MMC varies from 6 to 235.3 MVA by changing the DC link voltage from 10 to 400 kV. The switch types used for this system are provided in the appendix (Table A.1). To evaluate the impact of power rating, an evaluation is conducted with an increased current rating of the converter set to 960 A. For this case, the change in V_{dc} between 10-400 kV will increase the power from 12 to 470.7 MVA. Therefore, appropriate switch ratings should have been selected which are also provided in Table A.2 (appendix). The results, depicted in Fig. 5.12, illustrate

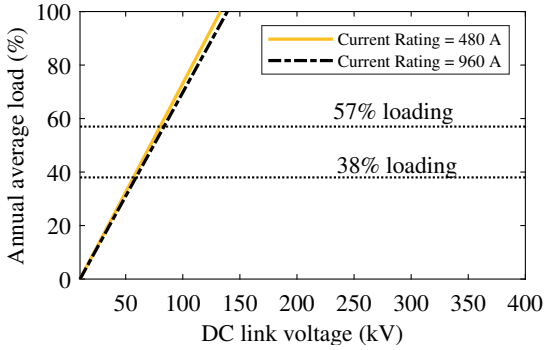

Figure 5.12: Sensitivity of the obtained results for feasibility boundary for SRS and MRS with higher rating switches.

that the boundary line changes trivially (m = 7.8 μ, V_{ref} = 10 kV), which is negligible. It can be concluded that the selection of MRS over other redundancy strategies is independent of the current rating and primarily hinges on the loading and DC link voltage. It is worth noting that the same conclusions were drawn in chapter 4, highlighting that switch rating selection remains independent of the current rating of the MMC.

5.5. PRACTICALITY AND OPERATIONAL CHALLENGES

The Mean Time to failure of the arm ($MTTF_{\text{arm}}$) considering the maintenance period ($T_{\text{O\&M}}$) is given by (5.13) [17].

$$MTTF_{\text{arm}} = \frac{\int_0^{T_{\text{O\&M}}} R_{\text{arm-x}}(t)\,dt}{1 - R_{\text{arm-x}}(T_{\text{O\&M}})} \tag{5.13}$$

Herein, $R_{\text{arm-x}}$ is arm reliability with various redundancies over the operating years. In Fig. 5.13, the required number of active redundant SM (n_{A}) is shown for the MRS scheme considering the required MTTF as a function of V_{dc} and $T_{\text{O\&M}}$. It can be observed that n_{A} must be increased to increase the $T_{\text{O\&M}}$, which will consequently reduce the O&M costs for MRS.

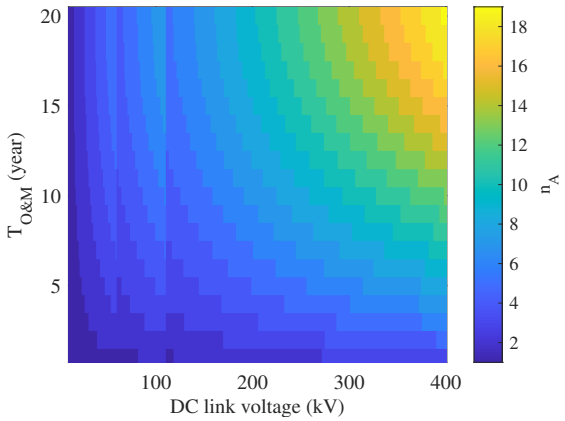

Figure 5.13: Required number of n_{A} in each arm for the MRS scheme as a function of DC link voltage and $T_{\text{O\&M}}$ at 100% loading for MTTF = 20 years.

This trade-off is investigated in more detail using Monte-Carlo Simulations (MCS). Fig. 5.14 shows an example of 10000 trials for a given MMC with $N_{\text{min}} = 48$ and $n_A = 2$, demonstrating that maintenance is required approximately six times over a 10-year B_{10} lifetime.

These findings are extrapolated to various MMC configurations. Fig. 5.15 presents the annual maintenance requirements for MMCs operating at 100% and 38% annual loading as a function of the V_{dc}. Based on the results of Fig. 5.15 (a), it is suggested that if the expected number of maintenance is once per year for a specific application, each arm of the MMC should include one active SM in the V_{dc} range of 10 kV to 33 kV. For DC link voltages ranging from 33 kV to 270 kV, two active SMs are required per arm to ensure operational continuity. For V_{dc} between 270 kV and 400 kV, three active redundant SMs ($n_{\text{A}} = 3$) are necessary. The same results can be applied if the annual average loading is 38% (Fig. 5.15 (b)). Also, note that the appropriate switch rating is considered according to chapter 4, which depends on annual loading and V_{dc}. This is evident in Fig. 5.15, where variations occur based on the annual loading of the converter, resulting in dips.

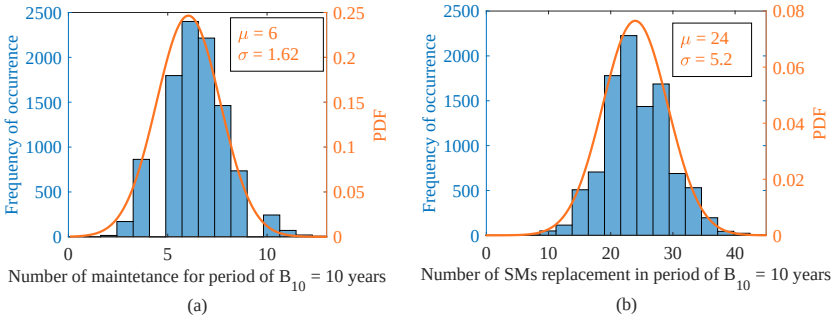

Figure 5.14: MCS results (10,000 trials) for MMC with $N_{\text{min}} = 48$ and $n_{\text{A}} = 2$ within the period of $B_{10} = 10$ years (a) the distribution of the required number of maintenance (b) the distribution of a number of faulty SMs that is going to be changed.

Specifically, at 38% loading (Fig. 5.15 (b)), these dips take place at V_{dc} values of 28 kV, 90 kV, and 177 kV. These variations are attributed to changes in modularity induced by the utilization of different switch ratings. By adhering to these guidelines, the uninterrupted operation of the MMC can be guaranteed, and the maximum number of spare SMs can be shared. However, it is important to note that the expected maintenance intervals in certain applications may differ, such as every two years or every six months, as shown in Fig. 5.15. The MRS scheme remains applicable in such cases, with the corresponding number of n_{A} in each arm. Similarly, the MCS methodology can estimate the number of SM failures within a specified period. For instance, as shown in Fig. 5.16, the expected number of failed SMs can be estimated over a 10-year (B_{10}). As observed in Fig. 5.16, an increase in the number of active redundant SMs (n_{A}) within each arm results in a reduction in the number of faulty SMs experiencing a lifetime of $B_{10} = 10$ years. This decrease is attributed to the decreased voltage stress across the SMs. However, it is essential to note that the multiplication of n_{A} by a factor of 6 contributes to an increase in the CI of the MMC. Similar to the observations in Fig. 5.15, dips around 60 kV and 120 kV are evident, associated with changes in modularity.

Therefore, implementing the MRS enables the derivation of an optimal design for the MMC across various applications. This optimization, aligned with the O&M planning of the MMC, results in reduced operational losses and a lower CI. Table 5.7 showcases the application of the MRS scheme to previously published work and the amount of money that can be saved in $B_{10} = 10$ years. Through considerations of DC link voltage, annual loading, and O&M planning (assuming maintenance occurs every year), this approach facilitates accurate estimation of the optimal switch rating, arms-level redundancy (n_{A}), and spare SMs (n_{S}) for the replacement of faulty SMs.

5.6. CONCLUSION

The developed analytical model estimates the weighted reliability of the proposed scheme based on two probability distribution functions for converter failure as a function of time. Unlike ARS and SRS, this assessment method is needed because the converter

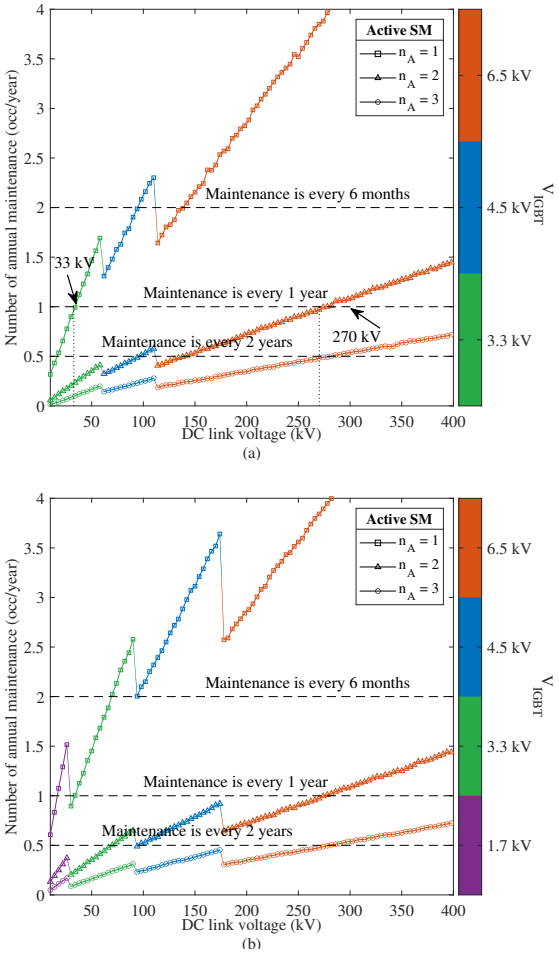

Figure 5.15: MCS results (10,000 trials) for estimating the number of maintenance frequency in the period of $B_{10} = 10$ years as a function of DC link voltage at (a) 100% loading, and (b) 38% loading .

reliability function structurally changes when the redundancy strategy is modified depending on the available spare and active SMs for MRS. Sensitivity analysis indicates that the proposed scheme becomes relatively more economically viable when the required B_{10} lifetime increases. Some dependence on increasing DC link voltage is also observed, especially for higher B_{10} lifetime. The economic viability of MRS is more when higher component costs are considered for the MMC. Further, this economic boundary between MRS and SRS for a 10 year payback has relatively limited dependence on the variation in component failure rate. Also, the economic viability of MRS is independent of the power capacity of the MMC, which was validated by using different switches with higher current ratings. It was shown that the MRS scheme becomes less favorable if its O&M cost is higher than other redundancy schemes. The effectiveness and appli-

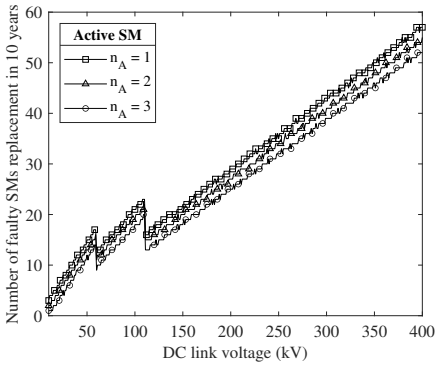

Figure 5.16: MCS results (10,000 trials) for estimating the number of faulty SM within the period of B_{10} = 10 years as a function of DC link voltage (at 100% loading).

Table 5.7: OPTIMAL DESIGN OF VARIOUS MMC

Ref	$V_{\mathbf{dc}}$ [§] **(kV)**	**Power (MW)**	**Red (%)**	**Saving by applying MRS**[‡]	
				$\mathbf{P_{l,ave}}$ = 38%	$\mathbf{P_{l,ave}}$ [†] = 57%
[15]	54	30	ARS (31)	109 K€	278.7 K€
[33]	100	100	ARS (32)	606.5 K€	577.7 K€
[34]	300	210	ARS (10)	935.8 K€	948.2 K€
[31]	320	500	ARS (8)	4.624 M€	5.163 M€
[35]	400	800	ARS (8.1)*	1.793 M€	3.742 M€
[35]	640	1200	ARS (8.2)*	3.156 M€	5.976 M€
[36]	640	1000	ARS (20)	3.954 M€	4.318 M€

§ pole to pole voltage * 8% redundancy is assumed

† Annual average loading of MMC shown in Fig. 5.8

‡ The savings are calculated for B_{10} = 10 years and includes operational losses and CI

cability of the MRS scheme are validated by proposing the MCS in which the optimum number of active redundant SM in each arm is determined with respect to the expected maintenance plan. MCS also estimates the number of failed SMs by emulating real-life scenarios. The efficacy of the MRS is demonstrated through its application in previously published studies.

REFERENCES

[1] F. Badrkhani Ajaei and R. Iravani, *Dynamic interactions of the mmc-hvdc grid and its host ac system due to ac-side disturbances,* IEEE Trans. Power Deliv. **31** (2016), 10.1109/TPWRD.2015.2512178.

[2] J. Xu, C. Zhao, Y. Xiong, C. Li, Y. Ji, and T. An, *Optimal design of mmc levels for electromagnetic transient studies of mmc-hvdc,* IEEE Trans. Power Deliv. **31** (2016), 10.1109/TPWRD.2016.2524648.

[3] H. Wang and F. Blaabjerg, *Reliability of capacitors for dc-link applications in power electronic converters—an overview,* IEEE Trans. Ind. Appl. **50** (2014), 10.1109/TIA.2014.2308357.

[4] S. S. Manohar, A. Sahoo, A. Subramaniam, and S. K. Panda, *Condition monitoring of power electronic converters in power plants — a review,* in *2017 20th International Conference on Electrical Machines and Systems (ICEMS)* (2017).

[5] M. Ahmadi, A. Shekhar, and P. Bauer, *Reconfigurability, modularity and redundancy trade-offs for grid connected power electronic systems,* in *2022 IEEE 20th International Power Electronics and Motion Control Conference (PEMC)* (2022).

[6] R. Billinton, S. Aboreshaid, and M. Fotuhi-Firuzabad, *Well-being analysis for hvdc transmission systems,* IEEE Trans. Power Syst. **12** (1997), 10.1109/59.589765.

[7] L. Guo, Y. Ding, M. Bao, C. Shao, P. Wang, and L. Goel, *Nodal reliability evaluation for a vsc-mtdc-based hybrid ac/dc power system,* IEEE Trans. Power Syst. **35** (2020), 10.1109/TPWRS.2019.2951711.

[8] J. Guo, X. Wang, Z. Bie, and Y. Hou, *Reliability modeling and evaluation of vsc-hvdc transmission systems,* in *2014 IEEE PES General Meeting | Conference Exposition* (2014).

[9] J. Xu, P. Zhao, and C. Zhao, *Reliability analysis and redundancy configuration of mmc with hybrid submodule topologies,* IEEE Trans. Power Electron. **31** (2016), 10.1109/TPEL.2015.2444877.

[10] J. Guo, J. Liang, X. Zhang, P. D. Judge, X. Wang, and T. C. Green, *Reliability analysis of mmcs considering submodule designs with individual or series-operated igbts,* IEEE Trans. Power Deliv. **32** (2017), 10.1109/TPWRD.2016.2572061.

[11] J. Xu, L. Wang, D. Wu, H. Jing, and C. Zhao, *Reliability modeling and redundancy design of hybrid mmc considering decoupled sub-module correlation,* International Journal of Electrical Power & Energy Systems (2019).

[12] J. Xu, H. Jing, and C. Zhao, *Reliability modeling of mmcs considering correlations of the requisite and redundant submodules,* IEEE Trans. Power Deliv. **33** (2018), 10.1109/TPWRD.2017.2757607.

[13] X. Xie, H. Li, A. McDonald, H. Tan, Y. Wu, T. Yang, and W. Yang, *Reliability modeling and analysis of hybrid mmcs under different redundancy schemes,* IEEE Trans. Power Deliv. **36** (2021), 10.1109/TPWRD.2020.3008281.

[14] J. Guo, X. Wang, J. Liang, H. Pang, and J. Gonçalves, *Reliability modeling and evaluation of mmcs under different redundancy schemes,* IEEE Trans. Power Deliv. **33** (2018), 10.1109/TPWRD.2017.2715664.

[15] G. Abeynayake, G. Li, T. Joseph, J. Liang, and W. Ming, *Reliability and cost-oriented analysis, comparison and selection of multi-level mvdc converters,* IEEE Trans. Power Deliv. (2021), 10.1109/TPWRD.2021.3051531.

[16] H. Li, X. Xie, A. S. McDonald, Z. Chai, T. Yang, Y. Wu, and W. Yang, *Cost and reliability optimization of modular multilevel converter with hybrid submodule for offshore dc wind turbine,* International Journal of Electrical Power & Energy Systems **120** (2020).

[17] B. Wang, X. Wang, Z. Bie, P. D. Judge, X. Wang, and T. C. Green, *Reliability model of mmc considering periodic preventive maintenance,* IEEE Trans. Power Deliv. **32** (2017), 10.1109/TPWRD.2016.2602888.

[18] P. Tu, S. Yang, and P. Wang, *Reliability- and cost-based redundancy design for modular multilevel converter,* IEEE Trans. Ind. Electron. **66** (2019), 10.1109/TIE.2018.2793263.

[19] J. E. Huber and J. W. Kolar, *Optimum number of cascaded cells for high-power medium-voltage ac–dc converters,* IEEE Journal of Emerging and Selected Topics in Power Electronics **5** (2017), 10.1109/JESTPE.2016.2605702.

[20] J. V. M. Farias, A. F. Cupertino, V. d. N. Ferreira, H. A. Pereira, S. I. Seleme, and R. Teodorescu, *Reliability-oriented design of modular multilevel converters for medium-voltage statcom,* IEEE Transactions on Industrial Electronics **67**, 6206 (2020).

[21] M. Ahmadi, A. Shekhar, and P. Bauer, *Switch voltage rating selection considering cost-oriented redundancy and modularity-based trade-offs in modular multilevel converter,* IEEE Trans. Power Deliv. (2023), 10.1109/TPWRD.2023.3263270.

[22] P. Yu, W. Fu, L. Wang, Z. Zhou, G. Wang, and Z. Zhang, *Reliability-centered maintenance for modular multilevel converter in hvdc transmission application,* IEEE Journal of Emerging and Selected Topics in Power Electronics **9**, 3166 (2021).

[23] B. Wang, X. Wang, Z. Bie, P. D. Judge, X. Wang, and T. C. Green, *Reliability model of mmc considering periodic preventive maintenance,* IEEE Transactions on Power Delivery **32**, 1535 (2017).

[24] F. Feng, J. Yu, Z. Yang, W. Dai, X. Zhao, S. Kamel, J. Wang, and G. Fu, *Dynamic preventive maintenance strategy for mmc considering multi-term thermal cycles,* International Journal of Electrical Power Energy Systems **116**, 105560 (2020).

[25] J. Wylie, M. C. Merlin, and T. C. Green, *Analysis of the effects from constant random and wear-out failures of sub-modules within a modular multi-level converter with varying maintenance periods,* in *2017 19th European Conference on Power Electronics and Applications (EPE'17 ECCE Europe)* (2017) pp. P.1–P.10.

[26] A. Shekhar, T. B. Soeiro, Y. Wu, and P. Bauer, *Optimal power flow control in parallel operating ac and dc distribution links,* IEEE Trans. Ind. Electron. **68** (2021), 10.1109/TIE.2020.2970675.

[27] A. Shekhar, L. B. Larumbe, T. B. Soeiro, Y. Wu, and P. Bauer, *Number of levels, arm inductance and modulation trade-offs for high power medium voltage grid-connected modular multilevel converters,* in *2019 10th International Conference on Power Electronics and ECCE Asia (ICPE 2019 - ECCE Asia)* (2019).

[28] K. Ilves, S. Norrga, L. Harnefors, and H.-P. Nee, *On energy storage requirements in modular multilevel converters,* IEEE Trans. Power Electron. **29** (2014), 10.1109/TPEL.2013.2254129.

[29] *Reliability Prediction of Electronic Equipment: MIL-HDBK-217D.*, Military standardization handbook (Department of Defense, 1983).

[30] R. Billinton and R. N. Allan, *Reliability evaluation of engineering systems: concepts and techniques,* (1992).

[31] J. V. M. Farias, A. F. Cupertino, H. A. Pereira, S. I. Seleme, and R. Teodorescu, *On converter fault tolerance in mmc-hvdc systems: A comprehensive survey,* IEEE Journal of Emerging and Selected Topics in Power Electronics **9**, 7459 (2021).

[32] A. Shekhar, T. B. Soeiro, L. Ramírez-Elizondo, and P. Bauer, *Offline reconfigurability based substation converter sizing for hybrid ac–dc distribution links,* IEEE Trans. Power Deliv. **35** (2020), 10.1109/TPWRD.2020.2966554.

[33] J. Kang, H. Kim, H.-J. Jung, D.-S. Lee, C.-K. Kim, H. A. Mantooth, and K. Hur, *On exploiting active redundancy of a modular multilevel converter to balance reliability and operational flexibility,* IEEE Transactions on Power Electronics **34**, 2234 (2019).

[34] H. Kim, J. Kang, J. W. Shim, J. Beerten, D. Van Hertem, H.-J. Jung, C.-K. Kim, and K. Hur, *Exploiting redundant energy of mmc–hvdc to enhance frequency response of low inertia ac grid,* IEEE Access **7**, 138485 (2019).

[35] R. Li, L. Yu, L. Xu, and G. P. Adam, *Coordinated control of parallel dr-hvdc and mmc-hvdc systems for offshore wind energy transmission,* IEEE Journal of Emerging and Selected Topics in Power Electronics **8**, 2572 (2020).

[36] M. Alharbi, S. Isik, and S. Bhattacharya, *A novel submodule level fault-tolerant approach for mmc with integrated scale-up architecture,* IEEE Journal of Emerging and Selected Topics in Industrial Electronics **2**, 343 (2021).

6

RECONFIGURABILITY IN MMC

This chapter begins with an introduction to the concept of reconfigurability in MMCs, specifically targeting the need for adaptable converter designs that can manage open-circuit faults (OCFs) in IGBTs. Reconfigurability enables the system to recover from faults without requiring additional hardware, which reduces cost and downtime while improving reliability. The chapter outlines the operation concept of MMCs during OCFs, a complete flow of detection, localization, and tolerance are developed, in which the methodology for integrating fault-tolerant reconfigurations is detailed. Additionally, this chapter provides experimental validation of the proposed method through physical tests on an MMC setup.

This chapter is based on:

- M. Ahmadi, A. Shekhar and P. Bauer, "Reliability Enhanced Fault-Tolerant Full-Bridge Modular Multilevel Converters using Reconfiguration during Open-Circuit Failures," in IEEE Transactions on Power Electronics, 2025.
- M. Ahmadi, F. Kardan, A. Shekhar and P. Bauer, "Influence of Controller Parameters on Open-Circuit Fault Localization Time in Full-Bridge Modular Multilevel Converter," accepted in 26th European Conference on Power Electronics and Applications (EPE), 2025.
- M. Ahmadi, Hitesh Dialani, Mladen Gagic, A. Shekhar and P. Bauer, "Design and Implementation of a Modular Multilevel Converter with Full Bridge Submodules with Software-in-the-Loop Control," accepted in IEEE 7th International Conference on DC Microgrids (ICDCM), 2025.

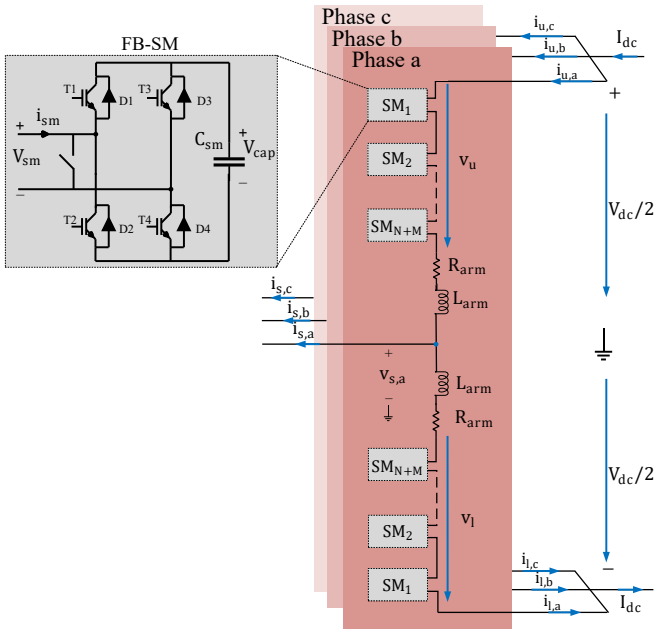

Figure 6.1: MMC configuration with FB SM.

6.1. INTRODUCTION

In most of the studies, the configuration of the SM is considered to be half-bridge (HB) due to its cost-effectiveness. However, many SM proposals and other SM configurations exist, among which the full-bridge (FB) is the most competitive option to handle DC link short-circuit faults [1]. Table 6.1 provides an overview of the existing MMC topologies with different SM configurations [1].

Table 6.1: COMMERCIALLY AVAILABLE MMC TECHNOLOGIES

Manufacturer	Product name	SM topology
Siemens	HVDC Plus	HB/FB
GE/Alstom	HVDC MaxSine	HB/FB
ABB	HVDC Light	HB
CEPRI	HVDC Flexible	HB

Since the FB SM will double the number of power electronics semiconductors, the capital cost of the MMC increases [2]. For this purpose, hybrid MMCs were introduced, where almost 30-50% of the SMs were configured as FB, and the rest as HB, to tolerate the DC link fault while reducing the capital cost [3, 4]. On top of this, there are also redundant SMs to tolerate the open-circuit fault (OCF) in the IGBT [1]. To improve the reliability of the MMC, redundancy concepts are used (chapter 2) whereby adding redundant SMs within the arms, the reliability of the MMC can improve by bypassing the

faulty SMs [5]. Several phases of fault detection, localization, and tolerance are developed to achieve this. In [6], fault detection and localization are developed in FB MMC. In [7], the voting theorem concept is proposed to detect and localize the faulty IGBT SM. The hot-redundant redundancy concept is introduced in [8] to achieve fault-tolerant operation. Methods in [9] provide a complete flowchart of fault detection, localization, and tolerance by applying hot-redundant redundancy. In [10], fault-tolerant operation of the MMC by using redundancy is achieved, while the modulation control strategy is adapted accordingly.

In [11], fault tolerance and ride-through operation are achieved by applying a new operation scheme for medium-voltage applications (MVAs). Authors in [12] proposed a fault-tolerance operation by alerting the control system to the measurements and sensors for SMs' capacitor voltage measurement. In [13], a detection method is proposed under light-load conditions of the MMC, where a variance parameter is applied to achieve precise fault detection. In [14], a fault-tolerance strategy in DC/DC MMC is proposed. Authors in [15] propose a fault localization strategy for MMC, which is applicable when the MMC operates as an inverter (AC/DC) or rectifier (AC/DC). Table 6.2 provides an overview of some relevant literature.

Table 6.2: COMPARISON OF FAULT DETECTION, LOCALIZATION, AND REDUNDANCY METHODS

Ref	FD†	FL‡	FT*	Redundancy	SM	HC§
[12]	✓	✓	✓	k-out-n/load-sharing	HB	Yes
[11]			✓	k-out-n/load-sharing	HB	No
[10]			✓	load-sharing	HB	No
[9]	✓	✓	✓	k-out-n	HB	No
[8]			✓	k-out-n	HB	No
[7]	✓	✓		-	FB	No
[6]	✓	✓	✓	k-out-n	FB	No
[13]	✓			-	HB	Yes
[14]			✓	k-out-n	HB	No
[15]		✓		-	HB	No
[16, 17]	✓	✓		-	HB	No
[18]	✓	✓	✓	k-out-n	HB	No

† Fault Detection ‡ Fault Localization * Fault Tolerance § Hardware Changes

As previously elaborated in Table 6.2, many studies address the open-circuit fault, ranging from detection concepts to localization and fault tolerance. However, few studies focus on the FB MMC. In this chapter, with a focus on FB SM, a new concept of reconfiguration is developed, which is comprehensively explained in Section 6.3. This chapter realizes the idea of detection, localization, redundancy, and reconfiguration to achieve a fault-tolerant MMC.

The configuration of the MMC with FB SM is shown in Fig. 6.1. The fault-tolerant operation through either redundancy or reconfiguration can be achieved by following the proposed algorithm given in Fig. 6.2. The MMC will typically operate in the event of an OCF in any of the four power electronic switches. The fault detection algorithm

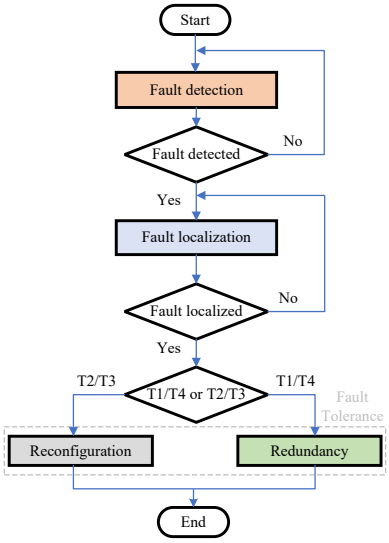

Figure 6.2: Complete algorithm of fault detection to tolerance in MMC.

can detect which pair of IGBTs (T1/T4, or T2/T3) the fault occurred in since the characteristics of the switches are identical. It is challenging to detect the exact IGBT in which the OCF occurred. This challenge is addressed in this study. After fault detection, fault localization and tolerance are achieved by either reconfiguration - if OCF occurs in T2 or T3 - or redundancy - if OCF occurs in T1 or T4.

In this study, load-sharing redundancy is applied, where the reference voltage will be increased. On the other hand, reconfiguration is performed by changing the faulty FB to HB. Hence, the objective of this chapter is to ride through the OCF in the SMs by giving a complete flow of detection, localization, and tolerance, where fault-tolerance is obtained by applying reconfiguration from FB to HB or employing redundant SMs in which the whole SM is bypassed. So, the main contributions are as follows:

- This chapter presents a control-based reconfigurability method for FB MMCs capable of managing open-circuit failures in two out of four IGBTs in an SM without hardware modifications.
- A complete framework is developed, encompassing fault detection, localization, and reconfiguration, ensuring continuous operation and fault tolerance.
- The proposed methodology is validated through a downscaled experimental setup, proving its effectiveness in real-world applications with minimal additional costs or complexity.

The reminder of the chapter is as follows: Section 6.2 provides details on how the prototype of the MMC setup is built using OPAL-RT as a hardware in the loop (HIL). Section 6.3 provides the basic mathematical model of the MMC's operation with redundant SMs and the behavior of the SM under OCF in any of the four IGBTs. Section 6.4 covers the

methodology of how to use reconfiguration or redundancy to tolerate the OCF. Section 6.5 briefly explains fault detection and localization. In Section 6.6, a scaled-down experimental setup is used to validate the effectiveness of this strategy. Finally, the chapter is concluded in Section 6.7.

6.2. MMC DESIGN

In the configuration described in this chapter, each arm of the MMC prototype includes four SMs, totaling 24 SMs for the entire system. The arms are coupled via inductors acting as filters and utilized for control. Each SM typically consists of a capacitor connected to the DC bus of either an HB or FB topology, with both configurations supported by the design used in this chapter [19].

Each SM has a local controller based on the Xilinx XC95144XL CPLD, programmable via JTAG. The OP5600 real-time simulator from OPAL-RT serves as the central controller for all 24 SMs and can be programmed from a computer. To reduce electromagnetic interference (EMI) and ensure high voltage isolation, communication between the OPAL-RT and CPLDs is via fiber-optic transmitters and receivers, with a custom PCB handling the electrical-optical signal conversion.

For practical system control, key parameters such as the capacitor voltage of each SM, arm current, arm voltage, and DC bus voltage are monitored and transmitted to the OPAL-RT. Capacitor voltages are sent via fiber optics, while LEM sensors measure the arm current, arm voltage, and DC bus voltage. These analog measurements are then relayed to the OPAL-RT. Fig. 6.3 illustrates the practical implementation of the lab-scale MMC prototype.

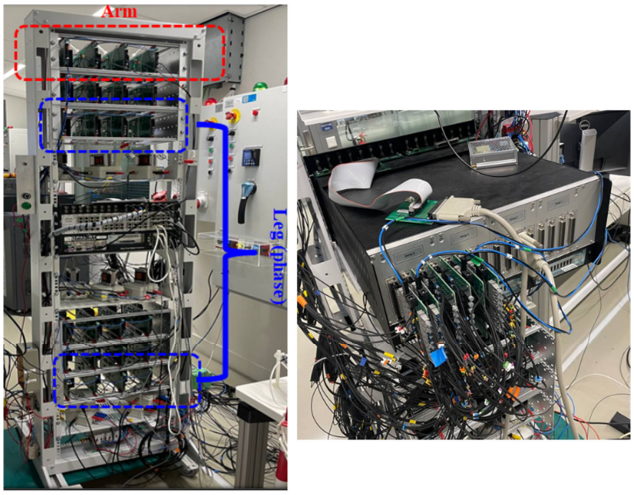

(a) (b)

Figure 6.3: Assembled lab scale MMC tower (a) front-end, (b) back-end.

6.2.1. INTERCONNECTION OF SYSTEM

A top-level overview of the MMC tower shown in Fig. 6.3 is demonstrated in Fig. 6.4. Each SM receives three fiber-optic signals from the OPAL-RT: an enable signal to activate the specific SM, the HB1 gate signal, and the HB2 gate signal, which correspond to the transmitted PWM signals to the OPAL-RT. A DIP switch on the PCB allows the CPLD to be configured for operation in either HB or FB mode.

Each SM sends two fiber-optic signals to the OPAL-RT: one for IGBT module temperature and one for capacitor voltage using PWM. An analog-to-digital circuit converts these measurements into digital signals, which are transmitted via an optical transmitter. The SM uses frequency modulation for both signals, and the OPAL-RT converts the PWM frequency back to voltage using an internal lookup table.

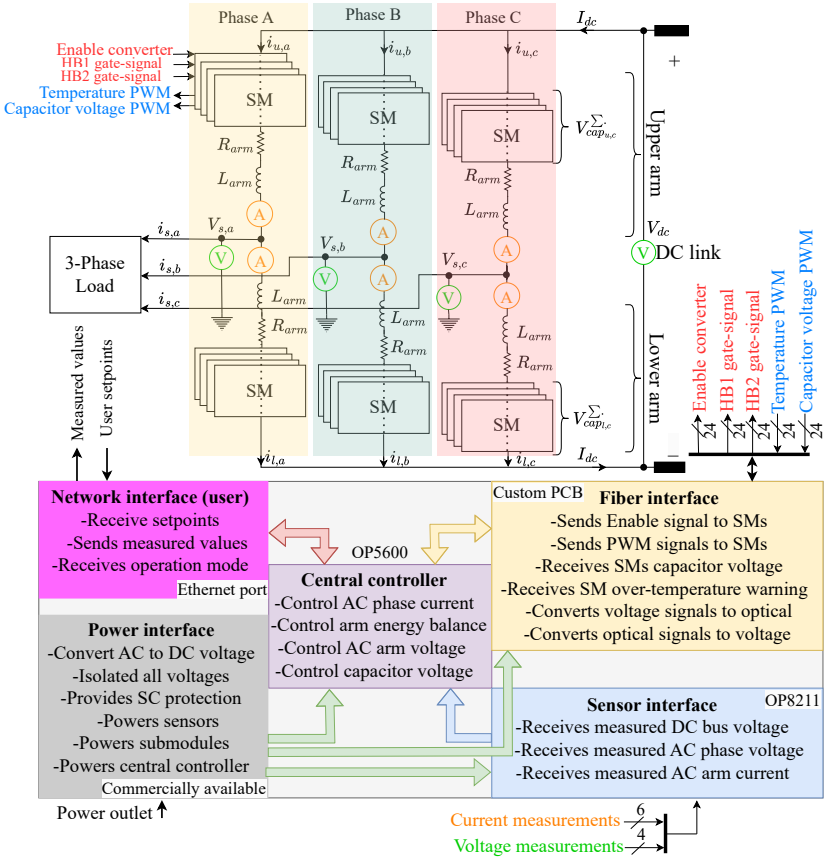

Figure 6.4: Top level interconnection of MMC tower.

A custom inductor is used to control the arm current delivered to the load, with each arm current measured by an S-6NP sensor. The LEM LV 25-P voltage transmitter is employed for phase and DC bus voltage measurements, sending the analog measurement signals to the OPAL-RT through the OP8211 interface.

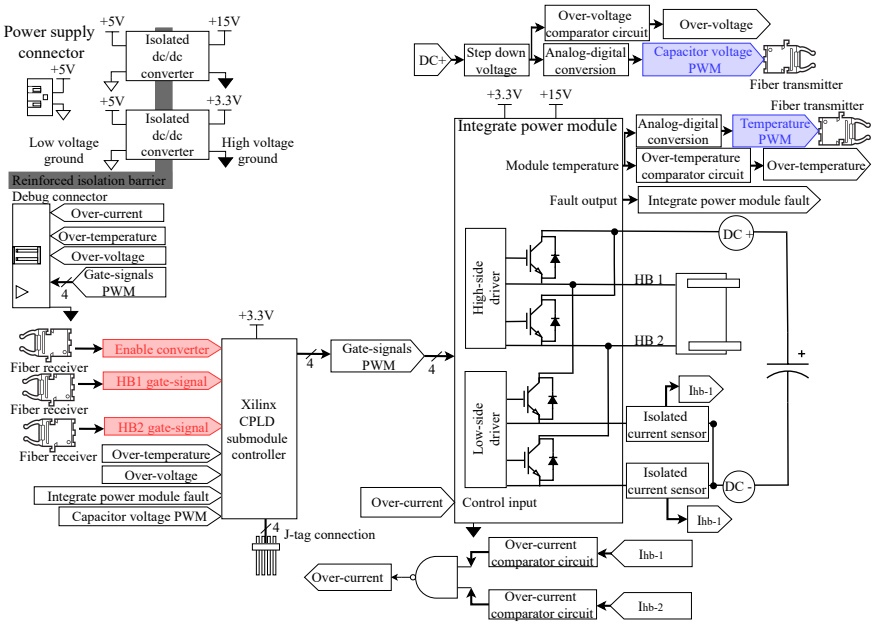

Figure 6.5: Top level schematic of the SM circuit.

6

The OPAL-RT serves as the central controller, enabling the user to implement custom control schemes, tune parameters in real-time, and monitor measured values to achieve the desired voltage and current.

This communication is established via an Ethernet port between the user's PC and the OPAL-RT. Commercially available isolated converters power all components at various DC voltage levels, ensuring safety and ease of use. Circuit breakers are installed in series with the power outlets for additional protection.

6.2.2. SM DESIGN

The MMC FB can be configured using either a FB or two HBs. To reduce complexity and cost and improve reliability, the PS219B4-S power module was selected, featuring three built-in IGBT HBs with integrated gate drivers and a temperature-sensing pin. For FB configuration, two HBs are used, and if HB configuration is desired, it can be achieved by disabling two gate signals from the CPLD.

Capacitor sizing is crucial due to its typically large size. To address this, each SM is divided into two separate PCBs—one for the IGBTs and one for the capacitors, as shown in Fig. 6.6. The IGBT board receives two PWM and enables signals from the OPAL-RT via fiber-optic receivers. At the same time, the DC capacitor voltage and module temperature are returned to the OPAL-RT. Fig. 6.5 shows the top-level schematic of each SM. A supplementary circuit protects against over-current, over-voltage, and over-temperature by comparing the signals to hardware-implemented thresholds. Although the power module includes built-in gate drivers, it does not feature dead-time control. The SM

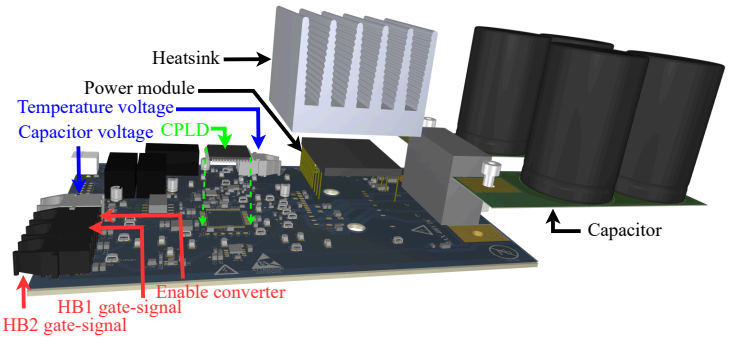

Figure 6.6: CAD rendering of the SM.

swiftly disables PWM signals through the CPLD in over-temperature or over-voltage conditions. The SM bypasses the CPLD for over-current conditions and directly shuts off the power module via the control pin for a faster response. A debug connector with the necessary signals facilitates troubleshooting, and isolated power supplies ensure proper isolation between SMs.

6

6.3. MMC OPERATION CONCEPT AND OCF BEHAVIOUR

6.3.1. MATHEMATICAL MODELS

The configuration of the 3-phase MMC with FB SM is given in Fig. 6.1. The modularity and scalability of MMC are obtained by connecting SMs in series, which makes the MMC applicable to many applications. From the FB SM configuration, it can be seen that four IGBTs and their body diode with a capacitor bank construct the FB SM. A bypass switch is also used to bypass the SM in case of SM failure. For each FB SM, the reconfiguration of the switches can provide different SM outputs, including zero, positive, and negative voltage. However, negative SM voltage, used to tolerate the DC link short-circuit in normal operation, is not considered in this study.

According to the circuitry of the MMC shown in Fig. 6.1 and based on Kirchhoff's law, the following equations can be obtained:

$$R_{\text{arm}} i_{\text{u}} + L_{\text{arm}} \frac{d i_{\text{u}}}{d t} = \frac{1}{2} {}_{dc} - v_u - v_s \tag{6.1}$$

$$R_{\text{arm}} i_{\text{l}} + L_{\text{arm}} \frac{d i_{\text{l}}}{d t} = \frac{1}{2} V_{dc} - v_l - v_s \tag{6.2}$$

Where v_u and v_l are defined as:

$$v_u = \sum_{i=1}^{N+M} V_{\text{SM},i}^{u} \tag{6.3}$$

$$v_l = \sum_{i=1}^{N+M} V_{\text{SM},i}^{l} \tag{6.4}$$

$$i_u = i_{cir} + \frac{1}{2} i_s \tag{6.5}$$

$$i_l = i_{cir} - \frac{1}{2} i_s \tag{6.6}$$

Here, $V^u_{\mathrm{SM},i}$ and $V^l_{\mathrm{SM},i}$ represent the voltage across the SM capacitors in the upper and lower arms, respectively. where v_u and v_l are the voltages of the upper arm and lower arm, respectively, and i_u and i_l are the upper arm and lower arm currents. i_{cir} is the circulating current that is calculated as follows:

$$i_{\mathrm{cir}} = \frac{1}{2}(i_u + i_l) \tag{6.7}$$

The DC and AC dynamics of the MMC can be obtained by summing and subtracting equations (2) and (3), respectively.

$$2L_{\mathrm{arm}} \frac{d i_{\mathrm{cir}}}{dt} + 2R_{\mathrm{arm}} i_{\mathrm{cir}} = V_{dc} - v_u - v_l \tag{6.8}$$

$$L_{\mathrm{arm}} \frac{d i_{\mathrm{s}}}{dt} + R_{\mathrm{arm}} i_{\mathrm{s}} = v_l - v_u - 2v_s \tag{6.9}$$

Ideally, the sum of v_u and v_l should equal V_{dc}, while $v_u - v_l$ should give perfectly sinusoidal AC outputs. So,

$$v_s = m\cos(\omega t + \phi)\frac{V_{dc}}{2} \tag{6.10}$$

where m is the modulation index with a value between $[0, 1]$. Assuming that there is no voltage drop across the arm's resistance:

$$v_u = \left(1 - m\cos(\omega t + \phi)\right)\frac{V_{dc}}{2} \tag{6.11}$$

$$v_l = \left(1 + m\cos(\omega t + \phi)\right)\frac{V_{dc}}{2} \tag{6.12}$$

6.3.2. LS-ARS OPERATION

The redundant SMs are used to increase the reliability of the MMC in case of SM failure. However, there are several methods of operating the redundant SMs. In this chapter, the LS-ARS is applied. In this redundancy strategy, all the existing SMs (original and redundant) share the load, so the voltage across each SM will be lower, as was detailed in chapter 3. However, in the case of an SM failure, the voltage across the remaining SMs increases as follows:

$$v_{u-ref} = \frac{1}{N + M - F_u}\left(1 - m\cos(\omega t + \phi)\right)\frac{V_{dc}}{2} \tag{6.13}$$

$$v_{l-ref} = \frac{1}{N + M - F_l}\left(1 + m\cos(\omega t + \phi)\right)\frac{V_{dc}}{2} \tag{6.14}$$

Where F_u and F_l are the number of faulty SMs in the upper and lower arms, respectively.

6.3.3. SM'S BEHAVIOR IN CASE OCF

In this section, the FB SM behavior under various conditions is evaluated. These conditions include inserted, bypassed 1, and bypassed 2 states. For each state, we analyze the behavior during normal operation and in the event of an OCF in one of the four IGBTs (T1, T2, T3, and T4). The SM voltage behavior is explained in detail, focusing on the voltage across the capacitor (V_{cap}) and the SM's ability to charge or discharge under different current flow scenarios (i_{SM}). The current behavior in the SM during OCFs is summarized in the following tables and figures.

INSERTED CONDITION

In the inserted state, the SM is actively contributing to the output voltage, allowing for the generation of $+V_{cap}$ or $-V_{cap}$ based on the system's requirements and current flow. During normal operation, the SM can either charge or discharge its capacitor depending on the current direction (i_{SM}). In case of an OCF:

- **Normal Operation:** The SM charges or discharges normally, with output voltages of $+V_{cap}$ depending on the current direction (in Table 6.3 (a) and Fig. 6.7 (a)).
- **OCF in T1:** When $i_{SM} < 0$, T1 fails to turn on, but the current forces to flow through D2, bypassing the capacitor. So, it is not possible to discharge the capacitor and its voltage only increases (in Table 6.3 (b) and Fig. 6.7 (b)).
- **OCF in T2:** Under an OCF in T2, the SM operates similarly and can be charged and discharged similarly to normal operation (in Table 6.3 (c) and Fig. 6.7 (c)).
- **OCF in T3:** A failure in T3 follows the same pattern, with the SM operating normally as OCF in T2 (in Table 6.3 (d) and Fig. 6.7 (d)).
- **OCF in T4:** This mirrors the case of T1. When $i_{SM} < 0$, the SM remains bypassed, preventing discharge (in Table 6.3 (e) and Fig. 6.7 (e)).

Table 6.3 and Fig. 6.7 show the voltage outputs and current paths for the inserted condition, and it can be concluded that OCF in T1 and T4 will deteriorate the proper operation of the SM. At the same time, OCF in T2 and T3 does not impact inserting the SM.

Table 6.3: SM'S OUTPUT VOLTAGE FOR INSERTED CONDITION AND CONSIDERING T1-T4 OCFS CONDITION

	Normal, (a)	OCF in T1, (b)	OCF in T2, (c)	OCF in T3, (d)	OCF in T4, (e)
Switch State	{T1,T2,T3,T4} {on,off,off,on}	{T1,T2,T3,T4} {OCF,off,off,on}	{T1,T2,T3,T4} {on,OCF,off,on}	{T1,T2,T3,T4} {on,off,OCF,on}	{T1,T2,T3,T4} {on,off,off,OCF}
$i_{sm} \geq 0$	$V_{sm} = V_{Cap}$, Charge	$V_{sm} = V_{Cap}$, Charge	$V_{sm} = V_{Cap}$, Charge	$V_{sm} = V_{Cap}$, Charge	$V_{sm} = V_{Cap}$, Charge
$i_{sm} < 0$	$V_{sm} = V_{Cap}$, Discharge	$V_{sm} = 0$, –	$V_{sm} = V_{Cap}$, Discharge	$V_{sm} = V_{Cap}$, Discharge	$V_{sm} = 0$, –

Table 6.4: SM'S OUTPUT VOLTAGE FOR BYPASSED CONDITION 1 AND CONSIDERING T1-T4 OCFS CONDITION

	Normal, (a)	OCF in T1, (b)	OCF in T2, (c)	OCF in T3, (d)	OCF in T4, (e)
Switch State	{T1,T2,T3,T4} {on,off,on,off}	{T1,T2,T3,T4} {OCF,off,on,off}	{T1,T2,T3,T4} {on,OCF,on,off}	{T1,T2,T3,T4} {on,off,OCF,off}	{T1,T2,T3,T4} {on,off,on,OCF}
$i_{sm} \geq 0$	$V_{sm} = 0$, –	$V_{sm} = 0$, –	$V_{sm} = 0$, –	$V_{sm} = V_{Cap}$, Charge	$V_{sm} = 0$, –
$i_{sm} < 0$	$V_{sm} = 0$, –	$V_{sm} = V_{Cap}$, Charge	$V_{sm} = 0$, –	$V_{sm} = 0$, –	$V_{sm} = 0$, –

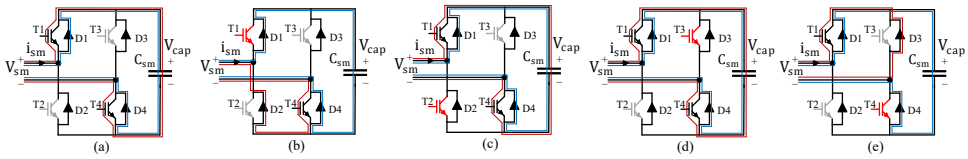

Figure 6.7: SM's behavior for the inserted mode in case of (a) normal operation, (b) OCF in T1, (c) OCF in T2, (d) OCF in T3, and (e) OCF in T4

.

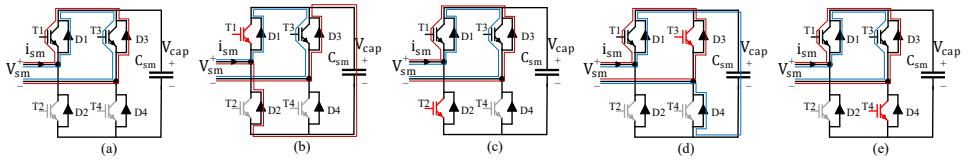

Figure 6.8: SM's behavior for the bypassed mode 1 in case of (a) normal operation, (b) OCF in T1, (c), OCF in T2, (d), OCF in T3, and (e) OCF in T4

.

BYPASSED CONDITION 1

In bypassed condition 1, the SM is bypassed, preventing the capacitor from affecting the output voltage. However, some capacitor charging may still occur in faulty conditions depending on the current flow.

- **Normal Operation:** Shown in Table 6.4 (a) and Fig. 6.8 (a), the output voltage is zero, and the SM is fully bypassed, with no charging or discharging of the capacitor.
- **OCF in T1:** When $i_{SM} < 0$, the SM is inserted and capacitor gets charged as shown in Table 6.4 (b) and Fig. 6.8 (b).
- **OCF in T2:** The SM is not impacted in this case and can be bypassed as required as given in Table 6.4 (c) and Fig. 6.8 (c).
- **OCF in T3:** In this scenario given in Table 6.4 (d) and Fig. 6.8 (d), an OCF in T3 increases the charging during bypassed conditions when $i_{SM} \geq 0$.
- **OCF in T4:** The behavior mirrors OCF in T2 -in Table 6.4 (e) and Fig. 6.8 (e)-, where the SM is bypassed as required.

Details of the current paths and SM voltage under bypass condition 1 are summarized in Table 6.4 and Fig. 6.8. It can be concluded that OCF in T1 and T3 will impact the SM's operation under bypassed condition 1 and charge the SM more than normal operation.

BYPASSED CONDITION 2

Bypassed condition 2 involves a different configuration of the bypass switches. The SM is inserted under certain fault conditions, which can cause the capacitor to charge in ways not typically seen in normal operation.

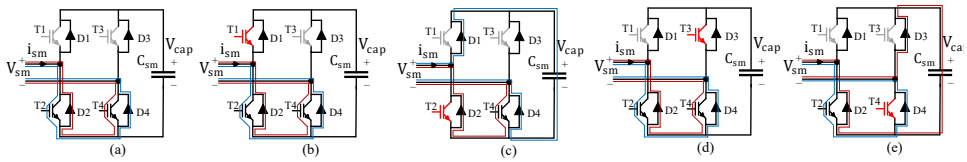

Figure 6.9: SM's behavior for the bypassed mode 2 in case of (a) normal operation, (b) OCF in T1, (c) OCF in T2, (d) OCF in T3, and (e) OCF in T4

.

- **Normal Operation:** The SM remains bypassed with zero output voltage as given in Table 6.5 (a) and Fig. 6.9 (a).
- **OCF in T1:** The SM is bypassed as expected as detailed in Table 6.5 (b) and Fig. 6.9 (b).
- **OCF in T2:** The capacitor charges more than usual under bypassed condition 2, when $i_{SM} \geq 0$ as given in Table 6.5 (c) and Fig. 6.9 (c).
- **OCF in T3:** Similar to T1, the SM is unaffected and can be bypassed without any problem as given in Table 6.5 (d) and Fig. 6.9 (d).
- **OCF in T4:** In this case, capacitor charges under bypassed condition 2, with increased V_{cap} during $i_{SM} < 0$ as given in Table 6.5 (e) and Fig. 6.9 (e).

Table 6.5 and Fig. 6.9 describe this state's current path and voltage output. As it was explained, only OCF in T2 and T4 will affect the SM's behavior under bypassed condition 2, which causes the capacitor to charge more compared to the normal operation.

Table 6.5: SM'S OUTPUT VOLTAGE FOR BYPASSED CONDITION 2 AND CONSIDERING T1-T4 OCFS CONDITION

	Normal, (a)	OCF in T1, (b)	OCF in T2, (c)	OCF in T3, (d)	OCF in T4, (e)
Switch State	{T1,T2,T3,T4} {off,on,off,on}	{T1,T2,T3,T4} {OCF,on,off,on}	{T1,T2,T3,T4} {off,OCF,off,on}	{T1,T2,T3,T4} {off,on,OCF,on}	{T1,T2,T3,T4} {off,on,off,OCF}
$i_{sm} \geq 0$	$V_{sm} = 0, -$	$V_{sm} = 0, -$	$V_{sm} = V_{Cap}$, Charge	$V_{sm} = 0, -$	$V_{sm} = 0, -$
$i_{sm} < 0$	$V_{sm} = 0, -$	$V_{sm} = 0, -$	$V_{sm} = 0, -$	$V_{sm} = 0, -$	$V_{sm} = V_{Cap}$, Charge

So, according to the explanations provided in Tables 6.3-6.5 and the dynamics of the MMC given in (6.8) and (6.9), the behavior of the circulating current is summarized in Table 6.6. As can be seen, it shows the ideal circulating current $\tilde{i}_{cir}$. For example, in case of a fault in T1/T4, the measured circulating current i_{cir} will be larger than the ideal values. These facts can be used later for fault detection and reconfigurability, which will be detailed in the subsequent section. Further details can be found in [9].

Table 6.6: CURRENT CHARACTERISTICS UNDER OCF

OCF in T2/T3	**OCF in T1/T4**
$\tilde{i}_{cir} \geq i_{cir}$	$\tilde{i}_{cir} < i_{cir}$

Table 6.7: FAULT TOLERANCE ACHIEVEMENT THROUGH REDUNDANCY AND RECONFIGURATION OF THE FB SM

State†	OCF in T1 (a), T4 (d)	OCF in T2 (b)	OCF in T3 (c)
Bypassed	Redundancy	Reconfiguration → T1, T2, T3, T4 (on, OCF, on, off)	Reconfiguration → T1, T2, T3, T4 (off, on, OCF, on)
Inserted	Redundancy	Reconfiguration → T1, T2, T3, T4 (on, OCF, off, on)	Reconfiguration → T1, T2, T3, T4 (on, off, OCF, on)

† For both current directions: $i_{sm} \geq 0$ and $i_{sm} < 0$

6.4. RECONFIGURABILITY METHODOLOGY

As detailed in Section 6.3, the OCF can occur in any of the switches, which inevitably increases the SM's voltage in inverter working mode [16]. Commonly, after fault occurrence, the SM is bypassed by turning on its bypass switch, which can be tolerated by using redundant SMs. However, there might be healthy IGBTs, and by applying the method of this chapter, the fault can be tolerated without any hardware changes. To achieve this, as shown in Fig. 6.10, the original number of levels can be kept in the case of OCF in T2 and T3, extending the system's lifetime significantly.

As shown in Fig. 6.10, if an OCF occurs in T2, the SM can still operate as an HB by keeping T1 all the time ON. The same operation can be achieved if the OCF takes place in T3 and by keeping T4 OFF all the time. However, the SM should be bypassed if OCF

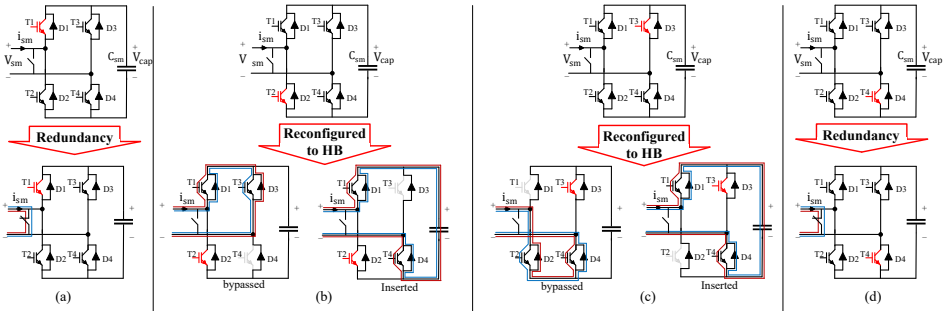

Figure 6.10: Reconfiguration and redundancy of SM under OCF in all IGBTs to achieve fault tolerance operation.

occurs in T1 and T4 without applying any hardware changes. There is also a challenge to determine in which switch the fault took place, as explained in Section II.C, since the operational behavior of the MMC and SMs are identical in the case of a T1/T4 or T2/T3 pair OCFs. So, an algorithm is developed, detailed in the subsequent section, to solve this issue.

6.5. FAULT DETECTION AND LOCALIZATION

In this chapter, and based on the MMC's characteristics before and after OCF, a complete fault diagnosis, localization, and tolerance are explained. For this purpose, a state observer is applied to detect the fault. The difference between the SM's voltage is considered for fault localization, and if it is more than the specified threshold, the faulty SM can be detected. Upon the high fault detection flag, the faulty SM will finally be bypassed (redundancy) or reconfigured to HB based on the information provided by the

fault detection algorithm.

6.5.1. FAULT DETECTION ALGORITHM

The state observer is one of the most widely used methods for fault detection, which is adopted in industry as well [9]. The working principle of this detector is to compare the measured output from the MMC with the observed value, and if the difference is greater than the threshold, the fault can be detected. By adopting this method, the fault can be detected within a few milliseconds, and it is even possible to determine in which pair of switches the OCF occurred.

The dynamics of the MMC in state-space form is given as:

$$\dot{x} = Ax + Bv + De \tag{6.15}$$

$$y = Cx \tag{6.16}$$

with

$$x = \begin{pmatrix} i_{\text{cir}} \\ i_s \end{pmatrix}, v = \begin{pmatrix} v_l \\ v_u \end{pmatrix}, e = \begin{pmatrix} V_{dc} \\ v_s \end{pmatrix}$$

$$A = \begin{pmatrix} -\frac{R_{\text{arm}}}{L_{\text{arm}}} & 0 \\ 0 & -\frac{R_{\text{arm}}}{L_{\text{arm}}} \end{pmatrix}, B = \begin{pmatrix} \frac{-1}{2L_{\text{arm}}} & \frac{-1}{2L_{\text{arm}}} \\ \frac{1}{L_{arm}} & -\frac{1}{L_{arm}} \end{pmatrix}$$

$$C = \begin{pmatrix} 1 & 0 \\ 0 & 1 \end{pmatrix}, D = \begin{pmatrix} \frac{1}{2L_{\text{arm}}} & 0 \\ 0 & -\frac{2}{L_{\text{arm}}} \end{pmatrix}$$

So, the observer is given as:

$$\dot{\hat{x}} = A\hat{x} + Bv + De + K(y - \hat{y}) \tag{6.17}$$

$$\hat{y} = C\hat{x} \tag{6.18}$$

in which $\hat{x}$ is the estimated value the observer gives. Also, K is the observer gain, which is shown as follows: based on the eigenvalues of the matrix $A - KC$, its value should be chosen as follows to meet the stability condition:

$$K = \begin{pmatrix} k & 0 \\ 0 & k \end{pmatrix}, \quad k > -\frac{R_{\text{arm}}}{L_{\text{arm}}}$$

Therefore, by comparing the observed current $\hat{i}_{\text{cir}}$ and the real current i_{cir}, the detection algorithm is shown in Fig. 6.11. Hence, if there is no OCF, the measured i_{cir} can track $\hat{i}_{\text{cir}}$ with a small error, also, the time step Δt and K should be appropriately selected to avoid false detection flags.

6.5.2. FAULT LOCALIZATION

In this study, the faulty SM is located by comparing the difference between maximum capacitor voltages within the arm's capacitors, as given in [20]. The faulty SM is located if the difference is more than the threshold. Fig. 6.12 shows the applied algorithm. If the threshold criterion is met, the timer starts, and if both conditions are met, the localization flag becomes high. Note that the threshold selection for fault localization should be 10% more than the capacitor voltage peak value to avoid false alarms.

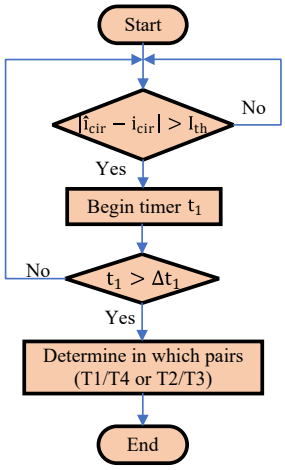

Figure 6.11: Flowchart of fault detection.

6.5.3. FAULT TOLERANCE

As explained, this chapter aims to achieve fault tolerance and capability in FB MMC by either applying redundancy (OCF in T1 or T4) or reconfiguring the FB to HB (OCF in T2 or T3).

RECONFIGURABILITY

If the OCF occurs in T2 or T3, the SM can still be operated as HB, but the dilemma here is that without hardware changes, it is challenging to detect which switch the OCF precisely took place. To achieve this, it is assumed that OCF occurred in T3 if the first voltage threshold is reached, the corresponding signals are sent where T4 will always be ON, and the other HB (T1, T2) will continue the operation. However, if the actual OCF occurred in T2, and the SM's behavior is given in Table 6.8.

Table 6.8: SM'S OUTPUT VOLTAGE UNDER T2 OCF CONDITION AND KEEPING RIGHT HB ALWAYS AS T3: OFF AND T4: ON AS PART OF RECONFIGURATION PROCESS

	Inserted, (a)	Bypassed, (b)
Switch State	{T1,T2,T3,T4} {on,OCF,off,on}	{T1,T2,T3,T4} {off,OCF,off,on}
$i_{sm} \geq 0$	$V_{sm} = V_{Cap}$, Charge	$V_{sm} = V_{Cap}$, Charge
$i_{sm} < 0$	$V_{sm} = V_{Cap}$, Discharge	$V_{sm} = 0$, –

As can be seen, this combination will not work as the SM's voltage keeps increasing. Therefore, the second threshold will be reached (V_{th2}), which shows the faulty IGBT is T2. Hence, the right-side HB (T3, T4) will continue the operation, and the left-side HB (T1, T2) will always be as T1: ON and T2:OFF(OCF). The algorithm for reconfiguration to HB is shown in Fig. 6.14.

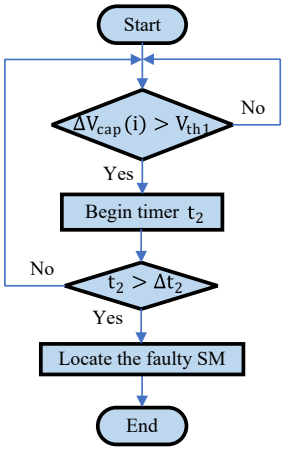

Figure 6.12: Flowchart of fault localization algorithm.

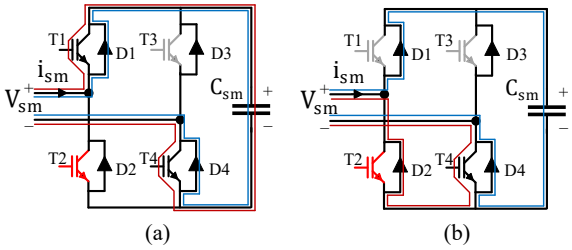

Figure 6.13: SM's current behavior under T2 OCF while keeping the right HB as T3: OFF and T4: ON for (a) inserted and (b) bypassed conditions.

REDUNDANCY

In the case of OCF in T1 or T4, the FB SM should be bypassed, and the number of operating SMs within that specific arm will decrease. This is a well-established concept, and the details can be found in many literature sources [21]. The fault tolerance in this case can be achieved by following the algorithm given in Fig. 6.15.

6.6. EXPERIMENTAL VALIDATION

In this section, the effectiveness of the proposed fault-tolerance methodology is validated, where a scaled down MMC with the given characteristics in Table 6.9 is used. As explained, the impact of both redundancy and reconfiguration is investigated. Here, the redundancy methodology is assumed to be load-sharing with $N = 3$ and $M = 1$, representing the redundant SMs. Fig. 6.16 presents a picture of the downscaled MMC in the lab. In this prototype, the OPAL-RT acts as the high-level controller, reads the analog and digital inputs from the hardware and sends the gating signals. Each SM also has its local circuitry, which includes the protection circuitry. This study uses the Nearest Level Modulation (NLM) for the modulation strategy. Also, the controller applied is adapted

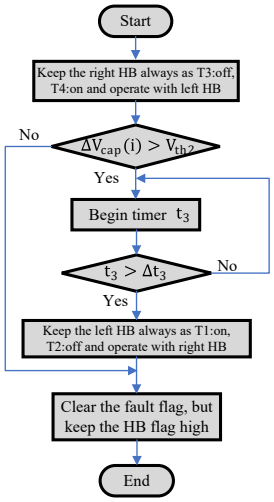

Figure 6.14: Algorithm for reconfigurability in case of OCF for T2 or T3.

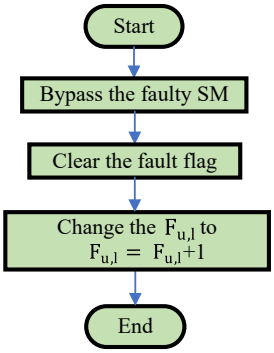

Figure 6.15: Redundancy algorithm for OCF in T1 or T4.

from [22].

Table 6.9: CHARACTERISTICS OF LAB SCALE MMC PROTOTYPE

Symbols	Item	Value
N+M	Number of SMs (including redundant)	3+1
V_{dc}	Pole-to-pole DC voltage	100 V
V_{SM}	Applied IGBT voltage	25 V
C_{SM}	SM capacitance	4 mF
L_{arm}	Arm inductance	4.3 mH
$R_{arm}(R)$	Arm resistance	0.5 Ω
$f_{Control}$ (NLM)	Transition rate of controller	2000 Hz
R_{Load}	Load resistance	10 Ω
k	Observer gain	5
I_{th}	Current threshold	5 A
V_{th1}	Voltage threshold 1	1 V
V_{th2}	Voltage threshold 2	1.5 V
Δt_1	Delay time 1	2 ms
Δt_2	Delay time 2	1 ms
Δt_3	Delay time 3	1 ms

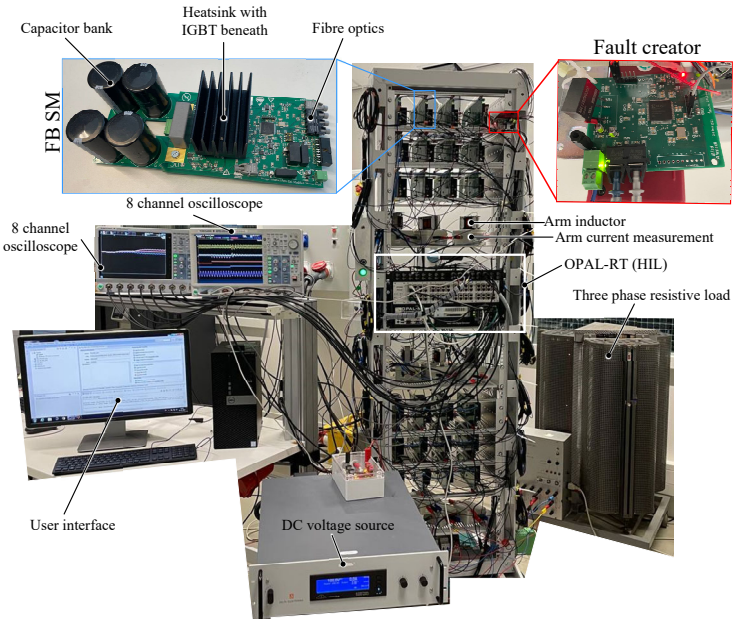

Figure 6.16: Experimental prototype of the three-phase FB MMC setup.

In this chapter, a fault creator is used to mimic better the OCF scenario, which connects to one of the SMs and overwrites the gating signals from OPAL-RT. Hence, it is possible to keep any arbitrary IGBT open, which mimics the OCF.

6.6.1. OCF IN T1 OR T4

The characteristics of the MMC under OCF in T1 or T4 are identical; therefore, the results are only shown for OCF in T1. Fig. 6.17 shows the MMC behavior in the case of T1 OCF. As can be seen, the fault can be detected in less than 10 ms before the fault signal goes high, which is the output of the observer by comparing the measured circulating current i_{cir} with the ideal i_{cir}. It can be seen from this difference, $i_{\text{cir}} - \hat{i}_{\text{cir}}$, that the fault occurred

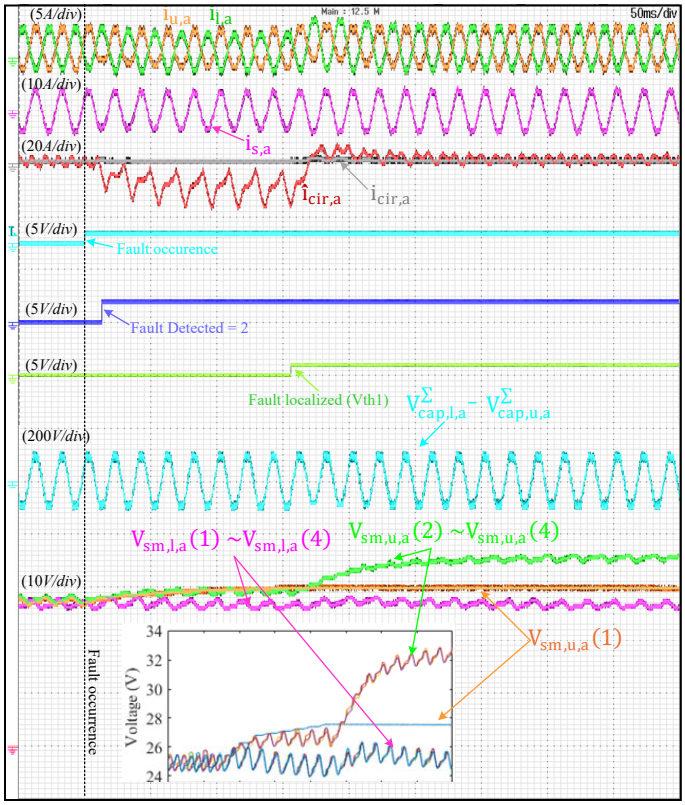

Figure 6.17: Experimental results when the proposed algorithm is applied at T1 or T4 OCFs.

in the pair of T1/T4. After the detection, the localization is achieved around 150 ms, and the difference between the faulty SM and the healthy ones will be more than V_{th1}. Other localization methods can perform localization faster, but this is not the scope of this study. Finally, after the faulty SM is localized, the voltage reference of the healthy SMs will be increased to 100/3 = 33.3 V.

6.6.2. OCF IN T3

The behavior of the MMC under T3 OCF is shown in Fig. 6.18. As can be seen, in less than 10 ms, the observer detects the fault, and since $i_{\text{cir}} < \hat{i}_{\text{cir}}$ correctly determines it. The faulty SM is localized after less than 20 ms, where the first fault localization flag goes high. Based on the algorithm, which ensures the fault occurred on T3, the FB SM is reconfigured to HB by always keeping the T3: OFF and T4: ON. The sorting algorithm will balance the voltage of the SMs in a similar way to that of other healthy SMs. In this case, the number of levels remains the same, and the SM where the OCF occurred is reconfigured to HB.

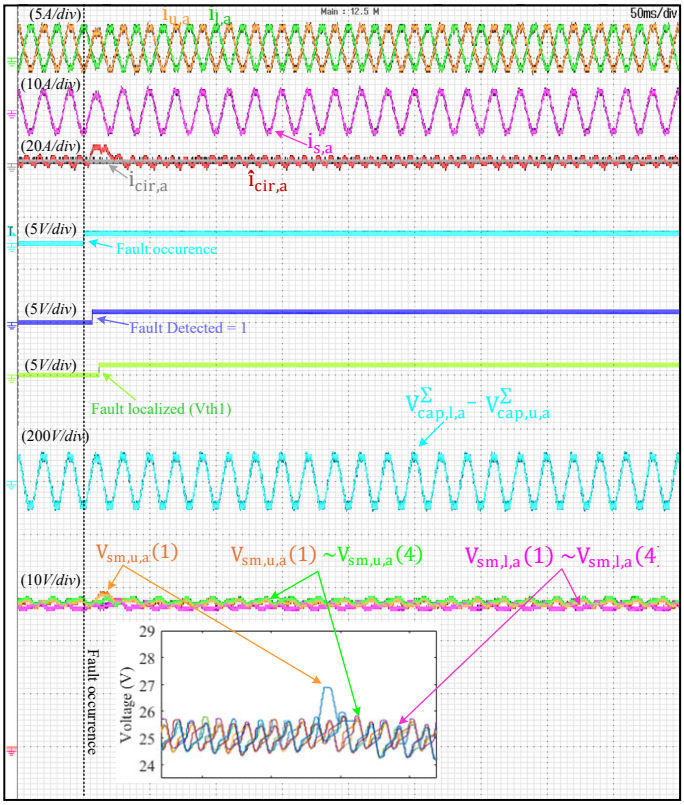

Figure 6.18: Experimental results when the proposed algorithm is applied at T3 OCF.

6.6.3. OCF IN T2

The behavior of the MMC in the case of OCF in T2 is identical to the T3 OCF. However, the reconfiguration algorithm first assures that the OCF occurred in T2, as explained in Table 6.8. So, as can be seen, the SMs will be charged more, which, in this case, will cause

the second voltage threshold to be reached. Hence, the controller realizes that the OCF occurred in T2 and reconfigures to HB by keeping the right half-bridge across T1 ON and T2 OFF. The results are presented in Fig. 6.19, where the fault is ridden through in less than 20 ms, and reconfiguration is obtained.

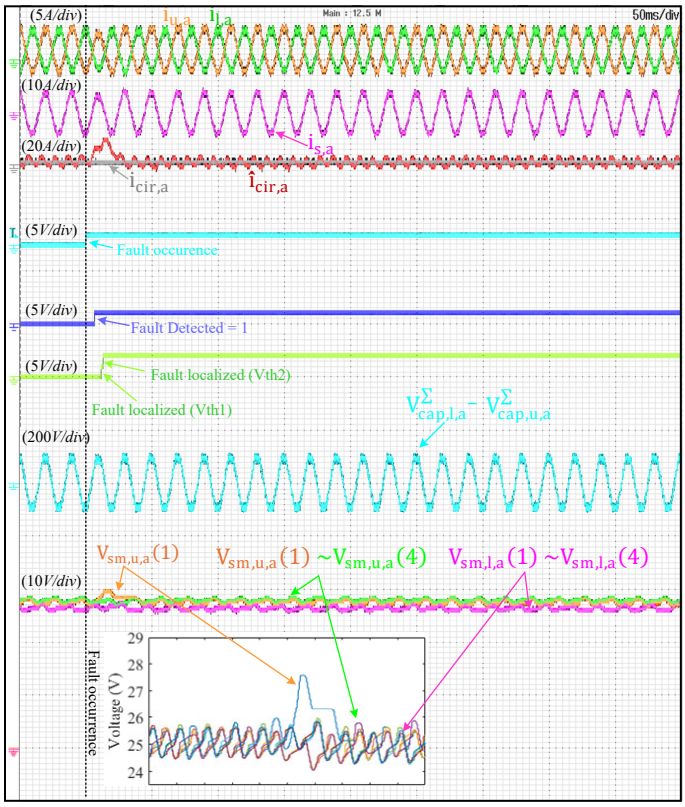

Figure 6.19: Experimental results when the proposed algorithm is applied at T2 OCF.

6.7. CONCLUSION

This chapter introduces a fault-tolerant reconfiguration method for FB MMC, addressing OCFs in IGBTs. The proposed approach demonstrates its effectiveness through an experimental setup without requiring additional hardware or significant cost increases. Focusing on reconfigurability through control logic adjustments ensures continuous operation and significantly enhances system reliability.

The experimental validation confirms the practicality of the proposed method, showcasing how it effectively detects faults, localizes them, and reconfigures the system for fault tolerance. The seamless transition between fault states and reconfiguration demonstrates the robustness of this method for high-reliability applications. This work con-

tributes to extending the operational lifetime of FB MMCs while reducing maintenance and downtime in critical power systems.

REFERENCES

[1] J. V. M. Farias, A. F. Cupertino, H. A. Pereira, S. I. Seleme, and R. Teodorescu, *On converter fault tolerance in mmc-hvdc systems: A comprehensive survey,* IEEE Journal of Emerging and Selected Topics in Power Electronics **9**, 7459 (2021).

[2] W. Lin, D. Jovcic, S. Nguefeu, and H. Saad, *Full-bridge mmc converter optimal design to hvdc operational requirements,* IEEE Transactions on Power Delivery **31**, 1342 (2016).

[3] J. Xu, P. Zhao, and C. Zhao, *Reliability analysis and redundancy configuration of mmc with hybrid submodule topologies,* IEEE Transactions on Power Electronics **31**, 2720 (2016).

[4] R. Zeng, L. Xu, L. Yao, and B. W. Williams, *Design and operation of a hybrid modular multilevel converter,* IEEE Transactions on Power Electronics **30**, 1137 (2015).

[5] M. Ahmadi, A. Shekhar, and P. Bauer, *Mixed redundancy strategy for modular multilevel converters in high-power applications,* IEEE Open Journal of the Industrial Electronics Society **5**, 535 (2024).

[6] K. Li, Z. Zhao, L. Yuan, S. Lu, and Y. Jiang, *Fault detection and tolerant control of open-circuit failure in mmc with full-bridge sub-modules,* in *2016 IEEE Energy Conversion Congress and Exposition (ECCE)* (2016) pp. 1–6.

[7] W. Zhou, H. Yang, M. Chen, W. Li, X. He, and J. Han, *Open-circuit failure detection and localization of full-bridge submodules for mmcs with single ring theorem,* in *2019 IEEE Applied Power Electronics Conference and Exposition (APEC)* (2019) pp. 1794–1799.

[8] K. Li, L. Yuan, Z. Zhao, S. Lu, and Y. Zhang, *Fault-tolerant control of mmc with hot reserved submodules based on carrier phase shift modulation,* IEEE Transactions on Power Electronics **32**, 6778 (2017).

[9] B. Li, S. Shi, B. Wang, G. Wang, W. Wang, and D. Xu, *Fault diagnosis and tolerant control of single igbt open-circuit failure in modular multilevel converters,* IEEE Transactions on Power Electronics **31**, 3165 (2016).

[10] B. Li, Z. Xu, J. Ding, and D. Xu, *Fault-tolerant control of medium-voltage modular multilevel converters with minimum performance degradation under submodule failures,* IEEE Access **6**, 11772 (2018).

[11] Q. Xiao, J. Wang, Y. Jin, L. Chen, H. Jia, T. Dragičević, and R. Teodorescu, *A novel operation scheme for modular multilevel converter with enhanced ride-through capability of submodule faults,* IEEE Journal of Emerging and Selected Topics in Power Electronics **9**, 1258 (2021).

[12] S. Yang, Y. Tang, and P. Wang, *Seamless fault-tolerant operation of a modular multilevel converter with switch open-circuit fault diagnosis in a distributed control architecture,* IEEE Transactions on Power Electronics **33**, 7058 (2018).

[13] C. Liu, F. Deng, X. Cai, Z. Wang, Z. Chen, and F. Blaabjerg, *Submodule open-circuit fault detection for modular multilevel converters under light load condition with rearranged bleeding resistor circuit,* IEEE Transactions on Power Electronics **37**, 4600 (2022).

[14] R. Razani and Y. A.-R. I. Mohamed, *Fault-tolerant operation of the dc/dc modular multilevel converter under submodule failure,* IEEE Journal of Emerging and Selected Topics in Power Electronics **9**, 6139 (2021).

[15] C. Liu, F. Deng, Q. Heng, R. Zhu, M. Liserre, Z. Wang, and W. Chen, *Fault localization strategy for modular multilevel converters under submodule lower switch open-circuit fault,* IEEE Transactions on Power Electronics **35**, 5190 (2020).

[16] Z. Geng, M. Han, Z. W. Khan, and X. Zhang, *Detection and localization strategy for switch open-circuit fault in modular multilevel converters,* IEEE Transactions on Power Delivery **35**, 2630 (2020).

[17] W. Zhou, J. Sheng, H. Luo, W. Li, and X. He, *Detection and localization of submodule open-circuit failures for modular multilevel converters with single ring theorem,* IEEE Transactions on Power Electronics **34**, 3729 (2019).

[18] J. Wang, H. Ma, and Z. Bai, *A submodule fault ride-through strategy for modular multilevel converters with nearest level modulation,* IEEE Transactions on Power Electronics **33**, 1597 (2018).

[19] M. Moranchel, F. M. Sanchez, E. J. Bueno, F. J. Rodriguez, and I. Sanz, *Six-level modular multilevel converter prototype with centralized hardware platform controller,* in *IECON 2015 - 41st Annual Conference of the IEEE Industrial Electronics Society* (2015) pp. 003863–003868.

[20] P. Hu, D. Jiang, Y. Zhou, Y. Liang, J. Guo, and Z. Lin, *Energy-balancing control strategy for modular multilevel converters under submodule fault conditions,* IEEE Transactions on Power Electronics **29**, 5021 (2014).

[21] J. V. M. Farias, A. F. Cupertino, H. A. Pereira, S. I. S. Junior, and R. Teodorescu, *On the redundancy strategies of modular multilevel converters,* IEEE Transactions on Power Delivery **33**, 851 (2018).

[22] K. Sharifabadi, L. Harnefors, H.-P. Nee, S. Norrga, and R. Teodorescu, *Dynamics and control,* in *Design, Control, and Application of Modular Multilevel Converters for HVDC Transmission Systems* (2016) pp. 133–213.

7

CONCLUSION

The research presented in this dissertation has addressed the critical challenges of reliability and cost-efficiency in MMCs. The core objective has been to enhance resilience and economic viability by leveraging redundancy, modularity, and reconfigurability. This conclusion synthesizes the study's outcomes, emphasizing key numerical improvements and their implications.

Reliability has been a central focus throughout this work. MMCs, extensively utilized in medium- and high-voltage applications such as HVDC systems and renewable energy integration, demand high reliability to ensure continuous operation and minimize downtime. Traditional reliability assessment methods, such as the MIL and FIDES methodologies, often fail to address real-world operating conditions' complexities. A new framework combining analytical approaches with MCS was proposed and implemented to overcome these limitations. This hybrid approach enabled more accurate reliability predictions by modeling dynamic operational stresses and incorporating redundancy strategies. For example, evaluating the reliability of MMCs using LS-ARS and SRS under a specific mission profile posed significant analytical challenges. However, employing MCS demonstrated that the problem could be resolved with over 99% accuracy, provided the number of trials exceeded 10,000. This capability underscores the robustness and precision of MCS in handling scenarios where analytical methods falter. Furthermore, a comparative analysis of existing reliability methodologies highlighted the variability in outputs derived from different methods, emphasizing that the absolute reliability values are less critical than the relative improvements achieved. For instance, in an MMC with specific characteristics, the B10 lifetime was estimated at approximately 0.2, 1, and 8.5 years without redundancy, using the MIL, FIDES, and Mission Profile methods, respectively. Despite these differences, adding an SM significantly enhanced the B10 lifetime, increasing it to 1.7, 10.5, and 18.3 years for the respective methods. This analysis clearly illustrates that irrespective of the chosen evaluation method, implementing even one redundant SM can remarkably improve the B10 lifetime, ranging from 200% to 1,000%. Such results highlight the transformative impact of redundancy

strategies on the reliability of MMCs, reinforcing the practical applicability and effectiveness of the proposed methodologies.

Another contribution of this research is the integration of modularity and cost considerations into the reliability design process. While the modular structure of MMCs offers scalability and flexibility, it also increases the number of components and, consequently, the potential points of failure. This dissertation thoroughly examined the trade-offs between component ratings, modularity levels, and reliability outcomes to address this challenge. For instance, in a 10 MW MMC with a 17 kV DC link, an initial switch voltage rating of 4.5 kV was deemed suboptimal. Based on the system's annual loading profile, selecting a lower switch rating, such as 1.7 kV or 3.3 kV, was more cost-effective, resulting in savings in CAPEX. Conversely, in an MMC application with a 320 MW power rating and a 160 kV DC link, the initial choice of a 3.3 kV switch rating was found to be non-optimal. In this case, selecting a higher switch rating would reduce OPEX by lowering conduction and switching losses despite a potential initial increase in CAPEX. It is crucial to emphasize that redundancy configurations were consistently designed to meet the reliability requirements of each MMC application, ensuring that cost optimization did not compromise system resilience. These findings underscore the feasibility of achieving reliability goals without incurring excessive costs, a critical consideration for large-scale deployments. A key aspect of this research was the incorporation of sensitivity analyses to account for variations in reliability assessment methods, component costs, and operational costs, which may arise from price fluctuations or differing system conditions. This approach ensures that the findings of this dissertation can be broadly applicable and valuable to academia and industry. One notable outcome from the sensitivity analysis was that, for various MMC applications with different power ratings, the optimal switch rating was predominantly influenced by the DC link voltage rather than the current rating. This insight provides a practical guideline for designing cost-efficient MMCs across a wide range of applications, reinforcing the applicability and relevance of the research outcomes.

Redundancy strategies were extensively examined as a means to enhance system robustness. The MRS proposed in this work integrates active redundant SMs with spare SMs that activate only in the event of a fault. Unlike traditional redundancy methods, which rely exclusively on either active or standby components, this hybrid approach strikes a balance between reliability and cost. A detailed analysis of a high-voltage MMC designed for HVDC transmission (operating at 320 kV) demonstrated the efficacy of MRS. The system's B10 lifetime was extended from 6.5 to 9.2 years, representing a significant improvement over standalone active redundancy strategies. Economically, applying MRS resulted in substantial cost savings across a wide range of MMCs with nominal power ratings between 30 MW and 1.2 GW. For example, in an MMC with a nominal power of 1.2 GW, MRS enabled 3 to 5 million Euros in savings over a 10-year period, with precise savings depending on the system's annual loading conditions. These outcomes were validated through MCS, ensuring robustness across diverse mission profiles and loading scenarios. The fundamental principle of MRS is to align maintenance frequency with redundancy levels. In systems with frequent maintenance intervals, a lower

level of redundancy is recommended, as this configuration minimizes both CAPEX and OPEX. Conversely, in applications where maintenance is infrequent due to logistical or cost constraints, a higher redundancy level becomes essential to ensure system reliability. However, this increase in redundancy is accompanied by corresponding increments in CAPEX and OPEX. These findings emphasize the flexibility and adaptability of MRS in optimizing the trade-offs between reliability, cost, and maintenance requirements. By tailoring redundancy levels to the specific operational and economic conditions of an MMC, MRS offers a practical and scalable solution for enhancing system resilience while maintaining cost efficiency.

Reconfigurability, a concept that has received limited attention in MMC designs, emerged as a pivotal focus of this research. The system's ability to dynamically bypass faulty components or rearrange its topology allows for continuous operation, even under fault conditions. This feature significantly enhances the reliability and availability of MMCs, particularly in critical applications. A fault detection and localization algorithm was developed and experimentally validated on a lab-scale MMC prototype. Specifically, faults were detected and localized within 150 ms of OCFs in T1 or T4 and within 30 ms for OCFs in T2 or T3. These results ensure minimal disruption to system performance and enable timely reconfiguration to maintain functionality. For instance, in the event of an OCF in T2 or T3, the reconfiguration method tolerates the fault, allowing the MMC to continue operating at nominal conditions without significant performance degradation. This approach validated the proposed methodology and highlighted its practical applicability in real-world scenarios. The ability to ensure continuous operation under fault conditions makes this reconfigurability approach especially valuable for remote or offshore installations where maintenance access is limited and often prohibitively expensive.

The contributions of this dissertation are not only numerical but also conceptual. Chapters 4, 6, and 7 provide a framework for enhancing MMC reliability cost-efficiently by applying the three main concepts introduced: redundancy, modularity, and reconfigurability (RMR). The methodologies presented here are applicable across a wide range of MMC applications, offering pathways to improve reliability without significantly increasing costs. This thesis has successfully addressed the dual challenge of improving reliability and reducing costs in MMCs. Integrating advanced reliability assessment techniques, cost-optimized modularity, mixed redundancy strategies, and fault-tolerant reconfigurability forms a cohesive framework that advances the state of the art in power electronics. These achievements pave the way for developing more robust, efficient, and economically viable MMCs, contributing to the global transition toward sustainable and reliable energy solutions.

7.1. CONTRIBUTIONS TO THE FUTURE RESEARCH

The integration of comprehensive reliability assessment techniques, cost-optimized redundancy strategies, and the application of reconfigurability for fault tolerance sets a new standard for ensuring reliability without imposing excessive costs. Future research,

which can be an extension or continuation of this work, is as follows:

- **Scalability of Reconfigurability**: While this thesis has validated reconfigurability through theoretical models and practical experiments, future work can focus on scaling this methodology. Research can explore the impact of larger MMC systems with higher power ratings, assessing whether the proposed fault-tolerant reconfiguration method holds for more complex systems.
- **Advanced Fault Detection Algorithms**: Although the fault detection algorithms presented in this thesis were successful, further improvement is possible by incorporating advanced machine learning algorithms or real-time digital twins. These could allow for faster and more accurate fault detection, potentially preventing damage to other system components.
- **Cost and Reliability Trade-offs for Other Converter Topologies**: Future work can extend the methodologies developed in this thesis to other converter topologies used in different applications. The cost-reliability trade-offs explored here for MMCs may present new findings when applied to bidirectional converters or AC/DC systems with different operational environments.
- **Exploration of Hybrid Redundancy Strategies**: While the mixed redundancy strategy proposed in this thesis has proven effective, future research can explore hybrid strategies that combine aspects of both mixed and active redundancy systems. Hybrid systems may better balance reliability, operational efficiency, and cost, especially in mission-critical applications.

A

APPENDIX

Details regarding the chosen switches are provided in Table A.1 for a current rating of 480 A. Additionally, Table A.2 outlines the switches selected when the current rating of the MMC is increased to 960 A.

Table A.1: SWITCH CHOICES RATING CURRENT OF 480 A

$V_{\mathbf{IGBT}}$ (kV)	**Model**
1.2	FF450R12ME4
1.7	FF450R12ME4
3.3	FF450R33TE3
4.5	FZ800R45KL3
6.5	FZ500R65KE3

Table A.2: SWITCH CHOICES RATING CURRENT OF 960 A

$V_{\mathbf{IGBT}}$ (kV)	**Model**
1.2	FF600RME4C
1.7	FF1000R17IE4P
3.3	FZ1000R33HE3BPSA1
4.5	FZ1000R45KL3B5
6.5	FZ500R65KE3 (Two parallel)

LIST OF PUBLICATIONS

JOURNALS

1. **M. Ahmadi**, A. Shekhar and P. Bauer, "Reliability Enhanced Fault-Tolerant Full-Bridge Modular Multilevel Converters using Reconfiguration during Open-Circuit Failures," in IEEE Transactions on Power Electronics, 2025.

2. **M. Ahmadi**, A. Shekhar and P. Bauer, "Switch Voltage Rating Selection Considering Cost-Oriented Redundancy and Modularity-based Trade-offs in Modular Multilevel Converter," in IEEE Transactions on Power Delivery, 2023.

3. **M. Ahmadi**, A. Shekhar and P. Bauer, "Mixed Redundancy Strategy for Modular Multilevel Converters in High-Power Applications," in IEEE Open Journal of the Industrial Electronics Society, 2024.

4. **M. Ahmadi**, A. Shekhar and P. Bauer, "Reliability Assessment for Modular Multilevel Converters Using Monte Carlo Simulations," in International Journal of Electrical Power and Energy Systems, 2025.

PEER-REVIEWED CONFERENCES

1. **M. Ahmadi**, A. Shekhar and P. Bauer, "Comparison of Military Handbook and the FIDES Methodology for Failure Rate Estimation of Modular Multilevel Converters," in IEEE 17th International Conference on Compatibility, Power Electronics and Power Engineering (CPE POWERENG), 2023.

2. **M. Ahmadi**, A. Shekhar and P. Bauer, "Reconfigurability, Modularity and Redundancy Trade-offs for Grid Connected Power Electronic Systems," in IEEE 20th International Power Electronics and Motion Control Conference (PEMC), 2022.

3. **M. Ahmadi**, A. Shekhar and P. Bauer, "Impact of the Various Components Consideration on Choosing Optimal Redundancy Strategy in MMC," in IEEE 20th International Power Electronics and Motion Control Conference (PEMC), 2022.

4. **M. Ahmadi**, R. van der Sande, A. Shekhar and P. Bauer, "Adequacy of Hybrid AC-DC Grids with Reliability Oriented Modular Multilevel Converter Design - A Case Study Using Modified RTS-24 Network," in IEEE 21st International Power Electronics and Motion Control Conference (PEMC), 2024.

5. **M. Ahmadi**, F. Kardan, A. Shekhar and P. Bauer, "Reliability Assessment of Modular Multilevel Converters: A Comparative Study of MIL and Mission Profile Methods," in 13th International Conference on Integrated Power Electronics Systems (CIPS), 2024.

6. **M. Ahmadi**, F. Kardan, A. Shekhar and P. Bauer, "Influence of Controller Parameters on Open-Circuit Fault Localization Time in Full-Bridge Modular Multilevel Converter," accepted in 26th European Conference on Power Electronics and Applications (EPE), 2025.

7. **M. Ahmadi**, Hitesh Dialani, Mladen Gagic, A. Shekhar and P. Bauer, "Design and Implementation of a Modular Multilevel Converter with Full Bridge Submodules with Software-in-the-Loop Control," accepted in IEEE 7th International Conference on DC Microgrids (ICDCM), 2025.

8. F. Kardan, **M. Ahmadi**, A. Shekhar and P. Bauer, "Load Profile Based Reliability Assessment of IGBT Module in Full-bridge DC/DC converter for Fast charging of EVs," in IEEE 23rd European Conference on Power Electronics and Applications (EPE ECCE Europe), 2023.

9. A. Shekhar, G. Rituraj, R. van der Sande, **M. Ahmadi**, R. Deshmukh, P. Bauer, V. Nougain, A. Lekic and P. Palensky, "Development of Reliable Power Electronic Systems using Real Time Digital Twin Based Power Hardware-in-the-Loop Testbed," in IEEE 15th PowerTech Belgrade, 2023.

ACKNOWLEDGEMENTS

Reaching the end of this Ph.D. journey has been both a demanding and deeply fulfilling experience. Along the way, I've had the good fortune to meet and work with many remarkable individuals who shaped my research and growth. I am sincerely grateful to all of you for your encouragement, knowledge, companionship, and support during this unforgettable chapter of my life.

Firstly, I would like to express my heartfelt thanks to my promotor, Prof. Pavol Bauer. Your support, trust, and leadership have been instrumental from the beginning. Your openness to new ideas, willingness to listen, and calm guidance through both challenging and exciting moments created the foundation on which this Ph.D. was built.

To my daily supervisor, Dr. Aditya Shekhar — thank you for the honest, sharp, and thoughtful way you've mentored me. Your dedication to research, as well as your clear sense of integrity and fairness, left a deep impression on me. From the earliest brainstorming sessions to our moments of reflection after conferences, I learned a great deal from you, both technically and personally. Working with you was not only productive but also genuinely enjoyable.

To my wife, Beheshteh — none of this would have been possible without you. You have been my greatest support through every high and low. Thank you for standing beside me through sleepless nights, difficult chapters, and moments of doubt. Your strength, love, and patience gave me courage when needed. I am endlessly grateful for your unwavering presence.

To my family — thank you for always believing in me, even when the path was unclear. Your support across the distance has been a source of motivation and comfort. The values you instilled in me and the sacrifices you've made are deeply appreciated, and this milestone is as much yours as it is mine.

In the lab, my days were made richer by the company and kindness of many. Mladen — thank you for the countless hours in the lab, for helping make the MMC setup a reality, and for all the chats that extended far beyond engineering. Whether it was brainstorming, troubleshooting, or just laughing about something totally unrelated, working with you was a true pleasure. I would like to sincerely thank Harrie and Bart for their invaluable support and dedication throughout my work in the lab.

Hitesh — what can I say? From solving technical puzzles together to bringing a cake for my birthday to helping with the "monstrosity" we built together in the lab — you were always there. Your generosity, patience, and good humor were a constant boost, and I feel lucky to have had you as a colleague and friend.

Joris — thank you for the many philosophical discussions that stretched well beyond a lunch break. Our long talks about life, meaning, and everything in between challenged my perspectives and offered a kind of intellectual companionship.

To Faezeh — I feel fortunate that we started this Ph.D. journey together. Thank you for being such a kind and thoughtful officemate and for the moments of collaboration,

encouragement, and laughter that helped keep things balanced along the way.

Junjie and Gangwei — my wonderful officemates — your discipline and focus were always impressive. I often found myself joyfully distracting you both just for some lighthearted conversation. Sharing a room with you made the day brighter and more fun.

Ibrahim — "let me tell you something": I always knew that if we started talking, we'd dive into hours of stories and debates. During our trip to Romania, the discussions that sometimes turned into friendly sparring sessions were unforgettable. Thanks for the laughs, the support, and the good vibes.

Marco, Cristian, Francesca, Lyu, Yang, Guangyao, Rohan, Calvin, Gautam, Joel, Darío, Alvaro, Nikos — I will always remember our warm conversations, relaxed meetups, and the little moments that made our group feel like home. Thank you for bringing such a cheerful spirit into the team.

A very special thanks to my mentor and friend, Alireza Javadian Sabet — your early guidance and friendship have meant a great deal to me. You've always been someone I could look up to and rely on.

Dhanashree — thank you for your kind support and guidance, especially regarding the OPAL-RT and MMC setup. Your expertise, reliability, and calm approach helped make complex challenges more manageable.

Sharmila — you are the true backbone of the DCE&S group. Your ability to handle everything with patience, grace, and efficiency made life so much easier for all of us. From sorting out travel and financial matters to handling countless administrative details, you were always there to help. Thank you for being so incredibly supportive.

Robin — my wonderful colleague, our trip to Denmark was truly memorable. I really enjoyed our long and insightful conversations in the lab, and your deep knowledge of MMC was always appreciated and helpful. Thank you for sharing both your expertise and your company.

Sachin — thank you for always being there with helpful advice, whether it was Ph.D.-related or not. I truly appreciated your support and your readiness to step in whenever help was needed.

Siddhesh — thank you for the good times in the lab; I really enjoyed our chats and moments of shared work.

Farshid — thank you for being a great friend and a much-needed source of balance during long days of work. Our shared breaks and outdoor chats helped me pause, recharge, and regain perspective.

Sohrab — thank you for always being there with your camera and your kindness. You so often sacrificed your time to take beautiful photos during our Ph.D. defenses, events, and gatherings.

Reza — thank you for taking care of my flowers when I couldn't; your kindness really meant a lot to me.

I would also like to thank others whose presence made my time at TU Delft unforgettable: Mohamad, Jianning, Wenli, Qobad, Gautham, and Zian.

To the many great friends who made my Ph.D. years colorful — Lu, thank you for your quiet support. Zhengzhao, Ruijun, Yawen, Tianming, Jundong, Heshi, Fan, and Haoyuan — thank you all for the wonderful energy you brought to our everyday life.

Finally, thank you to the entire DCES group for creating a warm, intellectually rich

environment. I truly appreciated the collective spirit of support, curiosity, and ambition. Special thanks to Hani, Sebastián, Laura, Wiljan, Felipe, Abdourahim, István, Zichen, Carina, Yongpeng, Koen, Margo, Bagas, Julian, Manfredo, Leila, Sourabh, Shibo, Lucia, Kalpesh, Fernando and Adnan.

There are surely more people who deserve mention — if you're reading this and we crossed paths during this time, know that I carry appreciation for you in my heart. Thank you for being part of this journey.

CURRICULUM VITÆ

Miad AHMADI

09-01-1994 Born in Kermanshah, Iran.

EDUCATION

2021 – 2025 Ph.D. in Electrical Engineering
Delft University of Technology (TU Delft), The Netherlands

2017 – 2019 M.Sc. in Electrical Engineering
Politecnico di Milano (Polimi), Italy

2012 – 2016 B.Sc. in Electrical Engineering - Electronics
Razi University, Iran

AWARDS

2022 Best Paper Award - PEMC 2022

2023 1^{st} Winner of IEEE IES SYPA - CPE POWERENG